PSU-IRL-SCI-408

Classification Numbers 1.5.1, 1.5.2, 1.5.3, 3.1.2, 3.1.4, and 3.2.1

THE PENNSYLVANIA
STATE UNIVERSITY

IONOSPHERIC RESEARCH

Scientific Report 408

PROPAGATION STUDIES USING A THEORETICAL IONOSPHERIC MODEL

by

Myung Ki Lee

March 1, 1973

The research reported in this document was supported by the National Science Foundation under Grant GA-27758; the Office of Naval Research under Grant N00014-67-A-0385-0017; and the National Aeronautics and Space Administration under Grants NGL 39-009-003 and NGR 39-009-002.

IONOSPHERE RESEARCH LABORATORY

University Park, Pennsylvania

Security Classification

DOCUMENT CONTROL DATA - R & D

(Security classification of title, body of abstract and indexing annotation must be entered when the overall report is classified)

1 ORIGINATING ACTIVITY (Corporate author)	2a. REPORT SECURITY CLASSIFICATION
Ionosphere Research Laboratory	2b. GROUP

3 REPORT TITLE

Propagation Studies Using a Theoretical Ionospheric Model

4 DESCRIPTIVE NOTES (Type of report and inclusive dates)

Scientific Report

5 AUTHOR(S) (First name, middle initial, last name)

Myung-Ki Lee

6. REPORT DATE	7a. TOTAL NO OF PAGES	7b. NO. OF REFS
March 1, 1973	137	

8a. CONTRACT OR GRANT NO	9a. ORIGINATOR'S REPORT NUMBER(S)
NSF GA-27758 ONR N00014-67-A-0385-0017 b. PROJECT NO NASA NGL 39-009-003 c. NGR 39-009-002 d.	PSU-IRL-SCI-408
	9b. OTHER REPORT NO(S) (Any other numbers that may be assigned this report)

10 DISTRIBUTION STATEMENT

Supporting Agencies

11 SUPPLEMENTARY NOTES	12. SPONSORING MILITARY ACTIVITY
	National Science Foundation Office of Naval Research National Aeronautics and Space Administ.

13 ABSTRACT

More is now known about the behavior of the ionospheric densities and temperatures as a function of solar activity, solar zenith angle, season, and geographical location. The currently available mid-latitude ionospheric and neutral atmospheric models are coupled with an advanced three dimensional ray tracing program to see what success would be obtained in predicting the wave propagation conditions and to study to what extent the use of theoretical ionospheric models is practical. The Penn State MK 1 ionospheric model, the Mitra-Rowe D region model, and the Groves' neutral atmospheric model are used throughout this work to best represent the real electron densities and collision frequencies. The Faraday rotation and differential Doppler velocities from satellites, the propagation modes for long distance high frequency propagation, the group delays for each mode, the ionospheric absorption, and the spatial loss are all predicted.

The prediction of the oblique incidence soundings shows that the group delays measured are bracketed by the predictions for a reasonable range of solar activities.

Comparison of the predictions of the model with the current techniques shows that the maximum percentage difference between the maximum usable frequencies for the paths considered are in all cases tested within 5%.

The prediction of the Faraday rotation and differential Doppler shift shows that the departure of the predictions from the measurements are no larger than the range of variation encountered in a given month.

Particular attention was paid to the interpretation of ionospheric absorption in terms of D region densities by clearly showing the percentage of the absorption that

(continued)

Security Classification

DOCUMENT CONTROL DATA - R & D

(Security classification of title, body of abstract and indexing annotation must be entered when the overall report is classified)

1 ORIGINATING ACTIVITY *(Corporate author)*	2a. REPORT SECURITY CLASSIFICATION
	2b. GROUP

3 REPORT TITLE

4 DESCRIPTIVE NOTES *(Type of report and inclusive dates)*

5 AUTHOR(S) *(First name, middle initial, last name)*

6 REPORT DATE	7a. TOTAL NO OF PAGES	7b. NO OF REFS
8a CONTRACT OR GRANT NO	9a. ORIGINATOR'S REPORT NUMBER(S)	
b. PROJECT NO		
c.	9b. OTHER REPORT NO(S) *(Any other numbers that may be assigned this report)*	
d.		

10 DISTRIBUTION STATEMENT

11. SUPPLEMENTARY NOTES	12 SPONSORING MILITARY ACTIVITY

13 ABSTRACT

takes place at different altitudes. The absorption figures calculated by the model suggest that the method can serve as a useful technique in checking models of the lower ionosphere.

PSU-IRL-SCI-408
Classification Numbers 1.5.1, 1.5.2, 1.5.3, 3.1.2, 3.1.4, and 3.2.1

Scientific Report 408

Propagation Studies Using a Theoretical Ionospheric Model

by

Myung Ki Lee

March 1, 1973

The research reported in this document was supported by the National Science Foundation under Grant GA-27758; the Office of Naval Research under Grant N00014-67-A-0385-0017; and the National Aeronautics and Space Administration under Grants NGL 39-009-003 and NGR 39-009-002.

Submitted by: J. S. Nisbet (A.J.F.)

J. S. Nisbet, Professor of
Electrical Engineering
Project Supervisor

Approved by: A J Ferraro

A. J. Ferraro, Acting Director
Ionosphere Research Laboratory

Ionosphere Research Laboratory

The Pennsylvania State University

University Park, Pennsylvania 16802

ACKNOWLEDGEMENT

The author would like to thank Professor J. S. Nisbet for his constant guidance and the numerous invaluable suggestions given throughout the course of this research.

The author also wishes to extend his gratitude to Professor W. J. Ross for his continuous encouragement.

Appreciation is also given to Professors A. J. Ferraro, J. J. Gibbons, G. J. McMurtry, and J. W. Robinson for their assistance given as members of the committee. The author is also grateful to Mr. Robert Divany for the computer programming and to the computresses of the Ionosphere Research Laboratory for their help in tabulating the data.

This work was supported in part by the National Science Foundation under Grant GA 27758, in part by the National Aeronautics and Space Administration under Grants NGR 39-009-002 and NGL 39-009-003, and by the Office of Naval Research under ~~Grant~~ Cnt. N00014-67-0385-0017.

TABLE OF CONTENTS

LIST OF TABLES

LIST OF FIGURES

ABSTRACT

More is now known about the behavior of the ionospheric densities and temperatures as a function of solar activity, solar zenith angle, season, and geographical location. The currently available mid-latitude ionospheric and neutral atmospheric models are coupled with an advanced three dimensional ray tracing program to see what success would be obtained in predicting the wave propagation conditions and to study to what extent the use of theoretical ionospheric models is practical. The Penn State Mk 1 ionospheric model, the Mitra-Rowe D region model, and the Groves' neutral atmospheric model are used throughout this work to best represent the real electron densities and collision frequencies. The Faraday rotation and differential Doppler velocities from satellites, the propagation modes for long distance high frequency propagation, the group delays for each mode, the ionospheric absorption, and the spatial loss are all predicted.

The prediction of the oblique incidence soundings shows that the group delays measured are bracketed by the predictions for a reasonable range of solar activities.

Comparison of the predictions of the model with the current techniques shows that the maximum percentage difference between the maximum usable frequencies for the paths considered are in all cases tested within 5%.

The prediction of the Faraday rotation and differential Doppler shift shows that the departure of the predictions from the measurements are no larger than the range of variation encountered in a given month.

Particular attention was paid to the interpretation of ionospheric absorption in terms of D region densities by clearly showing the percentage of the absorption that takes place at different altitudes. The absorption figures calculated by the model suggests that the method can serve as a useful technique in checking models of the lower ionosphere.

CHAPTER I

INTRODUCTION

1.1 General Statement of the Problem

To understand ionospheric radio wave propagation it is necessary to know the expected ray paths. These are needed to allow quantitative estimates to be made of the expected performance of systems employing propagation through the ionosphere. It is desirable to be able to predict the propagation paths, the fading modes, field strengths, and the relationship of these to solar and magnetic conditions. This requires a model that provides information on the electron and neutral densities as a function of location, season, time, and solar conditions as well as a ray tracing program to enable propagation conditions to be calculated for complete paths under any desired conditions.

It was desired to select from currently available mid-latitude ionospheric and neutral atmospheric models those that are best able to represent the real electron densities and collision frequencies. It was then desired to see how these could be coupled together in a consistent manner without discontinuities in boundary regions. It was then of interest to couple these with an advanced three dimensional ray tracing program to see what success would be obtained in predicting propagation conditions.

For many years it has been common to justify aeronomic programs on the basis of their relevance to radio wave

propagation. Theoretically based ionospheric models are now becoming available. It is of the utmost importance to study to what extent the use of theoretical models is practical and what improvements are vital to their application.

Chapter I introduces the problem and presents a comprehensive review of the relevant literature.

Chapter II describes the method of calculation in predicting the wave propagation conditions by combining the theoretical ionospheric model with the ray tracing program. The coupling of the ionospheric and neutral atmospheric models is discussed in section 2.1 to obtain the continuous profiles of electron density and the collision frequency. Section 2.2 describes the techniques for developing and interpolating the ionospheric models and magnetic field model to supply the necessary parameters to the ray tracing program so that the ray path for any desired conditions can be calculated. Initial information needed to run the program is also described briefly in section 2.3.

In the first section of Chapter III, predictions and observations for satellite propagation are compared under a variety of geographical, solar, and seasonal conditions. The horizontal gradient of the electron content along the satellite path is also discussed. In section 3.2 the prediction of the ray paths is described and the predictions of the oblique incidence soundings and the maximum usable frequency are compared with the experimental observations. In the last two sections the absorption of obliquely propagated high

frequency waves is re-examined and compared with the standard absorption measurement technique. The spatial loss due to the power spreading is also predicted to see its contribution to the path loss.

Chapter IV describes the prediction of the absorption of the high frequency radio waves and its comparison with the experimental observations for a variety of conditions. The variation of absorption with solar zenith angle, ground range, and solar activity is described and an empirical equation is derived.

Chapter V discusses the conclusions of this study and compares the results with other studies. Conclusions given in the first five sections relate to each of the specific problems posed in section 1.3. Suggestions for future work are given in section 5.6.

Appendix 1 describes the estimates of the initial azimuth angle and a great circle path for the location of the propagation path. Appendix 2 describes the main computer programs used in this study.

1.2 Previous Related Studies

1.2.1 Historical Summary of Ionospheric Prediction

Because the ionosphere varies from hour to hour and from day to day, etc., it is necessary to have a knowledge of this variability in order to select the optimum frequency. The selection of the best sky-wave frequencies for communication purposes over a given transmission path depends upon

the time of day, season of the year, phase of the sun-spot cycle, length of the path, and location of the path, as well as the conditions prevailing in the ionosphere over the path. The predictions are important for efficient frequency allocation, for the preparation of specifications for communication equipment, and for the operation, planning, and design of high frequency communication systems.

Current prediction techniques attempt to give values for several operational parameters. Those that have been commonly used are:

MUF	The "maximum usable frequency" for a given circuit and a given mode of propagation.
FOT	The "optimum working frequency" is defined as the value of the maximum usable frequency that is exceeded 90% of the days of the month. This frequency may be estimated for F2-layer propagation by multiplying the maximum usable frequency by 0.85.
M(3000)F2	The maximum usable frequency for a 3000 km path divided by the F2-layer critical frequency for the ordinary mode. It is often called M(3000)F2 factor.
MUF(ZERO)F2	The F2-layer maximum usable frequency for zero km.
MUF(4000)F2	The maximum usable frequency of the F2-layer for a 4000 km path.

f_oF2 The F2-layer critical frequency for the ordinary mode.

Predictions of the MUF are usually made for the monthly median value, which is the value equalled or exceeded 50% of the days during the month at a specified time of day. Many ionospheric observatories produce hourly values of the F2-MUF factor for reflections from the F2-layer.

Many theoretical methods have been developed for the evaluation of the F2-MUF factor which is the ratio of the maximum usable frequency propagated to the critical frequency of the F2-layer for the ordinary ray. The parabolic layer theory, the non-parabolic layer theory, and the transmission curve technique are the most popular methods.

The parabolic layer method depends upon the assumption that the F2-layer has a vertical electron density distribution parabolic in shape. Appleton and Beynon (1940, 1947) have developed, by assuming that the ionosphere has a parabolic electron density distribution, a direct method of calculating the maximum usable frequency reflected at oblique incidence by a thick parabolic layer for both short-distance (plane earth) and long-distance (curved earth) transmission and explained the results graphically. They also showed how to determine the MUF and skip distance for various values of the half thickness y_m, the height of maximum electron density h_m, and the base height h_o.

Newbern Smith (1939) gave a simple, rapid, graphical method for obtaining maximum usable frequencies and effective

reflection heights of radio waves, from vertical incidence measurements of the critical frequencies and the virtual heights of the various layers in the ionosphere. The method consists of the use of a "Transmission Curve", which is superimposed on the curve of frequency against virtual height, observed at vertical incidence. This transmission curve provided one of the most convenient and widely used methods for determining maximum usable frequencies.

Another method is the so called non-parabolic layer theory (N(h) profile method) given by Vickers (1959). This method is based on empirical relations derived from operational experience acquired over a long period of time. By producing a differential equation for the ray path which reduces, in the case of a parabolic electron density distribution, to that derived by Appleton and Beynon (1940), and solving that equation numerically, oblique incidence propagation characteristics and MUF factors were deduced. These MUF factors were compared with those which would have been obtained had a parabolic electron density distribution been assumed or had a transmission curve been used.

Up to this point most of the methods used in the determination of maximum usable frequencies for ionospheric propagation neglect the effects of the earth's magnetic field. Thomas, Haselgrove, and Robbins (1958a, b) and Thomas and Robbins (1958) have pointed out, however, that the inclusion of the magnetic field can appreciably affect the determination of the electron density distribution and

therefore the calculated MUF. Direct measurements of MUF (Wieder, 1955) have shown that the observed values are, on the average, about 3 percent higher than those obtained by the use of the transmission curves. Davies (1959) drew attention to influence of the geomagnetic field on MUF calculations using a transmission-slider technique and gave suggestions for improving MUF calculations.

As seen in the results of Hanson et al. (1958), Wieder (1955), and Silberstein (1958), the diurnal, seasonal, geographic variation of MUF factors and also a variation with sun-spot cycle could be seen.

The first automated high frequency (HF) path prediction computer program was developed in 1957 for the U.S. Army Signal Corps. This was later modified in several versions. The first fully automated program in which the oblique transmission equations for parabolic layers were used was developed in 1966 (Lucas and Haydon, 1966) by ESSA's Institute for Telecommunication Sciences and Aeronomy which preceeded the Institute for Telecommunication Sciences (ITS). In 1969 Barghausen et al. (1969) employed more extensive techniques which, though similar to the earlier ITS program, incorporated significant changes.

One of the basic principles employed in all ionospheric prediction is the relation of ionospheric characteristics to the sun-spot cycle. The actual prediction consists essentially of first predicting the solar activity and then from the mass of data available, the corresponding

trends of seasonal, diurnal and geographical variations of the ionosphere characteristics.

The basic ionospheric data used in the predictions are the E-, F1- and F2-layer ordinary wave critical frequencies (f_oE, f_oF1, and f_oF2, respectively) and the F2-M3000 factor. The synoptic numerical coefficient representations of the ionospheric characteristics are fundamental to all efficient HF computer prediction programs. These were first developed by ITSA and published in 1960 (Jones and Gallet, 1960) and developed further in 1962 (Jones and Gallet, 1962a; Jones and Gallet 1962b) and 1969 (Jones et al., 1969).

The basic form of the F2-layer predictions is a table of numerical coefficients defining a function which represents the world-wide and diurnal variations of ionospheric characteristics like f_oF2, MUF(ZERO)F2, M(3000)F2 median, and MUF(4000)F2 median. This function, referred to as the "numerical map" of the characteristics, has the form of a finite series of simple terms consisting of elementary functions of latitude, longitude, and time, each multiplied by the appropriate coefficient. A numerical map may then be written in the general form

$$\Omega(\lambda,\theta,T) = a_o(\lambda,\theta) + \sum_{j=1}^{H} [a_j(\lambda,\theta)\cos jT + b_j(\lambda,\theta)\sin jT]$$

where

$$a_j(\lambda,\theta) = \sum_{k=o}^{k} a_j^{(k)} F_k(\lambda,\theta)$$

$$b_j(\lambda,\theta) = \sum_{k=o}^{k} b_j^{(k)} F_k(\lambda,\theta)$$

λ = geographic latitude

θ = geographic longitude

T = universal time

H is the number of harmonics for representing the diurnal variation. Here $F_k(\lambda,\theta)$ denotes the orthonormal functions which are linear combinations of the geographic coordinate function $G_k(\lambda,\theta)$. In most applications it is convenient to express $\Omega(\lambda,\theta,T)$ explicitly in terms of the $G_k(\lambda,\theta)$. Then the new coefficient $U_{s,k}$ is used for defining the $a_j(\lambda,\theta)$ and $b_j(\lambda,\theta)$ in the form

$$a_j(\lambda,\theta) = \sum_{k=o}^{k} U_{2j,k} G_k(\lambda,\theta), \quad j = 0,1,\ldots,H$$

$$b_j(\lambda,\theta) = \sum_{k=o}^{k} U_{2j-1,k} G_k(\lambda,\theta), \quad j = 1,2,\ldots,H$$

Thus a numerical map $\Omega(\lambda,\theta,T)$ is defined by specifying the numerical coefficients to define the $a_j(\lambda,\theta)$ and $b_j(\lambda,\theta)$ in the above equations.

The "Ionospheric Predictions" issued monthly by the Ionospheric Propagation Predictions Group of ITS, ESSA Research Laboratories, Boulder, Colorado are based on this numerical map method. They are issued three months in advance and each issue provides the predicted sun-spot numbers derived from a regression analysis based on the solar cycle, tables of numerical coefficients that define the functions describing the predicted worldwide distribution of f_oF2 and M(3000)F2, and maps for each even hour of universal time of MUF(ZERO)F2 and MUF(4000)F2. Davies (1965) and Ostrow (1966) explained the details of applying these numerical and graphical prediction maps and discussed the calculation of MUF and FOT for transmission by F2-layer alone, transmission by the regular layers (E-F1, F2), and transmission with the effects of the sporadic E E_s for both distances less than 4000 km and distances greater than 4000 km.

Prediction of the long-term operational parameters of high frequency sky-wave telecommunication systems developed by Barghausen et al. (1969) was an application of the numerical technique to the parabolic layer theory. The ionospheric parameters for the specific path such as critical frequency of the layer, height of the maximum electron density of the layer, height of the bottom of the layer, and semithickness of the layer were obtained from the numerical world maps, and an empirical relationship between the maximum height of the F2-layer and M(3000) was used. Then the

parabolic layer theory was applied and the maximum usable frequency, take-off angle, and virtual height of reflection for all frequencies were calculated. This program predicts the long-term operational parameters such as maximum usable frequency (MUF), and optimum working frequency (FOT), based on the circuit reliability and service probability. A method for predicting estimates of the short term operational MUF based upon measurements of the local magnetic activity in the vicinity of the circuit was also incorporated into this program (Davies, 1970).

There are still many areas where further study, modification, or extension of the prediction model and methods are desirable. One may improve the prediction technique by using a ray tracing program which would be more adaptable when consideration must be given to ionospheric irregularities (tilts, spread F, sporadic E, etc.) that cause multipath, mixed modes, offpath scatter, asymmetrical paths, etc. Applying the ray tracing technique to a reasonable theoretical ionospheric model such as the Penn State Mk 1 Model should allow better predictions to be made.

1.2.2 Propagation in the Ionosphere and Ray Tracing

Since Kennelly and Heaviside (1902) independently suggested that long-range propagation of radio waves might be possible from England to America using the ionosphere as a reflector, numerous investigations of the ionosphere's

properties have been carried out for both practical and scientific purposes.

The first quantitative study of radio-ionosphere interactions was made by Appleton (1932) who formulated the Appleton-Hartree equation for the complex refractive index and the polarization of plane waves propagating in a homogeneous, anisotropic medium, such as the ionosphere. A very thorough discussion of them was given by Booker (1939, 1949), Ratcliffe (1959), Budden (1961), Kelso (1964), and Davis (1969).

The propagation of radio waves through the ionosphere can be described quite simply if the index of refraction does not change appreciably over the distance of a wavelength. In this case the W.K.B. solutions which Wentzel, Kramers and Brillouin (1920's) used extensively in quantum mechanics, often produce very good approximations to the analytical solution of the wave equations governing radio wave propagation in the ionosphere. A W.K.B. solution is, therefore, often said to be a mathematical expression of "ray" theory. The W.K.B. solutions play a most important part in the theory of the propagation of radio waves, and comprehensive reviews of their use may be found in texts by Budden (1961), Ginzburg (1961), Kelso (1964), and Davies (1969). This is the theory on which ordinary ray tracing programs are based.

There are, of course, varying degrees of sophistication in ray tracing. All ray tracing methods rest on the

same foundation which can be stated mathematically in a variety of equivalent ways. For example, Snell's law and Fermat's principle are the underlying principles on which all ray tracing techniques are based. An extension of Fermat's principle leads to a corresponding extension of Snell's law and could be used to derive all other equations used for ray tracing. However, a variety of mathematical approaches can be chosen to meet their own logical or computational purposes. Extensive descriptions of programs have been given by Croft (1969), Kelso (1968), and Jones (1966, 1970).

The ray tracing program used for this work is the Three Dimensional Ray Tracing Computer Program developed by Jones (1966) at the National Bureau of Standards. This ray tracing program has been in use now for over three years by people scattered all over the world. The method of tracing rays based on the principles of Hamiltonian Optics developed by Haselgrove (1955) is used in this program. The method involves the solution of a set of six simultaneous differential equations in terms of the three position coordinates and three variables indicating the direction of the wave normal.

The program calculates ray paths by numerically integrating the following six differential equations similar to those described by Haselgrove (1955).

$$\frac{dr}{dt} = (V_r - \text{Real}\{n\frac{\partial n}{\partial V_r}\})/\text{Real}\{nn'\}$$

$$\frac{d\theta}{dt} = (V_\theta - \text{Real}\{n\frac{\partial n}{\partial V_\theta}\})/(r\,\text{Real}\{nn'\})$$

$$\frac{d\phi}{dt} = (V_\phi - \text{Real}\{n\frac{\partial n}{\partial V_\phi}\})/(r\sin\theta\,\text{Real}\{nn'\})$$

$$\frac{dV_r}{dt} = \frac{\text{Real}\{n\frac{\partial n}{\partial r}\}}{\text{Real}\{nn'\}} + V_\theta \frac{d\theta}{dt} + V_\phi \sin\theta \frac{d\phi}{dt}$$

$$\frac{dV_\theta}{dt} = \frac{1}{r}\left(\frac{\text{Real}\{n\frac{\partial n}{\partial \theta}\}}{\text{Real}\{nn'\}} - V_\theta \frac{dr}{dt} + rV_\phi \cos\theta \frac{d\phi}{dt}\right)$$

$$\frac{dV_\phi}{dt} = \frac{1}{r\sin\theta}\left(\frac{\text{Real}\{n\frac{\partial n}{\partial \phi}\}}{\text{Real}\{nn'\}} - V_\phi \sin\theta \frac{dr}{dt} - rV_\phi \cos\theta \frac{d\theta}{dt}\right)$$

where the variables r, θ, and ϕ are the spherical polar coordinates of a point on the ray path; V_r, V_θ, and V_ϕ are the components of the wave normal direction in r, θ, and ϕ direction, normalized so that

$$V_r^2 + V_\theta^2 + V_\phi^2 = \text{Real}\{n^2\}$$

n is the complex phase refractive index and n' is the complex group refractive index. These are expressed as follows.

$$n^2 = 1 - \frac{X}{1 - jZ - \frac{Y_T^2}{2(1-X-jZ)} \pm \{\frac{Y_T^4}{4(1-X-jZ)^2} + Y_L^2\}^{1/2}}$$

where

$$X = \frac{Ne^2}{\varepsilon_o m\omega^2} = \frac{\omega_N^2}{\omega^2} = \frac{f_N^2}{f^2}$$

N = electron density

m = mass of an electron

ε_o = free space permittivity

ω = $2\pi f$, angular wave frequency

f = wave frequency

f_N = plasma wave frequency

Y_L = longitudinal component of the geomagnetic field parameter Y along the wave normal direction

Y_T = transverse component of Y

$Y = \frac{|e|B_o}{m\omega}$

$f_H = \frac{1}{2\pi} \frac{|e|B_o}{m}$, electron gyro frequency

B_o = the flux density of the earth's magnetic field

e = charge of an electron

$Z = \nu/\omega$

ν = electron collision frequency

$n' = n + f\frac{dn}{df}$, the complex group refractive index

The group path length is used as an independent variable t in the above six simultaneous differential equations, whereas Haselgrove uses phase path length. The group path is defined by

$$t = \int_{\text{path}} n'\cos\alpha ds$$

where α is the angle between the ray direction and the wave normal direction.

Jones (1970) explained that the six simultaneous differential equations give the same path as that obtained by the equations of Haselgrove if there are no collisions.

If there are electron collisions, so that n and n' are complex, then ray paths calculated using the equations of Haselgrove (1955) satisfy Fermat's principle,

$$\delta \int_{\text{path}} \text{Real}\{n\}\cos\alpha ds = 0$$

whereas, ray paths calculated using the above six equations satisfy

$$\delta \int_{\text{path}} \sqrt{\text{Real}\{n^2\}}\cos\alpha ds = 0$$

which is a better approximation to the ray path in a lossy medium. Jones (1970) mentioned that this ordinary ionospheric ray tracing program works well at HF (3-30 MHz). For the extension to lower frequencies, Jones also described the ray tracing in complex space to calculate the correct path in a lossy medium and compared the results with the phase integral method and the full wave solutions.

In addition to the six basic equations necessary to calculate the ray path, the program also integrates

$$\frac{dP}{dt} = \frac{\text{Real}\{n^2\}}{\text{Real}\{nn'\}}$$

to give the phase path, and integrates

$$\frac{dA}{dt} = \frac{10}{\log_e 10} \frac{2\pi f}{C} \frac{|\text{imag}\{n^2\}|}{\text{Real}\{nn'\}}$$

to give the absorption in db. One of the computer outputs for the propagation from Annapolis to State College is shown in Table 1.

The refractive index equations used in this ray tracing program are based on the Appleton-Hartree formulas. The following quantities are calculated in the program.

$$n^2,\ nn',\ n\frac{\partial n}{\partial r},\ n\frac{\partial n}{\partial \theta},\ n\frac{\partial n}{\partial \phi},\ n\frac{\partial n}{\partial V_r},\ n\frac{\partial n}{\partial V_\theta},\ n\frac{\partial n}{\partial V_\phi},\ \text{and}\ n\frac{\partial n}{\partial t}$$

In order to calculate the above quantities, the following quantities are provided:

$$X,\ \frac{\partial X}{\partial r},\ \frac{\partial X}{\partial \theta},\ \frac{\partial X}{\partial \phi},\ \text{and}\ \frac{\partial X}{\partial t}$$

from the electron density model,

$$Y,\ \frac{\partial Y}{\partial r},\ \frac{\partial Y}{\partial \theta},\ \frac{\partial Y}{\partial \phi},\ Y_r,\ \frac{\partial Y_r}{\partial r},\ \frac{\partial Y_r}{\partial \theta},\ \frac{\partial Y_r}{\partial \phi},$$

$$Y_\theta\ \frac{\partial Y_\theta}{\partial r},\ \frac{\partial Y_\theta}{\partial \theta},\ \frac{\partial Y_\theta}{\partial \phi},\ Y_\phi,\ \frac{\partial Y_\phi}{\partial r},\ \frac{\partial Y_\phi}{\partial \theta},\ \text{and}\ \frac{\partial Y_\phi}{\partial \phi}$$

from the magnetic field model, and

Table 1: One of the Ray Tracing Computer Outputs for the Propagation Between Annapolis and State College

Ordinary 00A Theoretical Profile for D- and E-Region. Date: 08/16/72

** Transmitter Information **

Frequency: 3.360000 MHZ Azimuth: 327.000 Degrees Elevation: 53.000 Degrees

	Height KM	Range KM	Azimuth Deviation XMTR Degrees	Azimuth Deviation Local Degrees	Elevation XMTR Degrees	Elevation Local Degrees	Group Path KM	Phase Path KM	Absorption DB
-2.E-07 at XMTR	0.0	0.0	0.0	0.0	53.000	53.000	0.0	0.0	0.0
-3.E-07 ENTR ION	58.742	43.753	0.012	-0.012	52.996	53.394	73.368	73.368	0.0
-3.E-03 VERT REV	120.348	122.195	0.442	-0.448	43.743	-0.134	203.719	159.712	17.688
4.E-03 APOGEE	120.723	126.447	0.346	-0.351	42.833	-14.584	211.219	162.250	17.920
3.E-04 EXIT ION	57.500	195.367	-0.288	0.294	15.450	-53.395	323.407	246.862	28.728
0. VERT REV	0.0	238.185	-0.234	0.240	-1.072	53.009	395.215	318.671	28.728
0. HOP	0.0	238.185	-0.234	0.240	-1.072	53.009	395.215	318.671	28.728

Wave Polarization

	Real	Imag
Entering Ionosphere	0.102	0.929
Exiting Ionosphere	-0.018	-0.988

	Latitude North	Longitude East	Altitude KM
Transmitted	39.00	-76.50	0.0
Received	40.78	281.95	0.0

Timing: 33.12 Seconds

Cost: $3.64

$$Z, \frac{\partial Z}{\partial r}, \frac{\partial Z}{\partial \theta}, \frac{\partial Z}{\partial \phi}$$

from the collision frequency model.

Therefore, when using this program, one must specify the ionospheric models which define electron density, collision frequency, and the earth's magnetic field as a function of position in space. The models chosen for this work are described in the following four sections.

For low frequencies (below about 1 MHz) and especially for very low frequencies, the ionosphere cannot always be regarded as a slowly varying medium and full wave solutions are often required for many problems. Jones (1970) explained that even though ray theory breaks down for low frequency (LF) radio waves, it can be best approximated to the full wave solution by extending Fermat's principle in complex space, which is the criteria of the ray path to have a minimum attenuation in addition to a minimum wave interference. This is the basis for the complex ray tracing program. Jones (1970) stated that applying ray tracing in complex space to a plane wave incident on a plane stratified medium gives a result that agrees exactly with the results obtained by the phase integral method in the complex plane, and that agrees satisfactorily with the full wave solution above 30 KHz for all of his results shown. Below this frequency, the amplitude errors for vertical polarization and phase error for both vertical polarization and

horizontal polarization increase with decreasing frequency, and therefore, the full wave solution is needed.

In general solutions for full wave equations can only be obtained through numerical integration using computers, except for certain restricted ionospheric models and propagation conditions. There are usually three ways of approaching the full wave solutions based on the type of dependent variables for the integration.

Clemmow and Heading (1954) and Budden and Clemmow (1957) obtained the coupled forms of the differential equations governing radio wave propagation in the ionosphere.

Budden (1955a, 1955b) described the methods for obtaining numerical solutions of the differential equations which govern the propagation of long and very long radio waves in the ionosphere at vertical and oblique incidence. In this method he obtained the first order simultaneous differential equations for plane wave propagation as derived from Maxwell's equations and the constitutive relations for the ionosphere and calculated the reflection coefficient matrix whose elements relate the total reflected wave to the total incident wave when the ionosphere is assumed to be horizontally stratified. The dependent variable is then the reflection coefficient matrix and not the wave field vector.

Barron and Budden (1959) resorted to another dependent variable, however, termed the admittance matrix which is related to the reflection coefficient matrix. The wave

admittance approach is used here, although the wave fields are variables preferred by others such as Pitteway (1965).

Pitteway (1965) extended Budden's technique to include the calculation of the wave fields and the polarization of long radio wave propagation in the ionosphere. A constraint was added onto one of the two separate independent solutions required in constructing the wave fields which are the dependent variables for the integration. Piggot, Pitteway, and Thrane (1965), using Pitteway's method, presented some of the characteristics of the waves reflected from the proposed ionospheric models and compared these results with ground measurements, made on low and very low frequency waves.

Seliga (1965) derived the generalized equations which include collision frequency dependence on the electron energy and outlined the numerical techniques for their solution similar to that of Pitteway (1965).

In the derivation of the Appleton-Hartree theory, the collision frequency of an electron was assumed to be independent of the electron velocity. However, laboratory experiments made by Phelps and Pack (1959) have shown that the collision frequency of electrons is very nearly proportional to the square of their velocity. Under these circumstances Sen and Wyller (1960), Budden (1965), and Deeks (1966) have deduced the generalized magneto-ionic theory to describe the propagation of a plane electromagnetic wave through a magneto-ionic medium in which the collision

frequency of monoenergetic electrons is proportional to the electron energy. It was shown that the classical Appleton-Hartree formulas can be best approximated by using the collision frequency called the effective collision frequency or equivalent collision frequency.

In the present work attention has been confined to those cases for which ray tracing is adequate and no attempt has been made to use full wave propagation programs with the models.

1.2.3 The Penn State Mk 1 Ionospheric Model

The Penn State Mk 1 Ionospheric Model has been described by Nisbet (1970a, b). This model provides a computer program that allows a model of the complete electron density profile in mid-latitudes to be calculated from 120 km to 1250 km as a function of latitude, longitude, day number, time, and solar activity.

Table 2 shows one of the computer outputs. Electron densities are listed for a given longitude, latitude, time (both universal time and local time), day number, and solar activity expressed in 10.7 cm solar flux. It also gives the values of electron content, the peak electron density, the percentage probability of observing sporadic E with a critical frequency greater than 0.5 MHz, the average value of the peak electron density when sporadic E is observed, and the standard deviation of the log-normal distribution.

The Penn State Mk 1 Ionospheric Model is constructed as follows:

Table 2: One of the Computer Outputs of the Penn State Mk 1 Ionospheric Model

PENN STATE MK. I IONOSPHERIC MODELS FOR SUMMER SOLSTICE.
EAST LONGITUDE = -122.60 LATITUDE = 37.50
S 10.7 = 137.20 S 10.7 (I.A.U.) = 141.76 DAY = 197.00 MONTH = 7

UNIVERSAL TIME =	0.0	2.00	4.00	6.00	8.00	10.00	12.00	14.00	16.00	18.00	20.00	22.00
LOCAL TIME =	15.83	17.83	19.83	21.83	23.83	1.83	3.83	5.83	7.83	9.83	11.83	13.83
ALTITUDE	ELECTRON DENSITY METERS -3 X10-9 (CM. -3 X10-3)											
120.00	71.30	36.62	1.79	1.79	1.79	1.79	1.79	32.05	63.53	105.32	123.63	110.66
130.00	117.60	40.18	1.55	1.55	1.55	1.56	1.56	31.05	107.74	161.59	180.45	166.35
140.00	148.95	58.98	1.94	1.96	1.98	2.00	2.01	43.35	141.52	191.77	209.15	195.76
150.00	168.44	78.55	2.24	2.26	2.27	2.28	2.29	62.41	162.23	208.21	224.65	212.83
160.00	182.39	93.76	2.33	2.32	2.32	2.31	2.30	77.63	176.47	216.68	232.65	223.29
170.00	193.47	106.00	2.26	2.24	2.21	2.18	2.16	88.62	187.49	221.05	237.14	230.38
180.00	203.64	117.19	2.12	2.08	2.03	1.99	1.95	97.13	198.66	225.26	241.83	237.16
190.00	215.02	128.68	1.94	1.89	1.82	1.77	1.73	104.19	213.89	232.71	249.78	246.35
200.00	229.77	141.71	1.76	1.69	1.62	1.57	1.52	110.84	236.90	246.10	263.37	260.22
210.00	257.54	166.12	1.59	1.51	1.43	1.38	1.33	118.62	288.53	267.52	284.42	280.61
220.00	309.97	217.75	1.42	1.34	1.26	1.21	1.17	129.50	372.47	318.38	330.98	331.64
230.00	366.11	267.40	1.83	1.19	1.11	1.06	1.02	153.01	436.27	381.07	393.69	390.68
240.00	422.76	321.80	10.06	1.05	0.98	0.93	0.90	194.40	491.45	443.84	457.94	450.52
250.00	476.22	377.92	34.50	0.93	0.86	0.82	0.79	237.80	533.54	501.78	519.50	507.41
260.00	523.16	431.66	83.60	0.83	0.76	0.72	0.69	278.22	560.67	550.78	574.36	557.95
270.00	561.21	479.09	156.97	0.74	0.68	0.64	1.17	311.17	573.22	588.20	619.50	599.59
280.00	589.12	517.37	244.39	4.74	0.60	4.61	7.13	334.03	573.04	613.03	653.25	630.92
290.00	606.73	544.99	331.56	19.70	4.38	19.19	24.81	346.29	562.68	625.68	675.16	651.60
300.00	614.68	561.73	406.49	53.96	19.14	51.18	58.20	348.98	544.80	627.46	685.85	662.12
320.00	606.55	566.27	498.22	178.21	108.48	155.75	151.22	333.36	495.66	605.82	678.90	657.37
340.00	575.88	542.36	517.47	308.09	241.25	248.56	222.36	302.43	439.78	562.91	645.13	627.72
360.00	532.97	502.30	491.47	379.38	333.15	287.14	246.14	267.10	385.05	510.59	596.59	583.85
380.00	485.28	455.50	444.61	390.95	360.67	282.29	236.73	233.02	335.06	456.50	542.15	533.80
400.00	437.50	407.89	391.85	367.08	345.03	256.04	212.26	202.48	290.97	404.82	487.38	482.83
420.00	392.20	362.69	340.66	328.21	309.81	223.12	183.88	175.98	252.73	357.52	435.40	433.93
440.00	350.59	321.37	294.15	286.14	269.44	190.72	156.77	153.32	219.84	315.23	387.66	388.63
460.00	313.08	284.42	253.27	246.36	230.70	161.67	132.81	133.99	191.61	277.92	344.66	347.51
480.00	279.61	251.75	217.98	210.94	196.17	136.70	112.40	117.49	167.39	245.23	306.38	310.64
500.00	249.92	223.06	187.79	180.32	166.45	115.70	95.35	103.36	146.58	216.67	272.50	277.80
550.00	189.92	166.05	130.91	122.73	111.17	77.72	64.86	76.01	106.28	160.19	204.36	211.14
600.00	145.89	125.27	94.00	86.04	76.62	54.98	47.03	56.91	78.32	119.90	154.79	162.00
650.00	113.49	96.09	70.76	63.56	55.92	42.14	37.29	43.53	58.95	91.04	118.66	125.71
700.00	89.65	75.32	56.79	50.49	44.22	35.42	32.39	34.37	45.76	70.42	92.30	98.87
750.00	72.23	60.81	48.86	43.39	38.07	32.16	30.09	28.45	37.14	55.89	73.20	79.13
800.00	59.75	51.00	44.60	39.75	35.05	30.66	29.05	24.95	31.86	45.93	59.57	64.78
850.00	51.07	44.67	42.40	37.97	33.63	29.99	28.60	23.08	28.86	39.39	50.12	54.62
900.00	45.27	40.80	41.29	37.12	32.97	29.69	28.39	22.16	27.27	35.31	43.81	47.65
950.00	41.57	38.53	40.73	36.71	32.67	29.56	28.31	21.73	26.46	32.90	39.78	43.06
1000.00	39.30	37.24	40.46	36.52	32.54	29.50	28.27	21.53	26.05	31.53	37.30	40.15
1050.00	37.94	36.53	40.32	36.43	32.47	29.47	28.25	21.44	25.85	30.76	35.82	38.37
1100.00	37.15	36.14	40.25	36.38	32.44	29.46	28.24	21.40	25.76	30.34	34.96	37.30
1150.00	36.69	35.92	40.21	36.36	32.43	29.45	28.23	21.38	25.71	30.12	34.46	36.67
1200.00	36.42	35.80	40.19	36.35	32.42	29.45	28.23	21.37	25.68	29.99	34.17	36.29
1250.00	36.27	35.73	40.18	36.35	32.42	29.45	28.23	21.37	25.67	29.92	34.00	36.07
ELECTRON CONTENT =	2.06E 13	1.78E 13	1.32E 13	9.92E 12	8.79E 12	7.18E 12	6.33E 12	9.81E 12	1.58E 13	1.95E 13	2.26E 13	2.26E 13
PEAK ELECTRON DENSITY =	6.15E 05	5.69E 05	5.18E 05	3.92E 05	3.61E 05	2.89E 05	2.46E 05	3.49E 05	5.75E 05	6.28E 05	6.87E 05	6.64E 05
HEIGHT OF PEAK =	304.23	312.33	336.48	374.55	380.57	366.42	362.20	298.11	274.74	296.72	305.69	306.68
ESPROB PERCENT =	71.48	60.57	48.68	38.98	34.08	35.29	42.29	53.20	65.10	74.79	79.69	78.48
AVNES/1000. CM-3 =	157.36	121.82	90.57	66.14	49.27	39.52	36.07	104.83	248.33	243.47	223.35	192.95
SIGMA ES =	0.58	0.64	0.68	0.70	0.69	0.65	0.59	0.53	0.48	0.46	0.48	0.52

E and F1 Region

1. An analytic fit to the CIRA (1965) neutral atmospheric model is used for all production and loss calculations.

2. The F1 region is treated using a photo-equilibrium model with 3 ionic constituents and 62 ionizing radiation groups each of which varies with solar activity. Solar zenith angles are calculated based on altitude, location, and time.

F2 Region

3. The F2-layer uses theoretical models arranged to fit boundary conditions of the peak electron density, the height of the peak, and the electron density at 1000 km.

4. Values of the peak electron density are obtained using the C.C.I.R. (1967) Report 340 atlas of ionospheric characteristics.

5. Values of the height of the peak are obtained from a model based on reduced ionograms.

Sporadic E Region

6. The model is log-normal in electron density

$$P(N_m E_s > n) = 0.5P\left[1-\mathrm{erf}\left(\frac{\log\frac{n}{\bar{n}}}{\sqrt{2}\sigma}\right)\right]$$

where

P = the probability of observing blanketing sporadic E

$\bar{n}$ = the average peak electron density when sporadic E is observed

σ = the standard deviation of distribution.

The model assumes that the ion and neutral temperatures are equal and calculates the electron temperature. Details of the construction of this model have been given by Nisbet (1970a) and a series of tables of electron densities for this model have been given by Nisbet (1970b).

To give an idea of the agreement of the model with observations, observations are shown on the left of Figure 1 and predictions of the model are shown on the right. This is for a low solar activity. Figure 2 is another example. This time for a very high level of solar activity the model and observed ionosphere appear to behave very similarly, and the agreement in the F1 region is of the order of 20%.

1.2.4 The Mitra-Rowe Electron Density Model for the D Region

For the D region, the model developed by Mitra and Rowe (1972) was used. This is a middle latitude model, and the magnetic latitude for this model lies between 30 and 60 degrees.

It is a model which uses Lyman α, 1 - 8 Å X rays, 1027 - 1118 Å radiation, and galactic cosmic rays as the ionization sources.

The 10.7 cm solar flux is used to represent the low solar activity to moderate-high solar activity. Cosmic

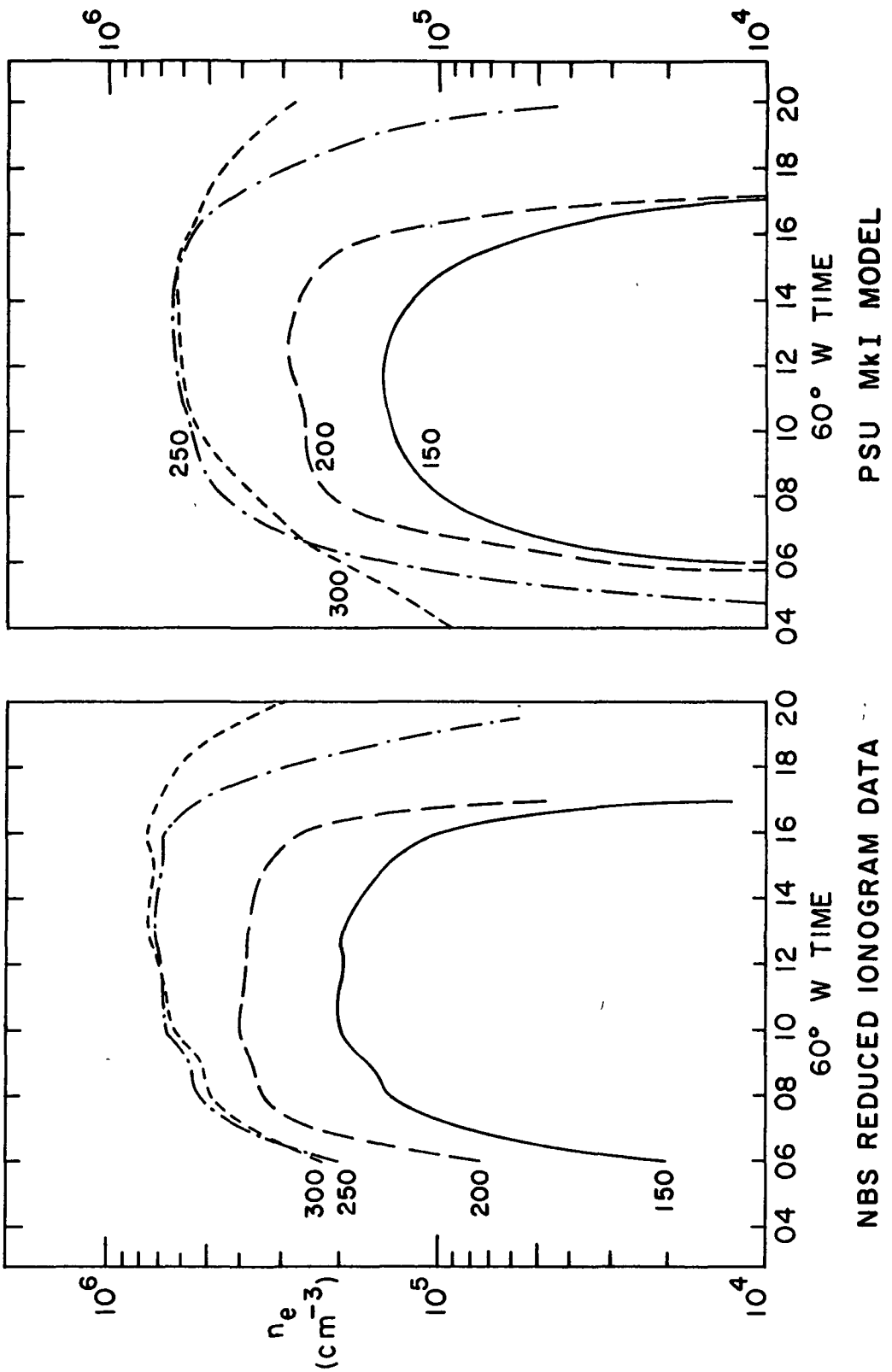

Figure 1 Electron Densities for St. Johns, Newfoundland, March 1961, $\bar{S}_{10.7}$ = 103

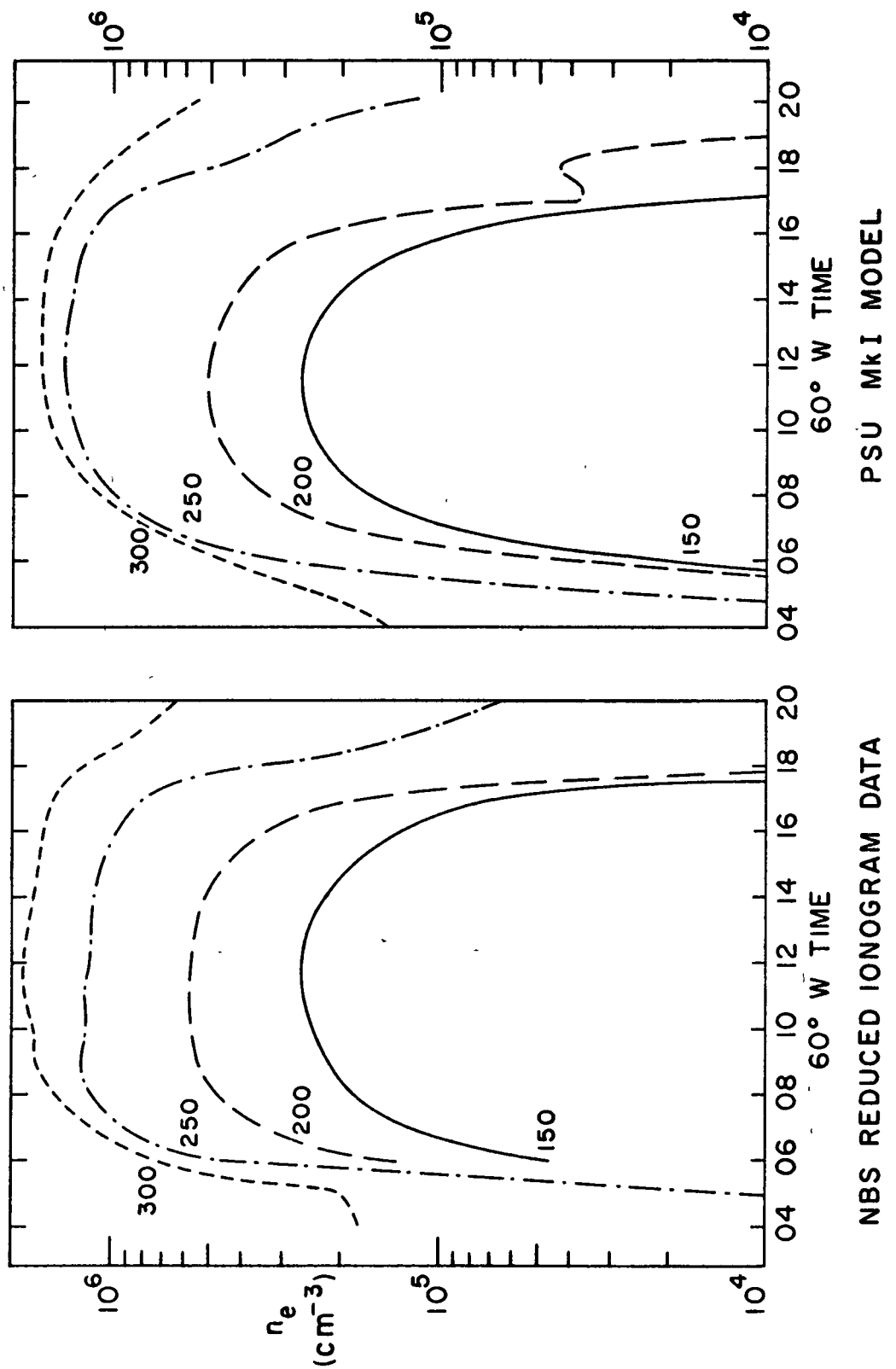

Figure 2 Electron Densities for St. Johns, Newfoundland, March 1959, $\bar{S}_{10.7}$ = 220

rays, 1 - 8 Å radiation, electron temperature, and the production of NO^+ and excited state O_2^+ are scaled with the phase of solar activity.

Six groups of ions are used to reproduce experimentally observed profiles of electron and ion densities. The ion chemistry of the D region was discussed in detail by Mitra and Rowe (1972). The simplified positive and negative ion chemistry used in the model is shown in Figure 3. This describes an ion chemical scheme consisting of a six-ion (four positive and two negative) model.

For major neutral constituents up to 90 km atmospheric model by Groves (1971) was used.

For minor neutrals, H_2O, O_3, and O were obtained from Bowman et al. (1970), and O_2 ($^1\Delta_g$) was obtained from Evans and Llewellgn (1970). CO_2 from Hays and Olivero (1970) and NO from Meira (1971) were also used in this model as were other minor neutral constituents.

Figure 4 shows the electron density profiles for three different solar zenith angles for April 1971. The solar activity of this month corresponded to $S_{10.7} = 140$. The model gives electron densities starting from 60 km.

1.2.5 The Collision Frequency Model

The neutral atmospheric model of Groves (1971) and the collision frequency calculations of Itikawa (1971) were combined to give the collision frequency profiles below 120 km. The Groves Model gives atmospheric temperature,

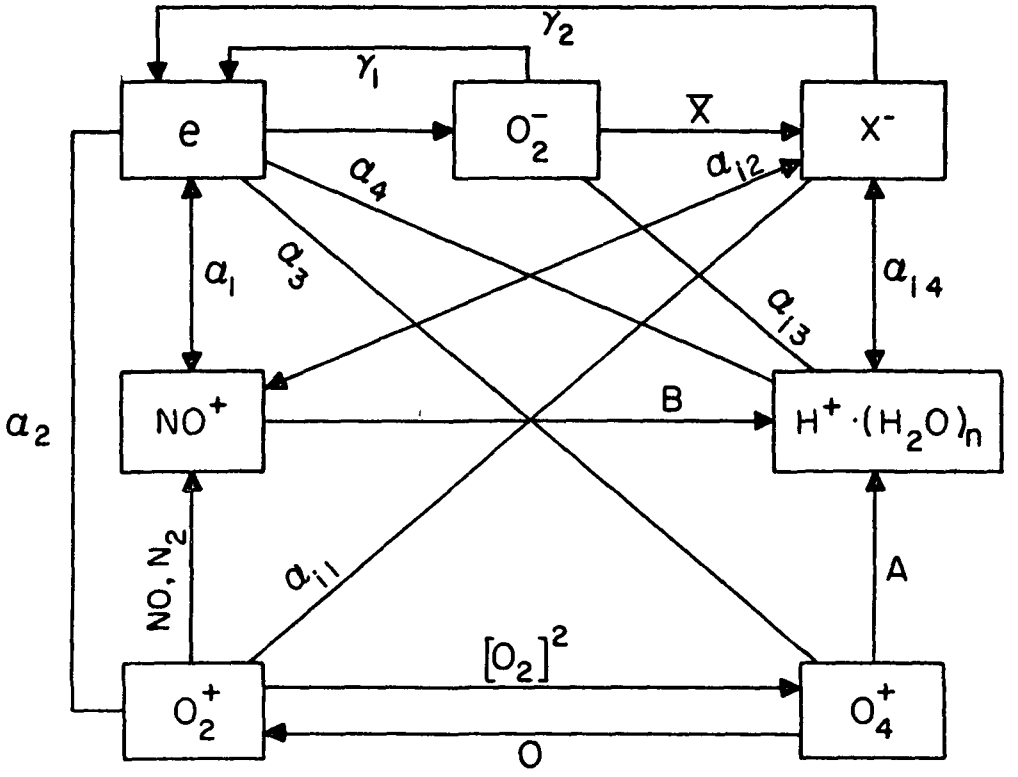

Figure 3 Six-Ion Model for D Region

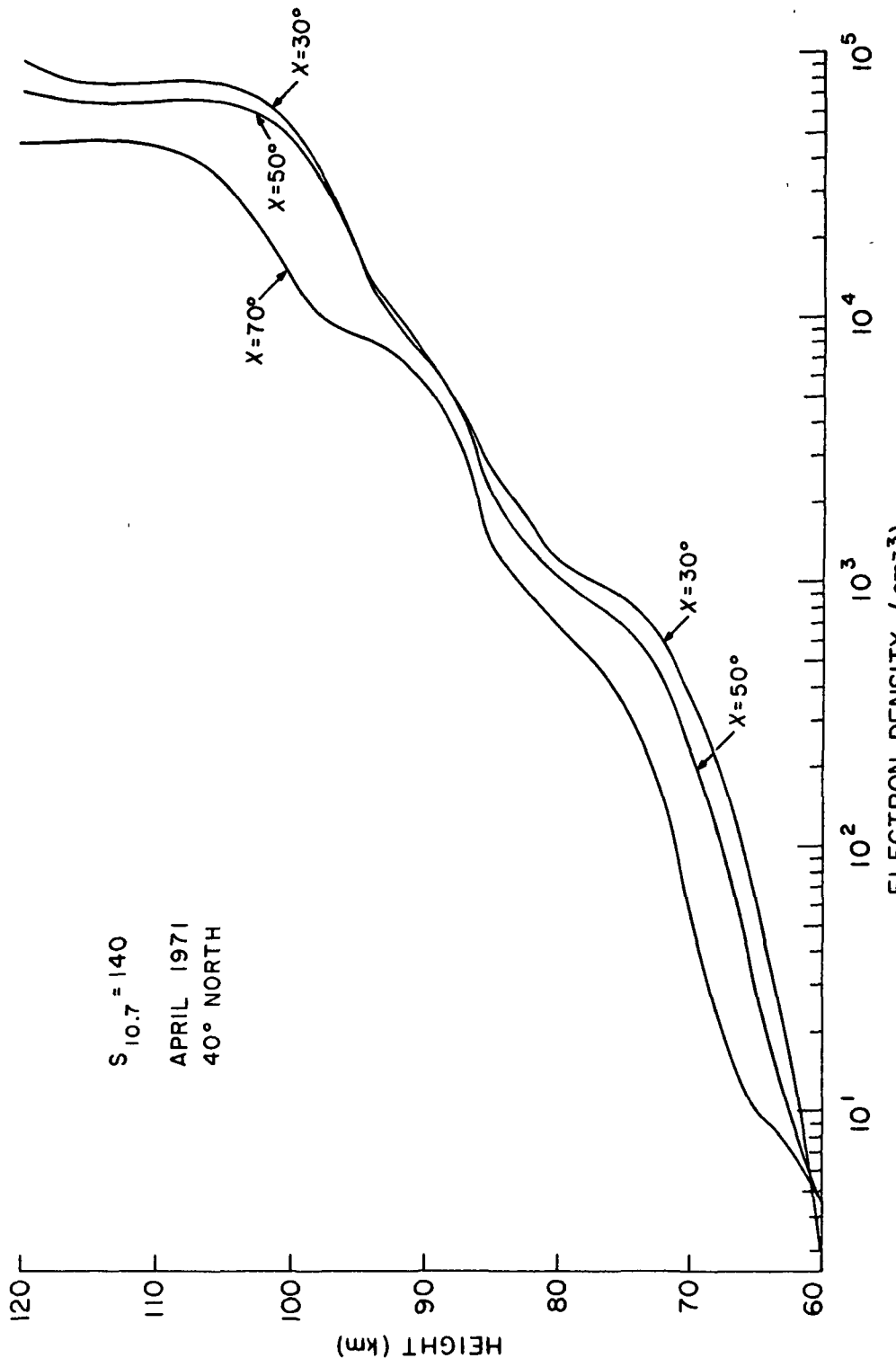

Figure 4 Electron Density Models Below 120 Km

pressure, and density for the first of each month and for 10° latitude intervals with values tabulated at 5 km intervals from 25 to 110 km.

Using the equation given by Jacchia (1970), the number densities of N_2, O_2, and O were deduced as follows.

$$n(N_2) = .7811 \frac{A\rho}{\bar{M}_o}$$

$$N(O) = 2A\rho \left(\frac{1}{\bar{M}} - \frac{1}{\bar{M}_o}\right)$$

$$n(O_2) = A\rho \left[\frac{1}{\bar{M}_o}(1+.21) - \frac{1}{\bar{M}}\right]$$

where

A = Avogadro's number = 6.02257×10^{-23} mole^{-1}

$\bar{M}_o$ = the sea-level mean molecular mass = 28.960

ρ = the density in g cm^{-3}

$\bar{M}$ = the mean molecular mass at each altitude

The variables ρ and $\bar{M}$ are also tabulated at 5-km intervals from 25 to 110 km in Groves' neutral atmospheric model.

Once the number densities of major neutrals were obtained, the collision calculations of Itikawa were employed to give the following equation for the mono-energetic collision frequency of electrons with neutrals.

$$\langle \nu_m \rangle^{en} = (1.292\times10^{-10}+2.135\times10^{-12}T-5.216\times10^{-17}T^2)\ n(O)$$

$$+ (3.923\times10^{-10}+8.600\times10^{-12}T-8.428\times10^{-16}T^2)\ n(N_2)$$

$$+ (7.936\times10^{-10}+4.292\times10^{-12}T-2.858\times10^{-16}T^2)\ n(O_2)$$

where

T = the absolute temperature of the electron.

The mono-energetic collision frequency of electrons with neutrals calculated in this way for middle latitude is shown in Figure 5. These calculations are compared with experimental observations and other theoretical expressions.

Figure 6 shows the seasonal and latitudinal variation of the collision frequency. At lower latitude the summer and winter profiles almost coincide. At higher latitudes the profiles for the two seasons differ appreciably.

Above 120 km the Penn State Mk 1 Model was employed to give both the electron-ion collision frequency and the electron-neutral collision frequency. The electron collision frequency with ions was obtained by assuming that electron, ion and neutral temperatures are equal. The collision frequency calculations of Itikawa were also used for the electron-ion collision frequency.

In Figure 7 the mono-energetic electron collision frequency with ions and neutrals is shown. Because the electron density changes are much larger than the neutral

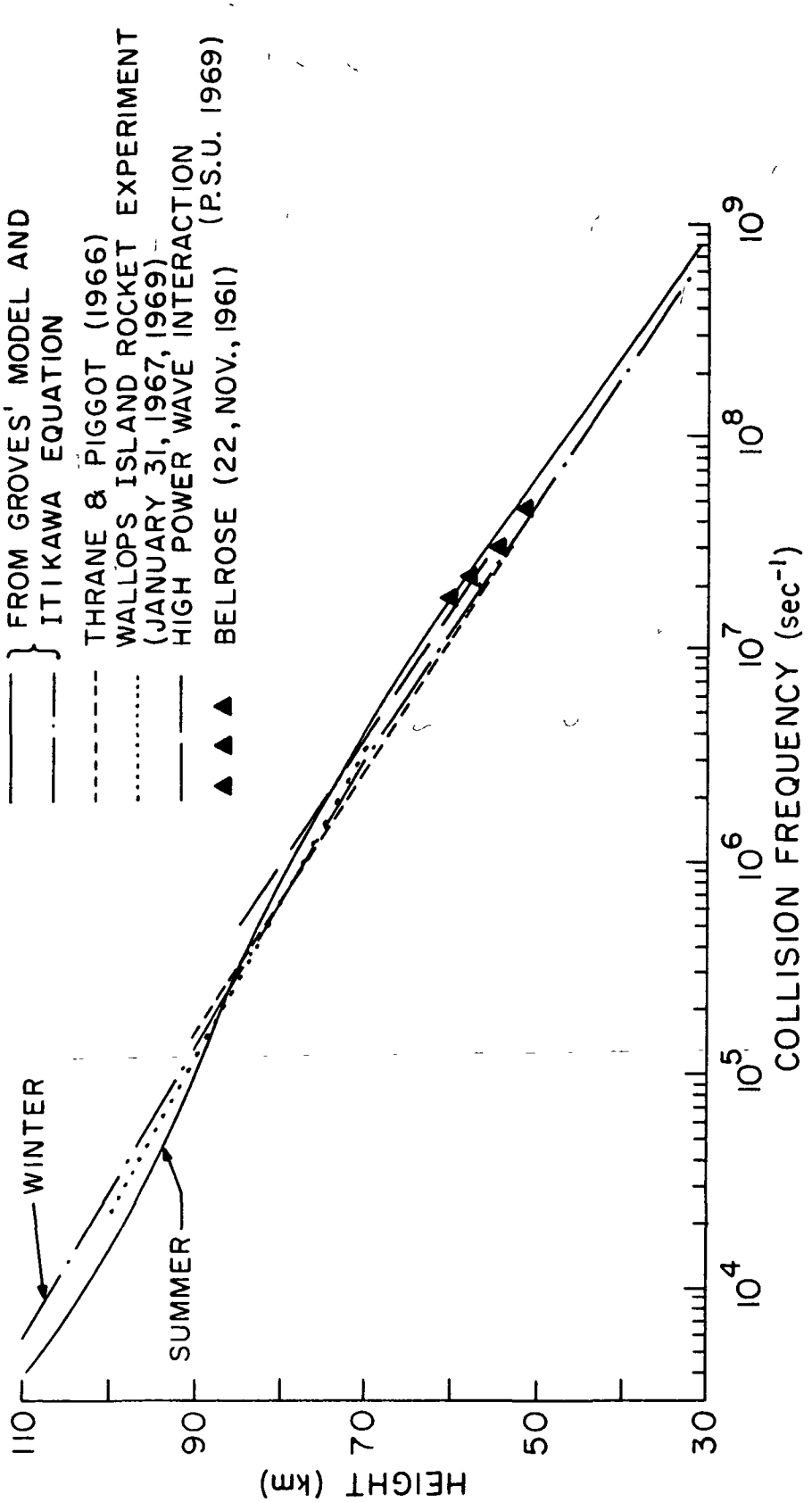

Figure 5 Neutral Collision Frequency Models

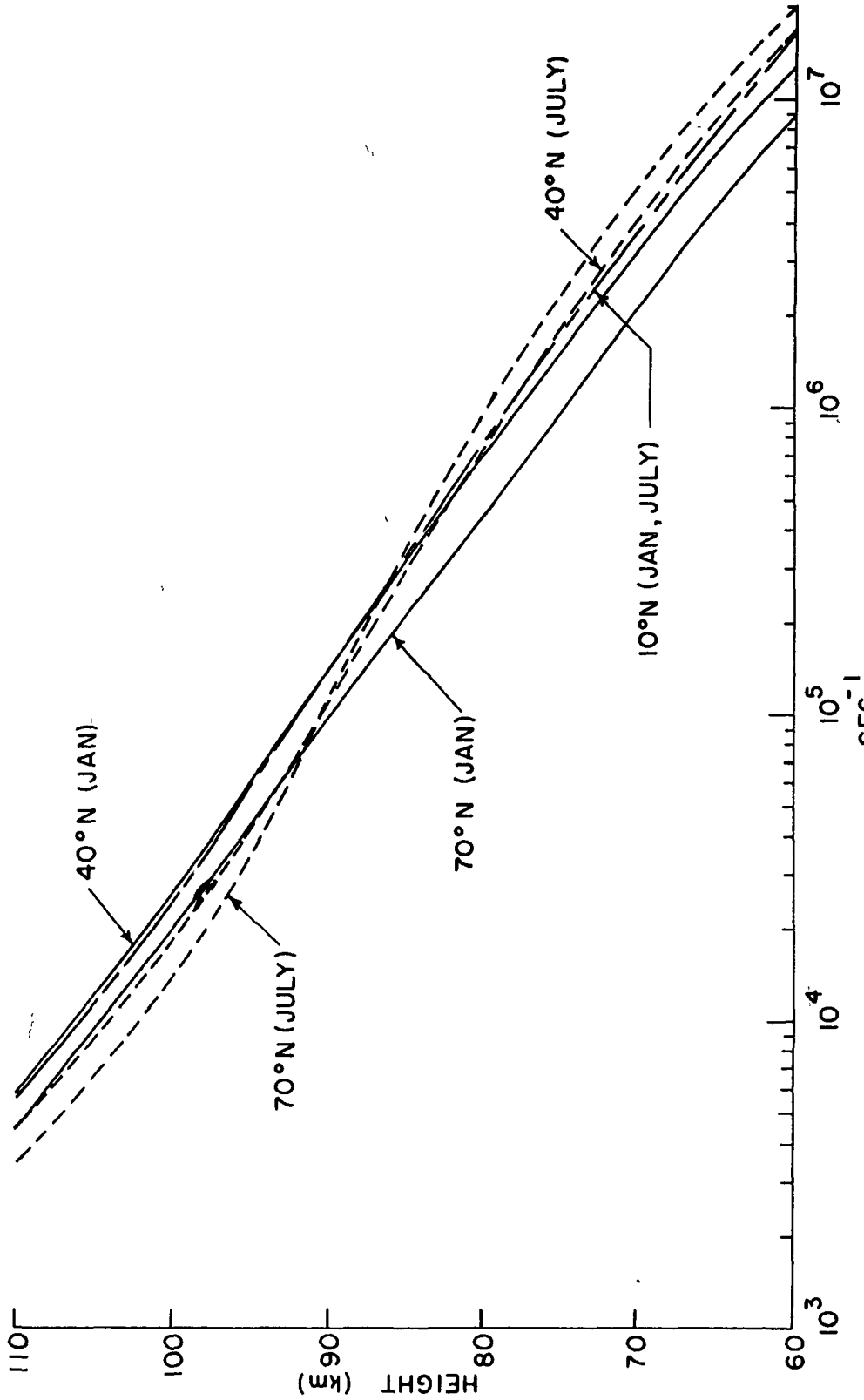

Figure 6 Seasonal and Latitudinal Variations of the Collision Frequency of Electrons with Neutral Particles

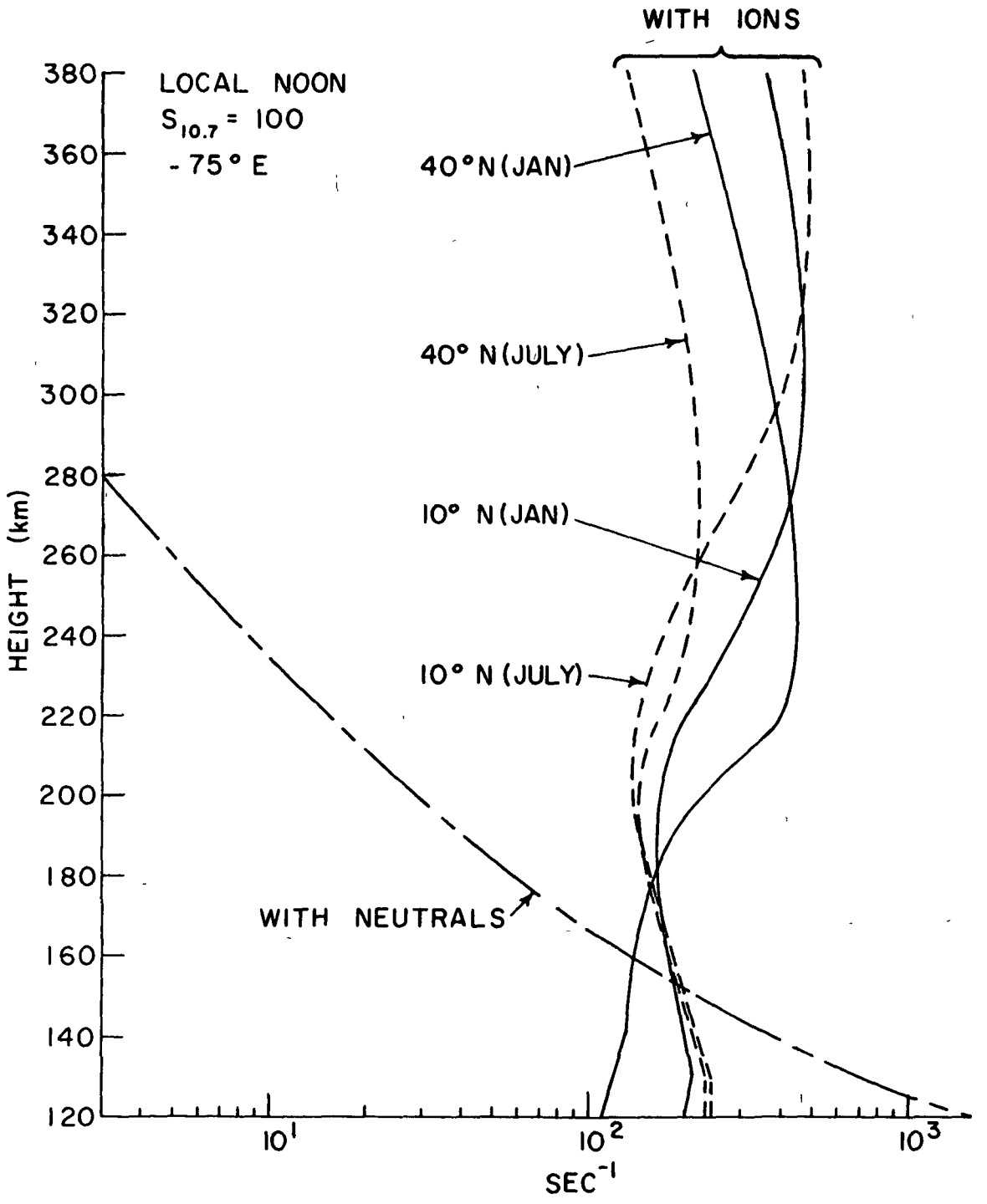

Figure 7 Seasonal and Latitudinal Variations of the Electron Collision Frequency with Ions and Neutrals Above 120 Km

density changes, the ion collision frequency varies by a much higher percentage. The Penn State Mk 1 Model allows the electron-ion collision frequency to be calculated for each model used.

1.2.6 The Earth's Magnetic Field Model

The earth's magnetic field is of primary importance in the ionospheric propagation of radio waves. It brings about a variety of phenomena in the radio wave propagation. Anisotropy in the medium arises from the gyration of moving electrons and ions in a magnetic field. The frequency of the gyration is called the gyromagnetic frequency or simply gyro frequency f_H.

When the plane-polarized wave is incident upon the ionosphere, it splits into two waves which are propagated independently. One is called the "ordinary wave", and the other is called the "extraordinary wave". Under this circumstance the refractive index is more complicated than that calculated when the effects of the magnetic field are not being taken into account. The real part of the refractive index can be greater or less than unity; and waves of frequency less than the electron plasma frequency can propagate in the medium.

For this work the magnetic field model described by Jensen and Cain (1962) was used. It is a series of coefficients for the spherical harmonic analysis of the magnetic field (Chapman and Bartels, 1962) as follows:

$$X = \sum_{n=1}^{6} \sum_{m=0}^{n} X_n^m \left[g_n^m \cos m\theta + h_n^m \sin m\theta\right] R^{n+2}$$

$$Y = \sum_{n=1}^{6} \sum_{m=0}^{n} Y_n^m \left[g_n^m \sin m\theta - h_n^m \cos m\theta\right] R^{n+2}$$

$$Z = \sum_{n=1}^{6} \sum_{m=0}^{n} Z_n^m \left[g_n^m \cos m\theta + h_n^m \sin m\theta\right] R^{n+2}$$

where

$$X_n^m = \frac{d}{d\phi} P_{n,m} (\cos \phi)$$

$$Y_n^m = \frac{m P_{n,m} (\cos \phi)}{\sin \phi}$$

$$Z_n^m = -(n+1)\, p_{n,m} (\cos \phi)$$

$$R = \frac{a}{a + h}$$

a = the radius of the earth

h = height above sea level

Here the function $P_{n,m} (\cos \phi)$ is a multiple of the associated Legendre function defined as follows:

$$P_{n,m} (\cos \phi) = \sin^m \phi \left[\cos^{n-m} \phi - \frac{(n-m)(n-m-1)}{2(2n-1)} \cos^{n-m-2} \phi + \frac{(n-m)(n-m-1)(n-m-2)(n-m-3)}{(2)(4)(2n-1)(2n-3)} \cos^{n-m-4} \phi - \ldots\right]$$

X, Y, and Z are, respectively, the north, east, and vertical (down) components of the magnetic field vector F in Figure 8. The Greek letters θ and ϕ are the longitude and the colatitude.

The coefficient g_n^m and h_n^m used in this program are those given by Jensen and Cain (1962).

Having defined X, Y, and Z, the dip angle, the magnetic flux density B, and the gyro frequency f_H can be computed.

$$I = \tan^{-1}\left(\frac{-Z}{\sqrt{X^2+Y^2}}\right) \qquad I \text{ in radians}$$

$$B = \sqrt{X^2+Y^2+Z^2} \qquad B \text{ in the unit of } 10^{-4} \text{wb/m}^2$$

$$f_H = 2.8\ B \qquad f_H \text{ in MHz}$$

One of the computer outputs is shown in Table 3 for an altitude of 300 km. This program provides the quantities I, B, and f_H for any longitude, latitude, and altitude.

1.2.7 Techniques for Measuring Ionospheric Absorption

There are several standard techniques for the measurement of ionospheric absorption of radio waves. Among these the A1, A2, and A3 methods are principal techniques for measuring ionospheric absorption.

A1 Method This is also known as the pulse-reflection method and consists of the measurement of the

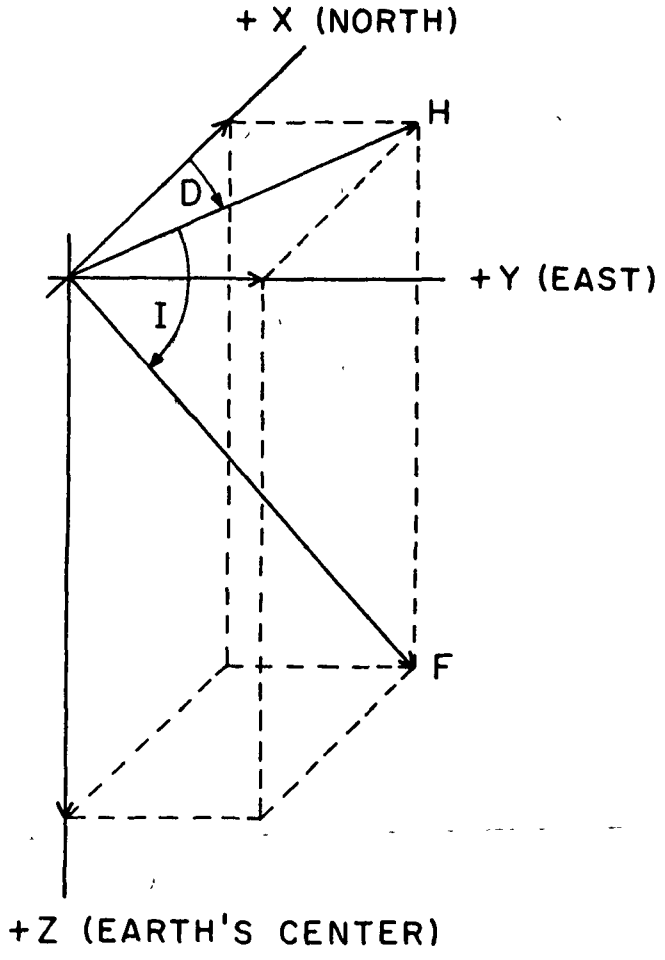

Figure 8 Geomagnetic Convention for Describing the Elements of a Magnetic Vector: X, Y, Z, H, D, I, and F or B

Table 3: One of the Computer Outputs Showing the Magnetic Field Variables for a Longitude of -80° and an Altitude of 300 km

Longitude	Latitude	SINX	Dip Angle	Dip Latitude	B	FH
-80.00	-90.00	-1.000000	-75.598541	-62.816528	0.517126	1.447952
-80.00	-80.00	-0.947749	-70.931824	-55.343262	0.486239	1.361468
-80.00	-70.00	-0.888492	-64.877548	-46.837723	0.439631	1.230966
-80.00	-60.00	-0.820031	-58.049713	-38.719727	0.384521	1.076658
-80.00	-50.00	-0.740834	-50.665222	-31.388412	0.330678	0.925899
-80.00	-40.00	-0.643541	-42.162933	-24.360229	0.286701	0.802762
-80.00	-30.00	-0.502964	-31.028229	-16.739487	0.257611	0.721311
-80.00	-20.00	-0.273408	-15.786946	- 8.046170	0.246290	0.689613
-80.00	-10.00	0.052749	3.003417	1.502741	0.256301	0.717644
-80.00	0.0	0.361997	22.249878	11.560610	0.289548	0.810734
-80.00	10.00	0.565525	38.988602	22.034515	0.340860	0.954408
-80.00	20.00	0.686140	52.385818	32.980804	0.399186	1.117719
-80.00	30.00	0.762991	62.936249	44.380707	0.453064	1.268579
-80.00	40.00	0.818096	71.338745	55.962799	0.493900	1.382919
-80.00	50.00	0.861826	78.054077	67.064911	0.516940	1.447432
-80.00	60.00	0.899036	83.183609	76.554932	0.521892	1.461298
-80.00	70.00	0.932361	86.415436	82.868704	0.513644	1.438201
-80.00	80.00	0.964654	87.401657	84.813950	0.501700	1.404758
-80.00	90.00	1.000000	87.137405	84.289063	0.496368	1.389828

amplitudes of the pulse echoes reflected from the E region of the ionosphere. The virtual height for all measurements generally ranges from 95 km to around 115 km depending on the frequency used and the ionospheric conditions such as time, season, and solar activities. The absorption measured in decibels, L, is given by (Mitra, 1970).

$$L = -20 \log \frac{I_d}{I_n} - 20 \log \frac{h_d'}{h_n'} \text{ (db)}$$

where

I_d = daytime amplitude

I_n = nighttime amplitude

h_d' = daytime virtual height

h_n' = nighttime virtual height

An excellent summary of this technique has been given in the IQSY Instruction Manual No. 4 (Piggot et al., 1963).

As in the other techniques the question of separating absorption contributions from the D- and E-layers has been a problem. A brief discussion of this problem was given by Mitra (1970).

Gnanalingam (1972) gave figures for the D- and E-region absorptions for the study of equatorial ionospheric absorption at Colombo, Ceylon. A substantial part of the absorption was found to take place near the reflection level. From his analytical method developed for the purpose of resolving absorption data, the percentage of absorption below 90 km and below 85 km was shown.

For both cases, the E region absorption was dominant. The percentage of absorption below 85 km was shown to be 45%, 35%, 32%, 29%, 24% for the frequencies 1.33, 2.0, 2.2, 2.6, and 3.2 MHz, respectively. As the frequency increases the percentage of absorption below 85 km decreases. The variation of absorption with solar zenith angle, season, and solar activity was also discussed.

A2 Method This is also called the cosmic radio noise method or riometer method. This technique was first introduced by Mitra and Shain (1953). The principle is that absorption is estimated by comparing the noise power received with the noise power that would have been received in the absence of the ionosphere at the same sidereal time. The absorption is estimated from the expression (Mitra, 1970).

$$L = 10 \log_{10}(P_o/P) \quad \text{db}$$

where

P = the signal power received

P_o = the signal power that would have been received in the absence of the ionosphere at the same sidereal time.

Details can be found in the IQSY Instruction Manual No. 4. The choice of the frequency is such that the riometer is of use on frequencies above the F-layer critical frequency

only. A typical frequency, used in high latitudes to measure polar cap absorption, is about 30 MHz.

From the cosmic Radio Noise measurements Saha and Venkatachari (1970) discussed the results of the measurements of the collision frequency and the electron temperature. The temperature values were significantly lower than those obtained by either incoherent scatter techniques or by rocket probe methods.

By calculating the absorption which a given riometer system would be expected to measure, Heisler and Hower (1970) discussed the interpretation of riometer measurements. By making a comparison between calculated and measured absorption, they concluded that nighttime absorption reported by many authors was only an apparent absorption arising from errors in setting the level of the quiet-day curve.

A3 Method This is the technique by which the absorption for the oblique radio wave path is commonly measured, usually at short distances. Recommended frequencies and distances for middle latitudes are 2 - 3 MHz and 100 - 400 km (Mitra, 1970).

In this method a continuous-wave transmitter is used and the receiver output is registered on a pen recorder. The antenna is designed to select the ordinary component, since the absorption is smaller for the ordinary than for the extra-ordinary.

Basically absorption by this technique is obtained

by comparing the daytime field strength with that of nighttime, since nighttime observations are used for calibration.

The absorption reduced to vertical incidence ($\perp$) for frequency f_Λ (used at oblique incidence), $L_\perp (f_\Lambda, 0)$, is given by (Schwentek, 1966)

$$L_\perp (f_\Lambda, 0) = - \cos \alpha L_\Lambda (f_\Lambda, \alpha)$$

$$= - \cos \alpha \; 20 \log \frac{E_d \cdot \ell'_d}{E_n \cdot \ell'_n}$$

where

α = the angle of incidence

E_d = daytime field strength

E_n = nighttime field strength

ℓ'_d = daytime half path length

ℓ'_n = nighttime half path length

For the determination of the daytime ionospheric absorption, calibration was made depending on where the nighttime reflection occurs. Schwentek (1966) showed that ℓ'_d/ℓ'_n is very close to unity and may usually be neglected, if calibration is possible using a sporadic E layer at night as a reflector. If the nighttime reflection is from the F region, calibration was made by multiplying the recorded field strength, E_n (true nighttime field strength), by $\ell'(F)/\ell'(E)$ and by a factor determined by the transmitting and receiving aerial polar diagrams for the direction involved.

Extensive studies with the A3 technique over a long period of time have been made in Germany (Schwentek, 1971) to determine the D region absorption. The method also has been used for the study of anomalous absorption in winter in middle latitudes.

Besides the A1, A2, and A3 methods, there are other techniques called the f_{min} method and the sweep-frequency method.

A critical examination of the techniques which have been used for measuring ionospheric absorption was made by Mitra (1970) in the special issue devoted to contributions from the Working Group on Electromagentic Probing of the Upper Atmosphere set up by the URSI. Comparison of different absorption techniques and their relative advantages and disadvantages were made in this issue and in the text of Davies (1969).

1.3 Specific Statement of the Problem

The specific problems carried out in this work are outlined below.

1.3.1. To develop a general theoretical approach to the radio wave propagation prediction techniques by combining the theoretical ionospheric model with the ray tracing program.

1.3.2 To compare some oblique incidence ionospheric

soundings with the prediction of the propagation conditions for an ionospheric model.

1.3.3 To compare the prediction of radio wave propagation using an ionospheric model with current prediction techniques for high frequency radio wave propagation for ground to ground paths.

1.3.4 To compare the predicted satellite to ground propagation conditions with observations.

1.3.5 To predict the path losses of high frequency radio waves and the contribution of absorption and spatial loss.

CHAPTER II

METHOD OF CALCULATION

2.1 Coupling of the Ionospheric and Neutral Atmospheric Models

In this work two ionospheric models are used. One is the Penn State Mk 1 Ionospheric Model representing the region above 120 km, the other is the Mitra-Rowe Model for the region below 120 km. Both models use different neutral atmospheric models. The Penn State Mk 1 Model uses an analytic fit to the CIRA (1965) neutral model; the Mitra-Rowe Model uses Groves' seasonal and latitudinal atmospheric model and extends it to 120 km by extrapolation.

In order to give the continuous gradient of electron density and collision frequency profiles at the boundary, the boundary conditions such as neutral constituents and temperature must be matched at 120 km.

The determination of boundary values for neutral constituents and temperature has been a problem for many years, and considerable controversy still exists (Mitra, 1972).

The following attempt was made to make the boundary values for two models continuous in both electron densities and collision frequencies above and below 120 km. After obtaining the profiles for electron density and collision frequency from each model, a modification was made by hand to make the profile smooth at the boundary. For most cases

two models showed a slight difference due to the incompatibility of the two International Reference Atmospheres.

The parameters needed for the ray tracing are the phase refractive index, the wave normal direction, the derivative of position and wave normal direction with respect to group path, and the derivatives of refractive index with respect to position and the wave normal direction. These quantities are supplied from the neutral atmospheric model, the electron density model and the spherical harmonic expansion of the earth's magnetic field which is an integral part of the Penn State Mk 1 Ionospheric Model. Figure 9 shows how the ionospheric model couples with the neutral atmospheric model to calculate the ray path using the ray tracing program.

2.2 Technique for Developing and Interpolating the Ionospheric Models and Magnetic Field Models

Once the propagation path has been located geographically, as shown in Figure 39 in Appendix 1, profiles of electron density have to be developed along the path. In evaluating the ionospheric parameters, some of the prediction techniques use several control points (reflection areas) such as the midpoint of the path, E-layer control point, and F2-layer control point. Since the characteristics of the ionosphere at the point of reflection affect the MUF, that point is called a "control point".

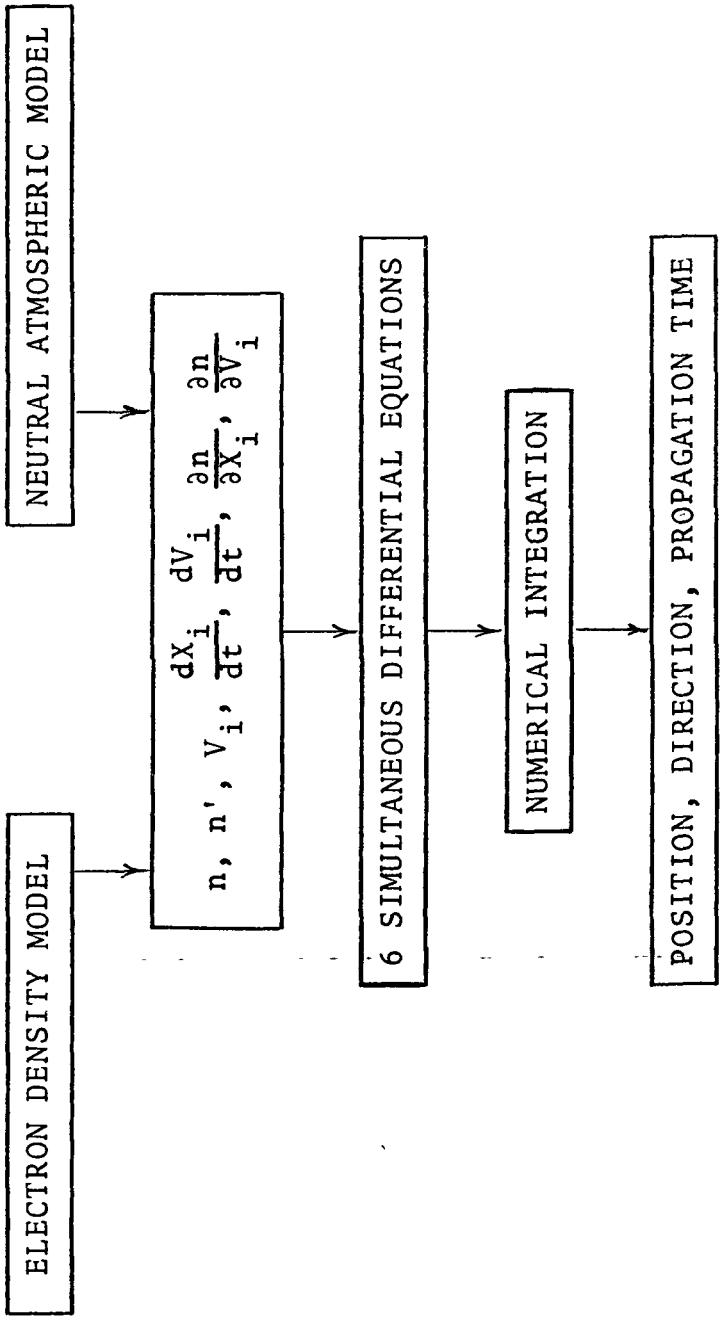

Figure 9 Schematic Diagram Showing the Coupling of the Models With the Ray Tracing Program

When the ionospheric irregularities (such as tilts that cause off-path and asymmetrical path) exist, transmission along the great circle may not be possible depending on the direction of tilts. The geomagnetic field also can cause the deviation of the path from the great circle path depending on the direction of the field.

Under these circumstances, it is necessary to obtain the electron density profiles all over the area involved in the transmission.

Taking these effects into consideration, the grid of the electron density profiles between the transmitter and the receiver was made and shown in Appendix 1.

The grid of the electron density profiles forms a three dimensional matrix, the element of which represents the electron density for a given longitude, latitude, and altitude. The interval between columns representing longitudes and the interval between rows representing latitudes can be chosen depending on the path length.

This is easily done by obtaining the electron density profiles for these longitudes and latitudes for a given day number, time (universal time), and solar activity expressed in 10.7 cm solar flux.

Once electron density profiles at every intersection of the column and the row are obtained, the vertical and the horizontal gradient of the electron density at any point along the ray path can be evaluated simply by using linear interpolation as follows. The gradient of the normalized

electron density X in the direction of r, θ, and ϕ are

$$\frac{\partial n}{\partial z} = \frac{n(I+1,J,K) - n(I,J,K)}{z(I+1) - z(I)}$$

$$\frac{\partial n}{\partial \lambda} = \frac{n(I,J,K+1) - n(I,J,K)}{\lambda(K+1) - \lambda(K)}$$

$$\frac{\partial n}{\partial \psi} = \frac{n(I,J+1,K) - n(I,J,K)}{\psi(J+1) - \psi(J)}$$

$$n = n(I,J,K) + \frac{\partial n}{\partial z} \cdot \Delta z + \frac{\partial n}{\partial \lambda} \cdot \Delta \lambda + \frac{\partial n}{\partial \psi} \cdot \Delta \psi$$

where

$n(I,J,K)$ = the electron density in cm^{-3} at Ith altitude, Jth longitude, and Kth latitude.

z, λ, and ψ = altitude, latitude (north), and longitude (east). Latitude and longitude are both in radians.

Thus,

$$X = K \cdot n/(f^2)$$

$$\frac{\partial X}{\partial r} = K \cdot \frac{\partial n}{\partial z}/(f^2)$$

$$\frac{\partial X}{\partial \theta} = - K \cdot \frac{\partial n}{\partial \lambda}/(f^2)$$

$$\frac{\partial X}{\partial \phi} = K \cdot \frac{\partial n}{\partial \psi}/(f^2)$$

where

X = normalized electron density

f = wave frequency in MHz

$K = 80.5 \times 10^{-6}$

r, θ, and ϕ = spherical polar coordinates

In a similar way, the grid of the earth's magnetic field elements is made.

From the magnetic field elements Z, X, and Y, as shown in Figure 8, the $f_{H,r}$, $f_{H,\theta}$, and $f_{H,\phi}$ which are r, θ, ϕ components of the gyro-frequency f_H, respectively are obtained with the proper signs by taking into consideration the use of spherical polar coordinates. Then the gradients of the normalized magnetic field vector Y (Y here is not the eastward magnetic field vector) and its components are obtained as follows:

$$\frac{\partial Y_r}{\partial r} = \frac{1}{f} \cdot \frac{f_{H,r}(I+1,J,K) - f_{H,r}(I,J,K)}{z(I+1) - z(I)}$$

$$\frac{\partial Y_r}{\partial \theta} = -\frac{1}{f} \cdot \frac{f_{H,r}(I,J,K+1) - f_{H,r}(I,J,K)}{\lambda(K+1) - \lambda(K)}$$

$$\frac{\partial Y_r}{\partial \phi} = \frac{1}{f} \cdot \frac{f_{H,r}(I,J+1,K) - f_{H,r}(I,J,K)}{\psi(J+1) - \psi(J)}$$

$$Y_r = \frac{f_{H,r}(I,J,K)}{f} + \frac{\partial Y_r}{\partial r} \cdot \Delta z + \left(-\frac{\partial Y_r}{\partial \theta}\right) \cdot \Delta\lambda + \frac{\partial Y_r}{\partial \phi} \cdot \Delta\psi$$

$$\frac{\partial Y_\theta}{\partial r}, \frac{\partial Y_\theta}{\partial \theta}, \frac{\partial Y_\theta}{\partial \phi}, Y_\theta, \frac{\partial Y_\phi}{\partial r}, \frac{\partial Y_\phi}{\partial \theta}, \frac{\partial Y_\phi}{\partial \phi}, Y_\phi$$

are obtained in the same way. Thus Y and its gradients are obtained as follows

$$Y = \sqrt{Y_r^2 + Y_\theta^2 + Y_\phi^2}$$

$$\frac{\partial Y}{\partial r} = \frac{1}{Y}\left(Y_r \cdot \frac{\partial Y_r}{\partial r} + Y_\theta \cdot \frac{\partial Y_\theta}{\partial r} + Y_\phi \cdot \frac{\partial Y_\phi}{\partial r}\right)$$

$$\frac{\partial Y}{\partial \theta} = \frac{1}{Y}\left(Y_r \cdot \frac{\partial Y_r}{\partial \theta} + Y_\theta \cdot \frac{\partial Y_\theta}{\partial \theta} + Y_\phi \cdot \frac{\partial Y_\phi}{\partial \theta}\right)$$

$$\frac{\partial Y}{\partial \phi} = \frac{1}{Y}\left(Y_r \cdot \frac{\partial Y_r}{\partial \phi} + Y_\theta \cdot \frac{\partial Y_\theta}{\partial \phi} + Y_\phi \cdot \frac{\partial Y_\phi}{\partial \phi}\right)$$

These are the quantities which must be supplied to the ray tracing program.

For the collision frequency model the gradient can be obtained in the same way as the gradient of the electron density was obtained.

For the constant collision frequency and electron density profiles, the program provides the way to calculate the gradients using the cubic interpolation and extrapolation.

2.3 Initial Information Needed to Run the Program

Once the ionospheric model, the neutral atmospheric model, and the magnetic field model are supplied to the ray tracing program, one can start to run the program to calculate the ray path. First the frequency, the elevation angle, and the azimuth angle must be adjusted for the

desired transmission for a given path. To get the proper initial guesses to run the program, the following are considered.

(1) The variation of the critical frequency along the great circle path. This will allow one to estimate the frequency.

(2) The variation of the height of peak along the great circle path. This will enable one to see the possible asymmetry of the ray path and the reflection height.

(3) The direction between the earth's magnetic field and the direction of the propagation to see the possible lateral deviation or asymmetry of the ray path.

With these general ideas, the frequency can be approximately chosen using the "secant law".

$$f_{ob} = f_v \sec \phi_o$$

where

f_{ob} = frequency of the wave incident obliquely on a flat layer

f_v = the equivalent vertical frequency

ϕ_o = the angle of incidence

By incorporating the critical frequency of the layer, the height of the peak, and the given path length, a crude approximation can be made to calculate the angle of

incidence and the maximum usable frequency. If virtual height can be used instead of the height of the peak, more accurate values can be obtained.

For long distance propagation, the earth's curvature must be taken into account. In this case Davies (1969) gave the following formulas.

$$f_{max} = f_c \left\{ \frac{4[h_o+(D^2/8a)]^2+D^2}{4[h_o+(D^2/8a)]^2} \right\}$$

$$\phi_o = \tan^{-1} \left\{ \frac{\sin(D/2a)}{1+(h_o/a)-\cos(D/2a)} \right\}$$

where

a = the earth's radius, 6370 km

h_o = height of the reflection from a thin layer

D = the distance (the ground range)

By using the height of the peak of the F2-layer for h_o, ϕ_o and f_{max} can be easily calculated.

The ITS Ionospheric Prediction method was used to provide the initial estimates. For a given path less than 4000 km, f_c and f_{max} can be found from the prediction map, and thus h_o and ϕ_o can be approximated using the formula given by Davies. For a distance greater than 4000 km, path MUF and path FOT can be predicted based on the two control point method.

With this information, the ray tracting program can be run using trial and error correction until the desired transmission paths are obtained.

CHAPTER III

RESULTS OF CALCULATION

3.1 Comparison of Satellite Propagation Measurements with Predictions

One of the most basic propagation measurements is the electron content from observation of the Faraday rotation or the differential Doppler shifts for satellite to ground propagation. These measurements have been described by Bowhill (1958, 1962), Ross (1965), Ross et al. (1968), da Rosa and Garriot (1969), and Garriot et al. (1970).

Such measurements have a very distinct relevance to the errors in navigational satellite systems, the errors in angular position of radio stars, and similar calculations when radio waves are propagated through the ionosphere at frequencies considerably in excess of the peak plasma frequency of the F2-layer.

A knowledge of the electron content for a given path allows a correction to be made for such errors. As shown in Table 2 the Penn State Mk 1 Ionospheric Model also provides the value for the electron content for a given longitude, latitude, time, day number, and solar activity. In this section the prediction by model calculation is made and compared with the satellite propagation measurements.

3.1.1 The Diurnal Variation of Electron Content

Figures 10 and 11 show the prediction of the diurnal

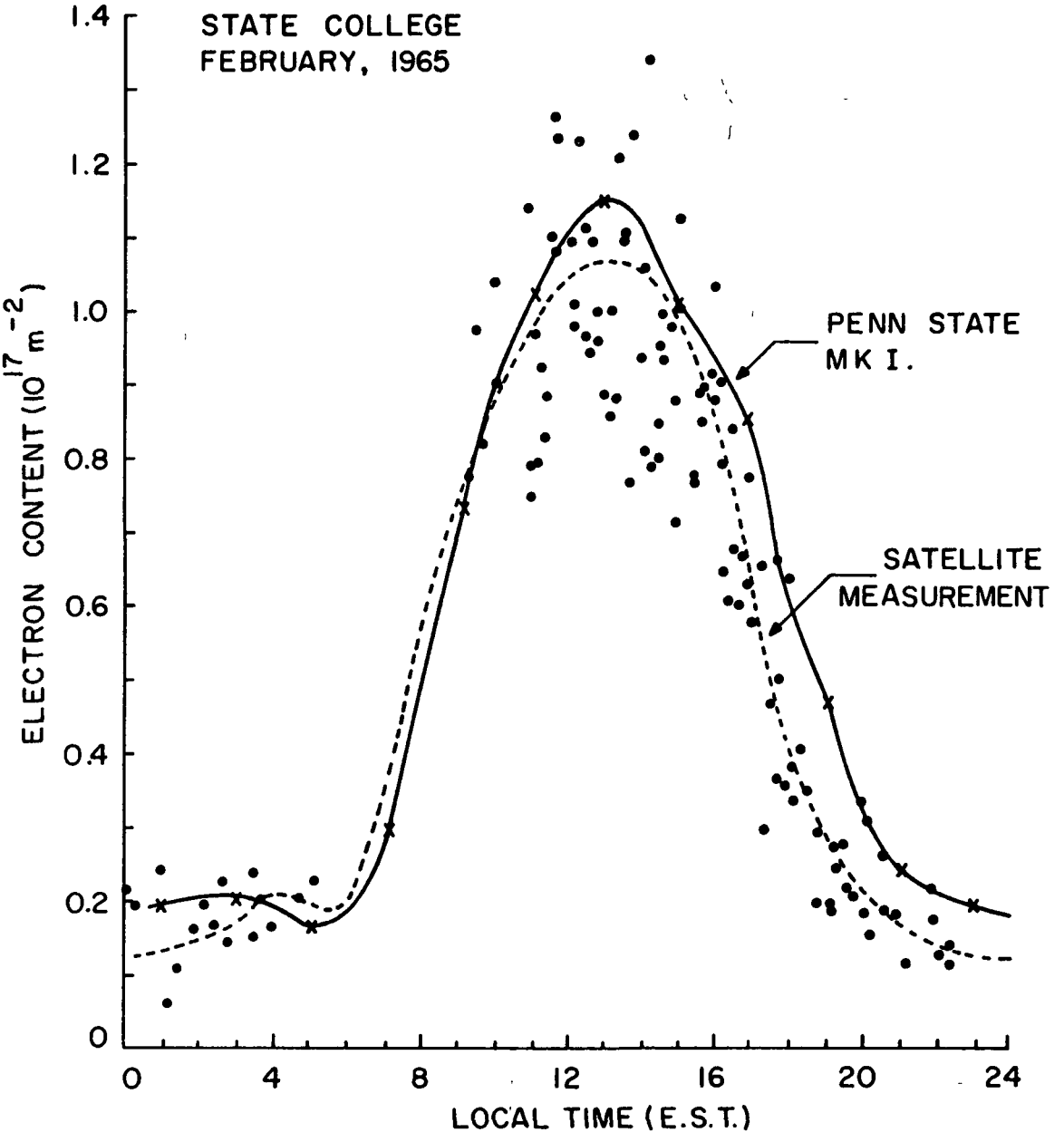

Figure 10 Diurnal Variation of Electron Content

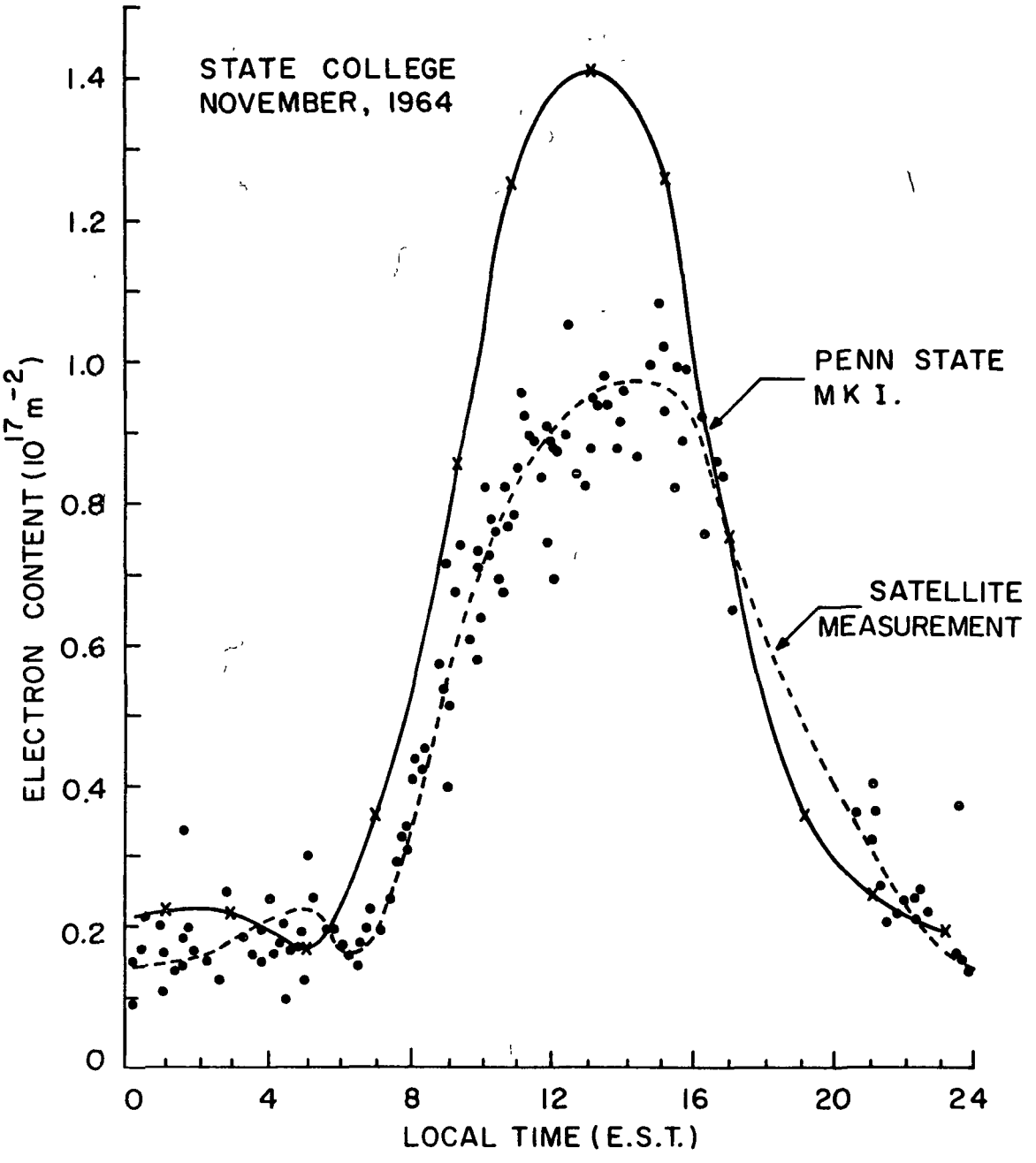

Figure 11 Diurnal Variation of Electron Content

variation of the electron content at University Park, Pennsylvania. Total electron content has been calculated for 285 passes of the S-66 satellite observed at University Park, Pennsylvania (40.8°N, 78°W) between October 24, 1964 and March 16, 1965. A detailed analysis of these results has been given by Solomon (1965).

The dotted line in the figure represents the average of this measurement. The Faraday rotation technique was used to calculate the content. The solid line is obtained from the Penn State Mk 1 Model calculations. In February 1964 and November 1964 the monthly mean value of 10.7 cm solar flux which was used for this calculation was approximately equal to 73. The day to day variations in 10.7 cm solar flux were relatively small for this period.

In Figure 10, as expected, both the prediction and the observation show that there seems to be a steady average increase in total electron content from about sun rise through the day to midafternoon. From sun rise through early afternoon in November 1964 the model calculation shows higher values than those obtained by satellite measurement as shown in Figure 11.

Figure 12 shows another comparison with the measurements made at Huancayo, Peru (12.05°S, - 75.35°E), of the polarization rotation of the 54 MHz signals from the Satellite 1961 Omicron 1 from September 1961 to February 1963 (Ross, 1966). This satellite was launched in a high-inclination orbit, approximately circular at about 1000 km

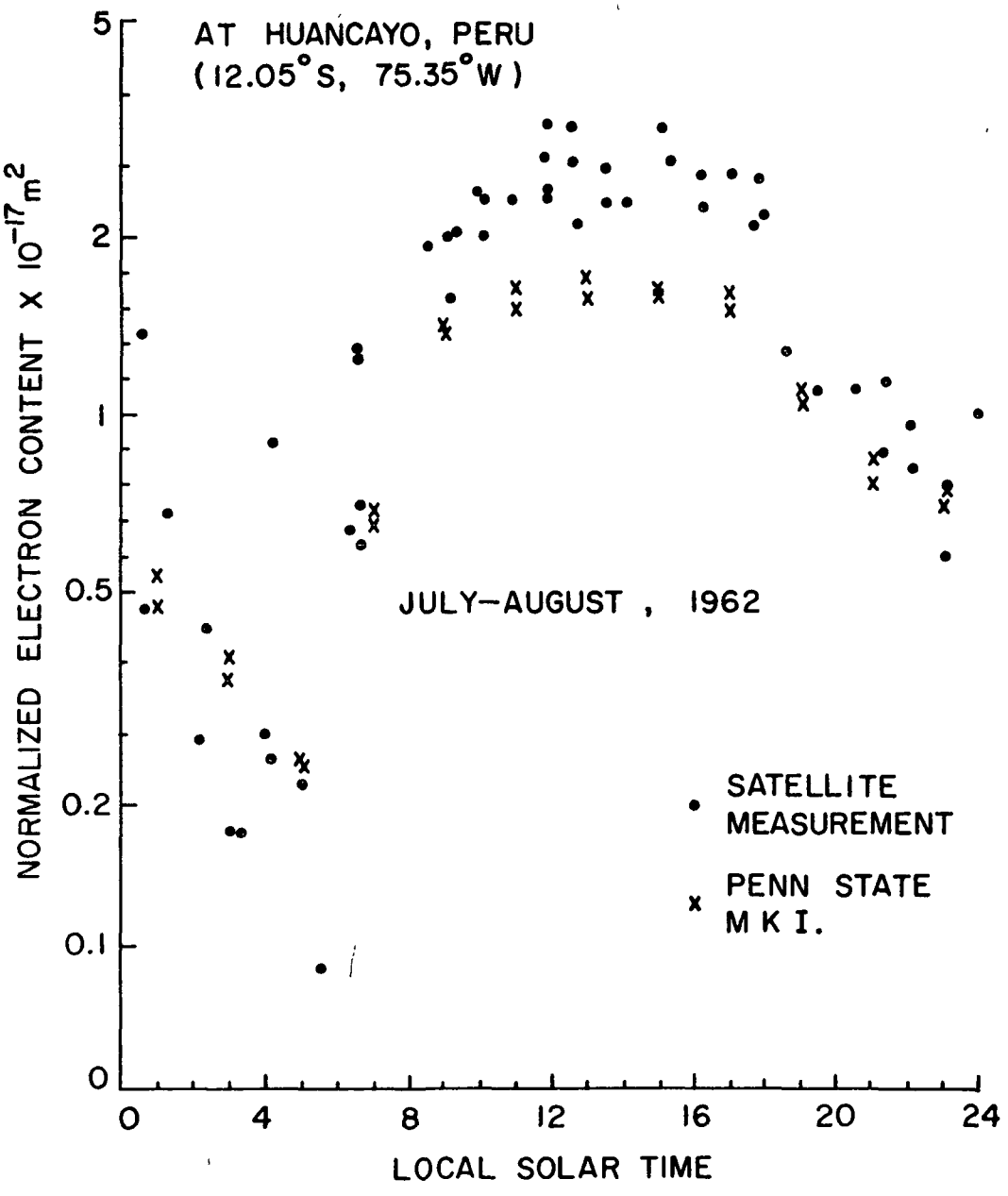

Figure 12 Average Diurnal Variation of Electron Content

altitude. The measurement of electron content, therefore, refers to the height range up to about 1000 km. The Penn State Mk 1 Model gives the values for the electron content up to 1250 km. Since the electron densities above 1000 km are very small, the electron content up to 1250 km is almost equal to the electron content up to 1000 km.

The satellite measurements and the predictions by the model calculation show similar diurnal variations. The model calculations are about 30% lower than the satellite measurement at the diurnal maximum. Even though the model assumptions break down at this low latitude, the agreement for the electron content seems to be comparable to the day to day variations.

Sometimes it is desired to know the diurnal variation of the electron content for different seasons with associated solar and magnetic activities. Figures 13, 14, and 15 show the diurnal variation of electron content at different seasons and different phases of the solar cycle at Stanford (37.5°N, - 122°E).

The solid lines were obtained from the Faraday rotation measurement made with the geostationary satellites (Garriot et al. 1969). The cross marks were again obtained from the model calculations. The monthly mean values of 10.7 cm solar flux in March, July, and December were used for spring equinox, summer solstice, and winter solstice, respectively.

For spring equinox the agreement between the predictions and the measurements is quite good except in 1968

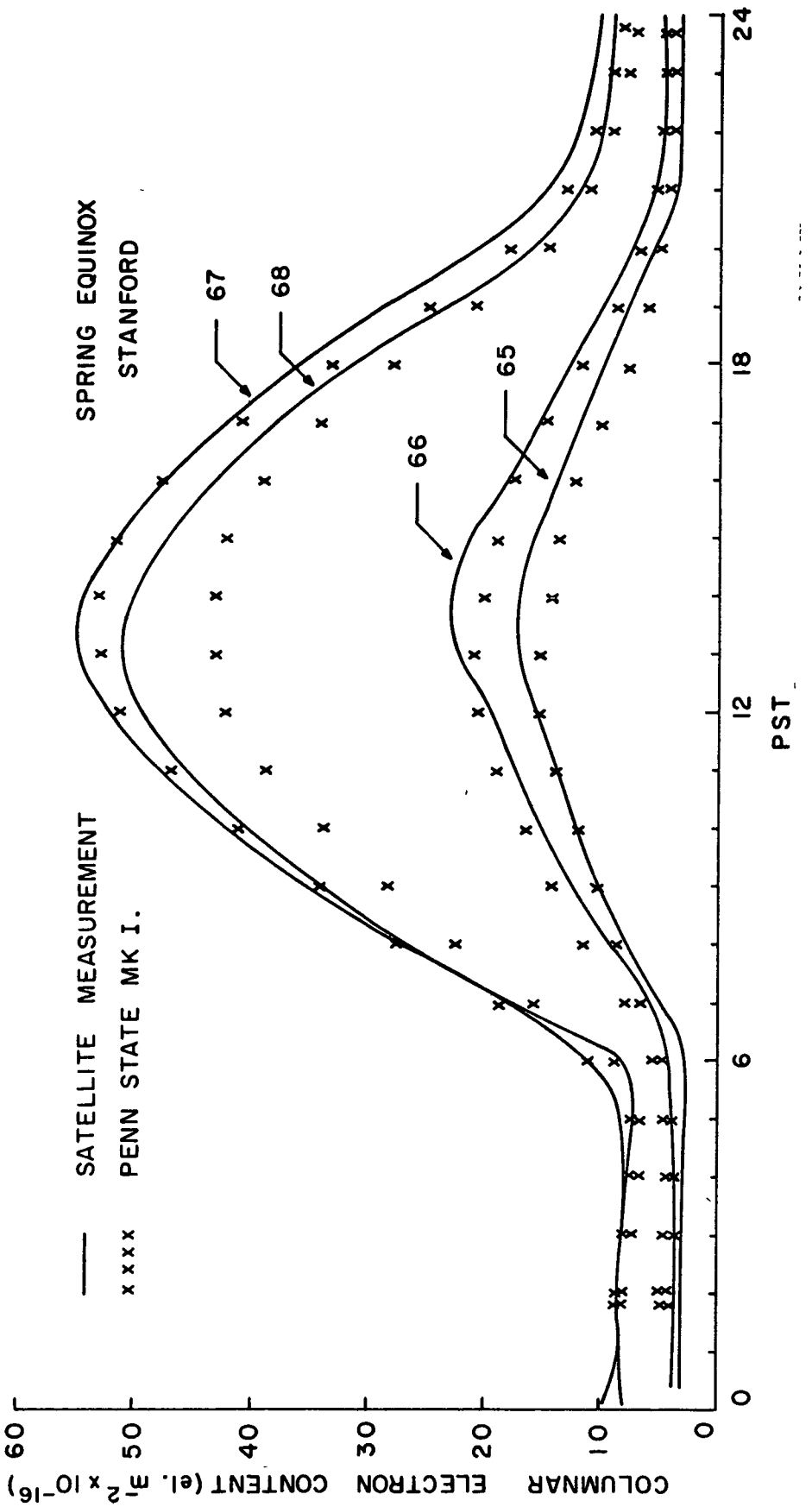

Figure 13 Diurnal Variation of Electron Content at Stanford for Spring Equinox at Different Phases of the Solar Cycle

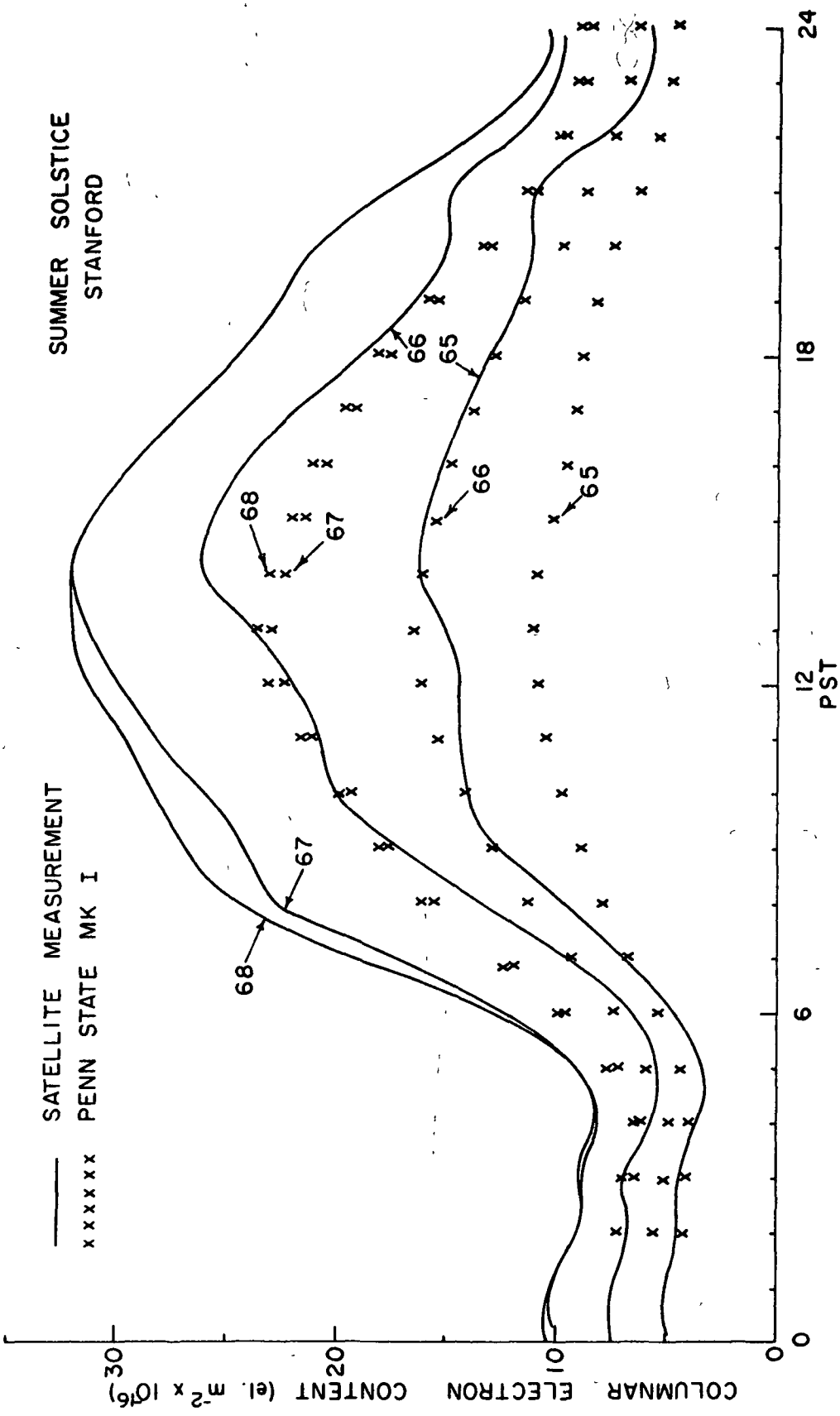

Figure 14 Diurnal Variation of Electron Content at Stanford for Summer Solstice at Different Phases of the Solar Cycle

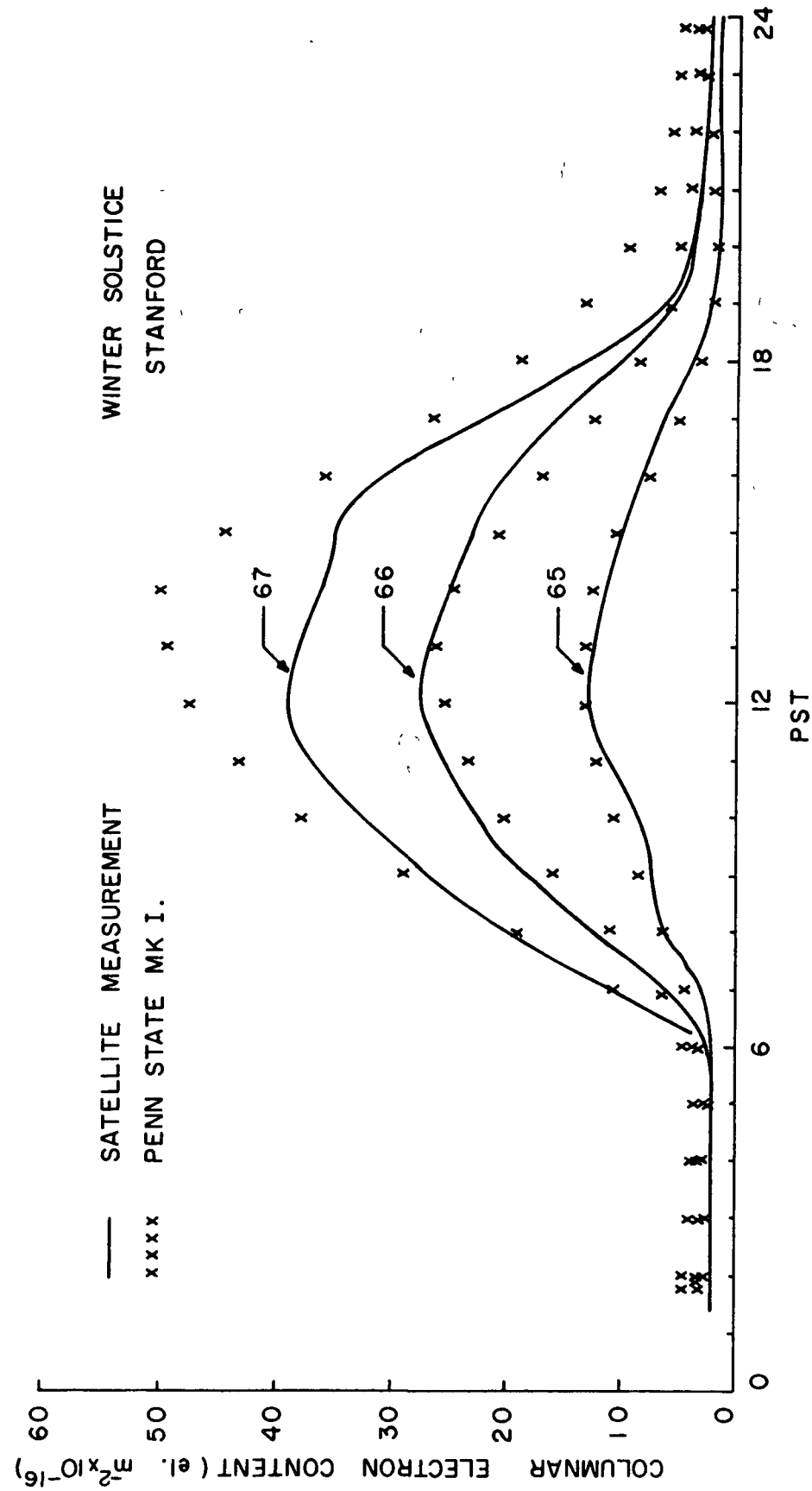

Figure 15 Diurnal Variation of Electron Content at Stanford for Winter Solstice at Different Phases of the Solar Cycle

solar year. The prediction for 1968 solar year shows about 10% lower values than the measurements during day time.

For summer solstice considerable discrepancies of up to 40% between the predictions and the measurements can be seen through all four solar years.

For winter solstice the prediction for 1967 solar year shows higher values than the measurement from the late morning through whole afternoon.

3.1.2 The Day-to-Day Variation of Electron Content

Figure 16 shows the electron content observed for a satellite on north to south passes over State College from October 1964 to September 1965. The contents correspond to different times of day as the satellite precesses. There is about a 30 to 40% difference between measurements and predictions from the middle of November to early December, whereas the predictions and the measurements are still good during May and June.

The day-to-day variations are of the same order as the diurnal variations of the electron content as shown in Figure 11 and Figure 14. The predictions are for monthly average conditions and it remains to be determined whether the departures are due to changes in the neutral atmosphere, the ionizing radiation or some other effects.

3.1.3 Horizontal Gradient of the Electron Content

Also of interest is the electron content gradient in

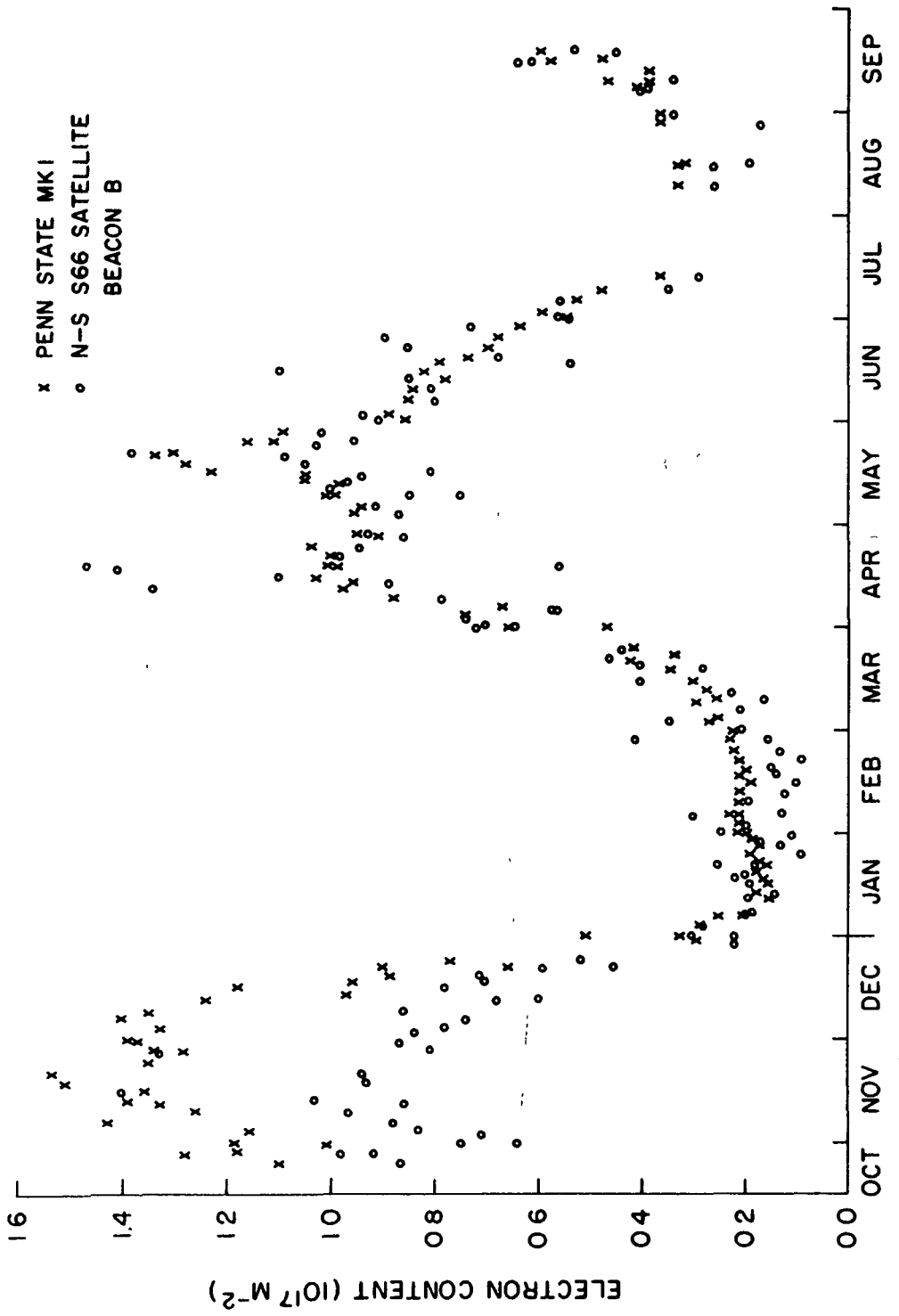

Figure 16 Day-to-Day Variation of Electron Content Through October 1964 to September 1965

the horizontal direction. In order to improve the satellite measurements, it is often necessary to predict what sort of horizontal gradient of the electron content is expected.

Figures 17, 18, and 19 show three examples of the comparison of satellite observations and the models. It is apparent that even when good agreement is obtained between actual and measured values of the electron contents the horizontal gradients may depart greatly from the values given by models. This is hardly surprising because effects such as gravity wave perturbations can greatly change the horizontal gradient without major effects on the average total profile. Wind structures which are not always regular can also change from one night to the next.

3.2 The Prediction of the Ray Paths, Oblique Incidence Soundings, and the MUF

3.2.1 The Prediction of the Ray Paths

An attempt was made to predict the possible ray paths between Washington (37°N, - 75°E) and London (52°N, 0°E) for April 10, 1971 and solar activities similar to those of this day.

Since there is a time difference in local time between Washington and London, specific time was chosen to see the effect of the changes in the medium on the propagation.

At 23:00 U.T. London will be in darkness and Washington in day light. This produces the electron density gradients shown in Figure 20. The ray paths are also shown for 2 hop-propagation and 3 hop-propagation and

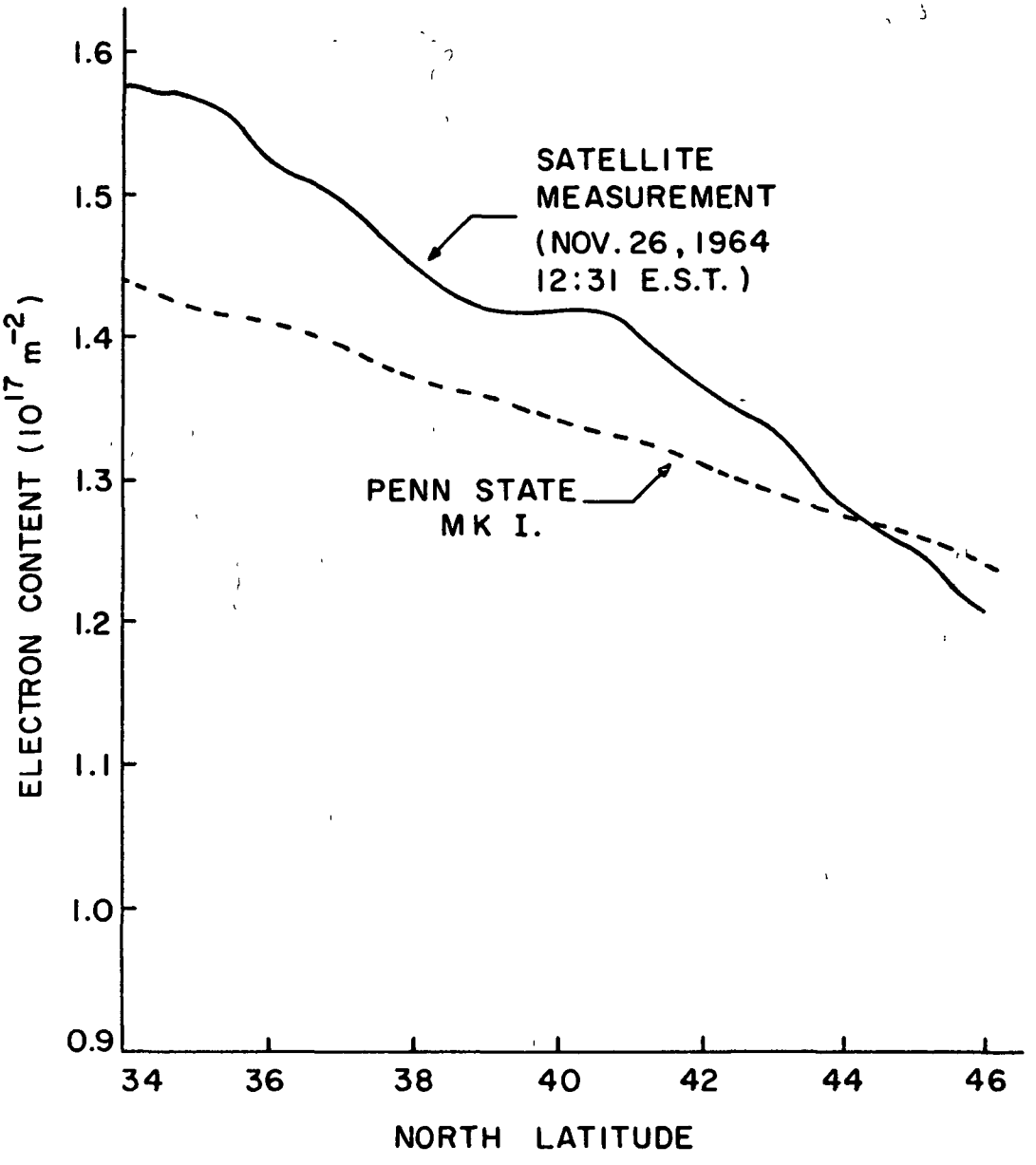

Figure 17 Daytime Gradient of Electron Content

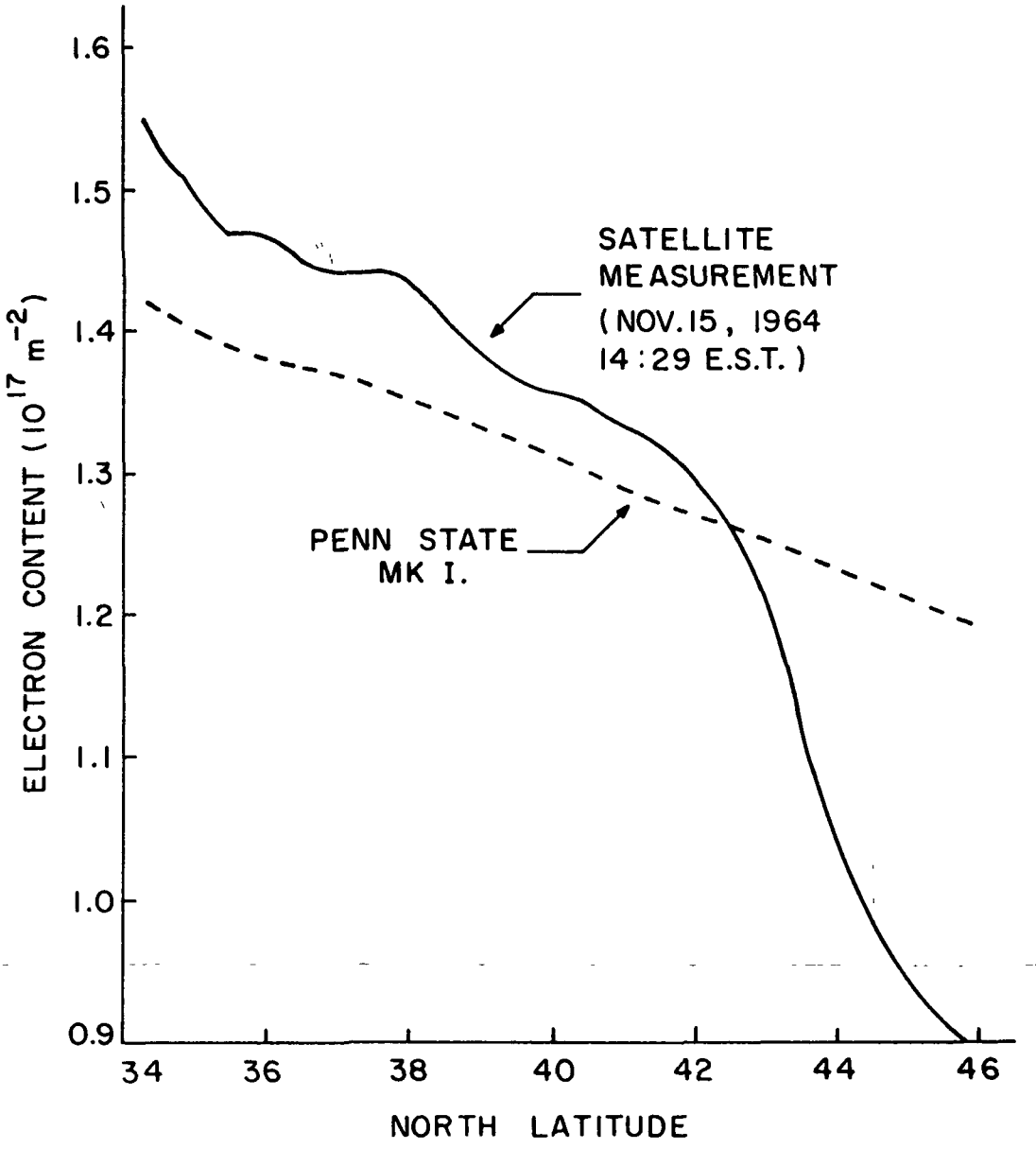

Figure 18 Daytime Gradient of Electron Content

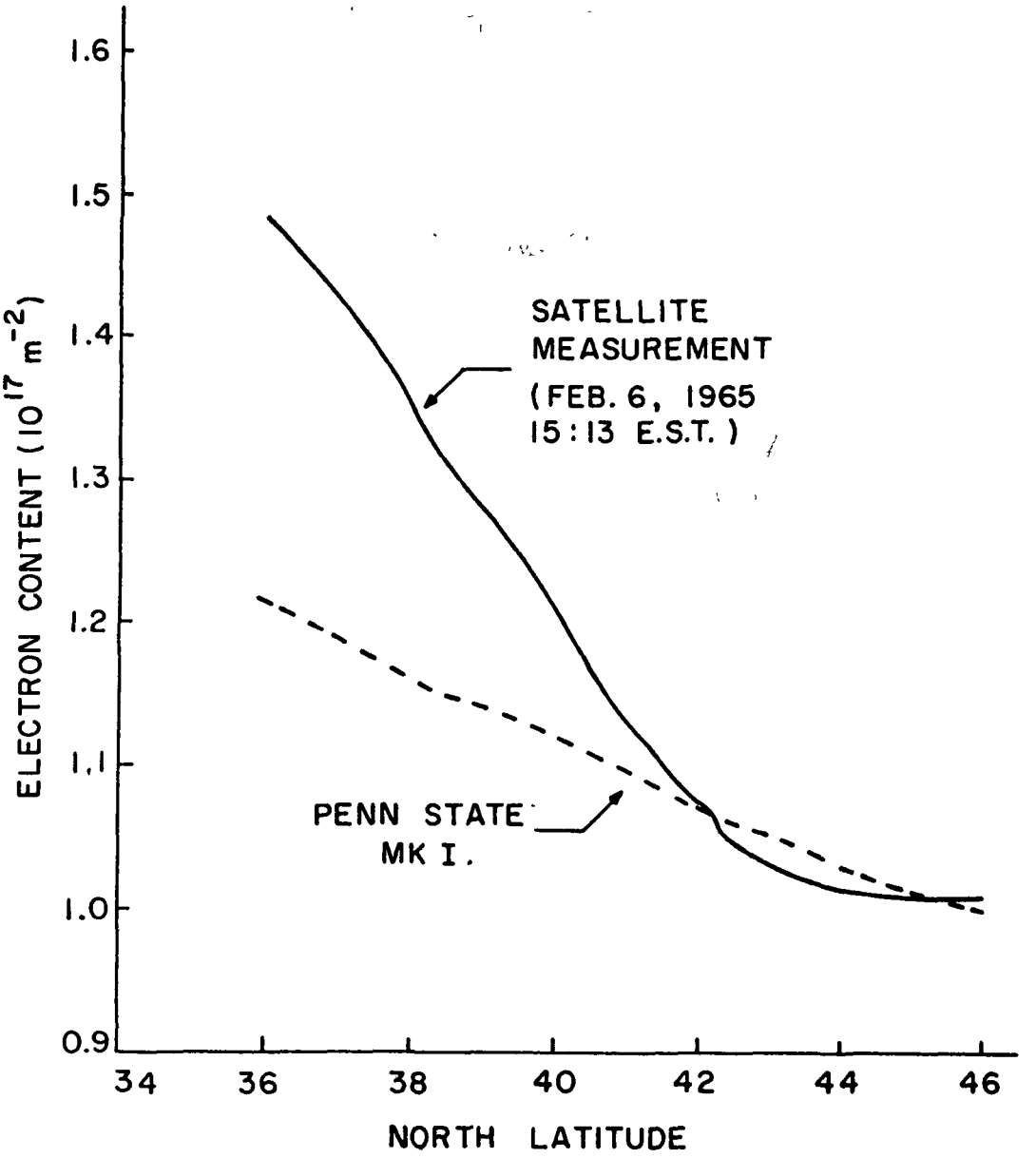

Figure 19 Daytime Gradient of Electron Content

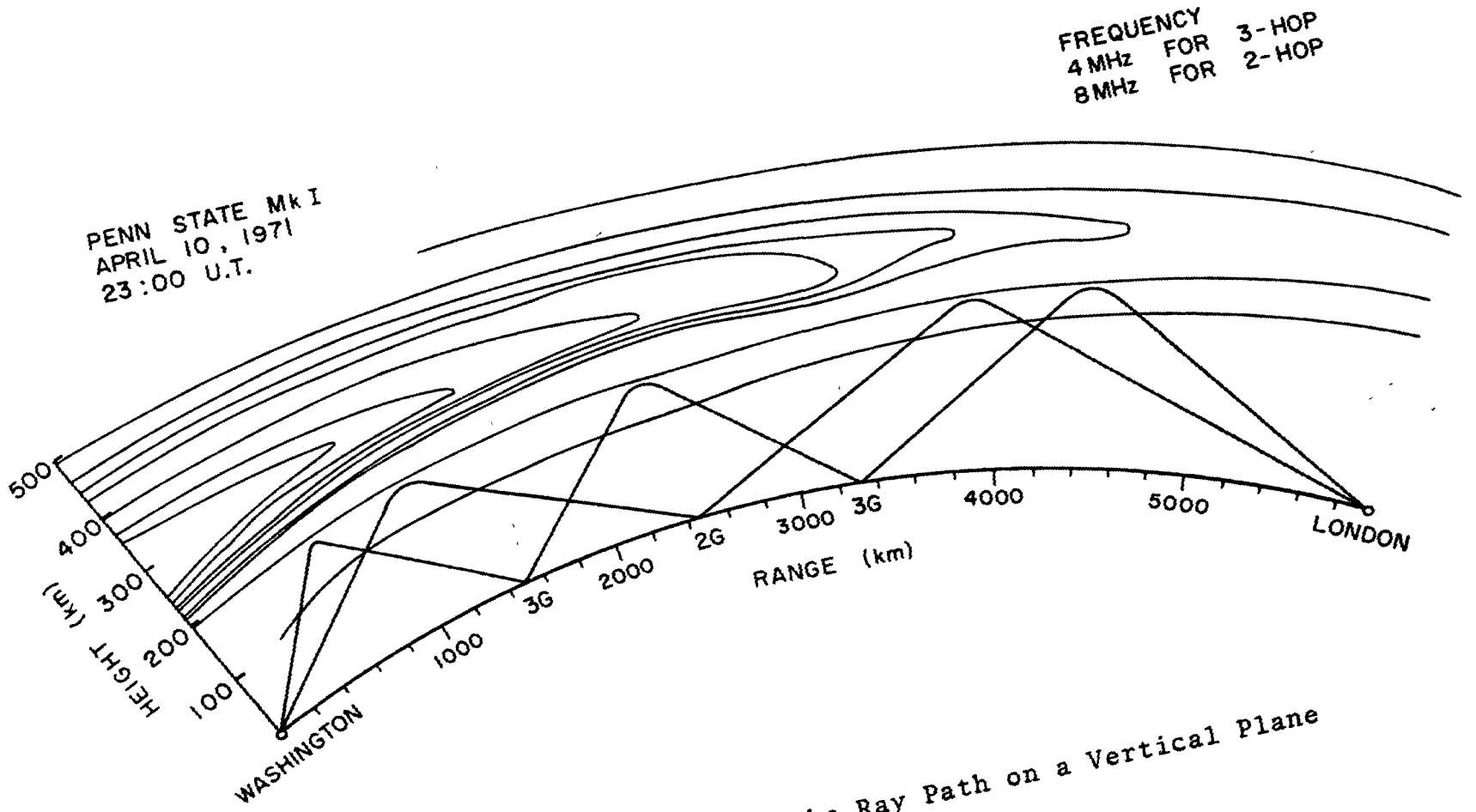

Figure 20 Projection of the Ray Path on a Vertical Plane

it can be seen that the distance between the paths is increasing as the reflection height increases. The reason for this is obvious from the map or plane view of the ray paths shown in Figure 21. The peak electron density can be shown along the ray path and the maximum (peak) electron density decreases as shown in Figure 21.

For the 2 hop-propagation, the ground reflection at 2G is in the sea east of Newfoundland. For the 3 hop case the first ground reflection is almost exactly at Halifax, Nova Scotia and the second in the mid-atlantic south of Greenland.

Figure 22 is another prediction of the propagation conditions at 7:00 U.T. At London the ionosphere was already sunlit and Washington was in darkness. Here the electron density gradients are rather different from before.

Figure 23 is a plane view of the same propagation conditions. As shown in the figure the first ground hop 3G has moved from Halifax, Nova Scotia out into the sea east of Newfoundland. The peak electron density gradients are almost at right angles to the ray path in this case.

For these predictions, the effect of the earth's magnetic field and the collision frequency of the electrons were neglected.

3.2.2 The Prediction of the Oblique Incidence Sounding and the Maximum Usable Frequency

Merely plotting ray paths is of limited interest and

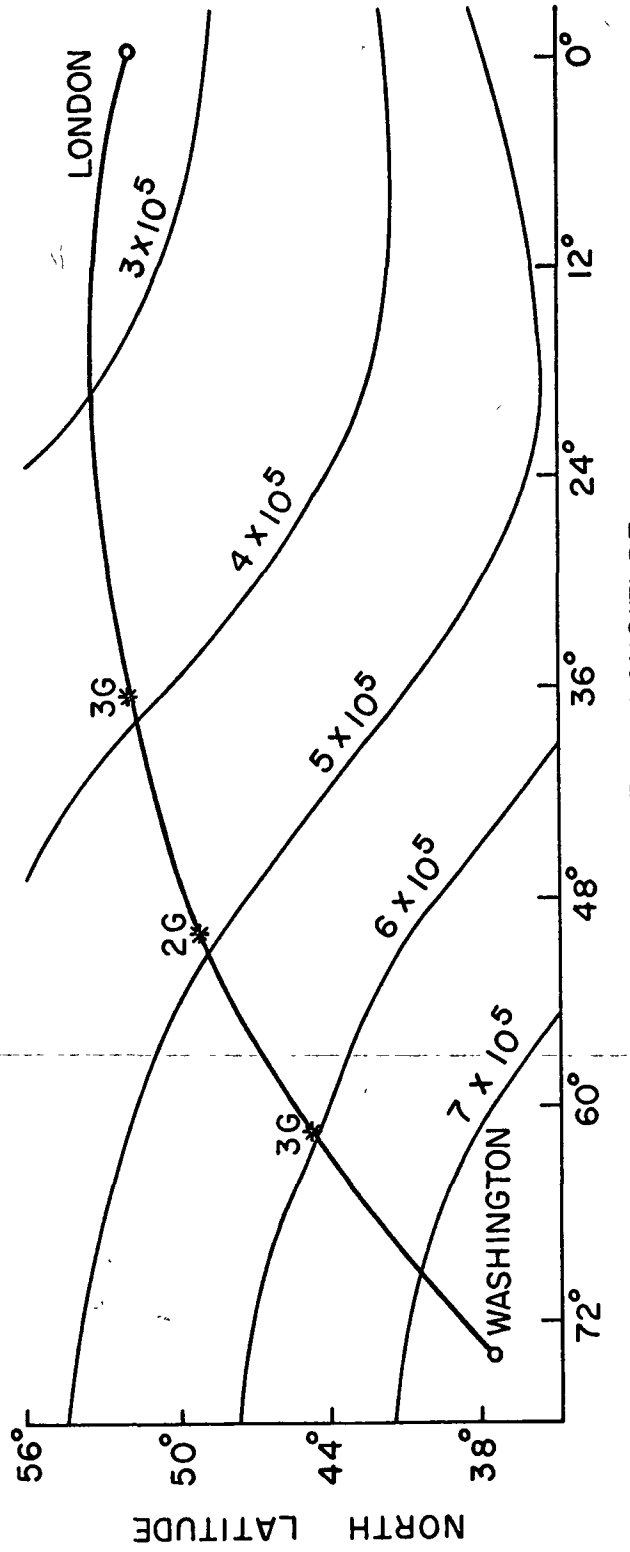

Figure 21 . Projection of the Ray Path on the Ground

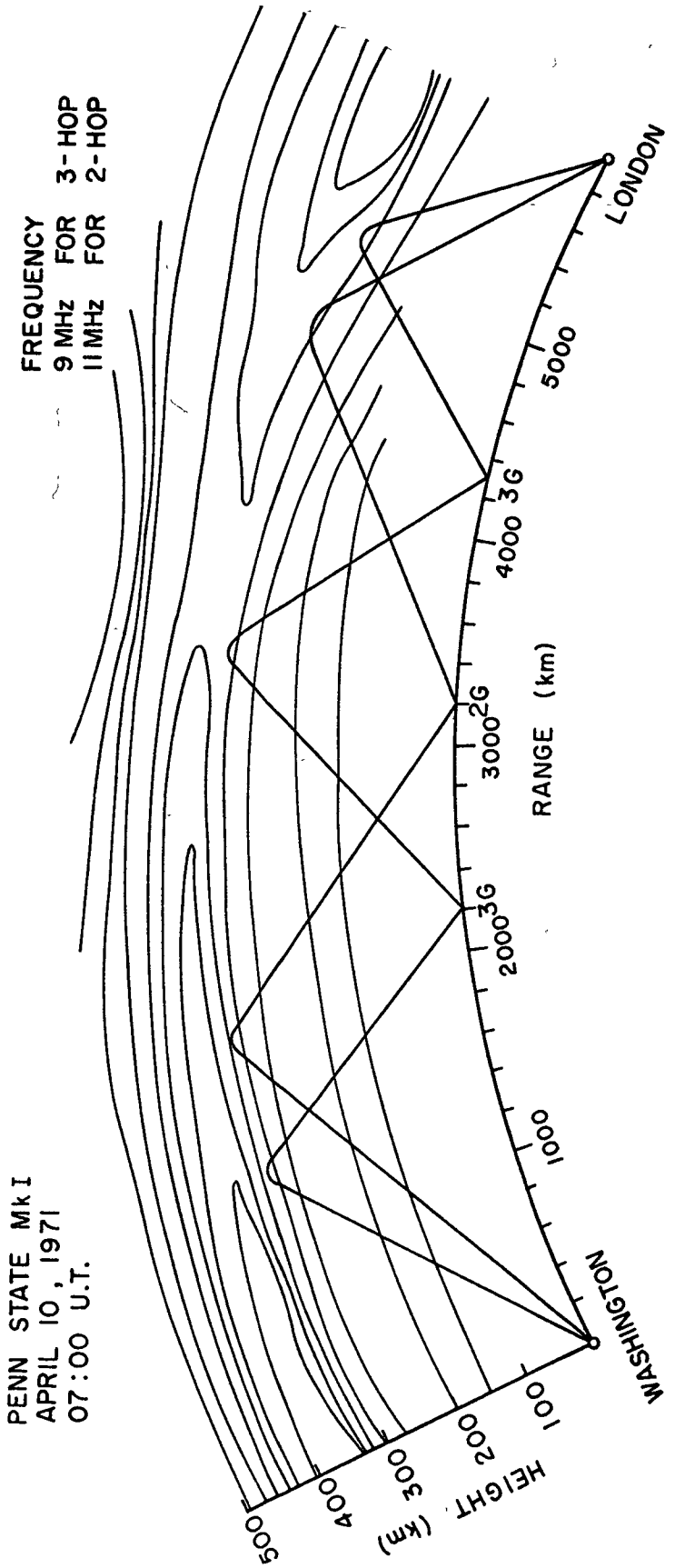

Figure 22 Projection of the Ray Path on a Vertical Plane

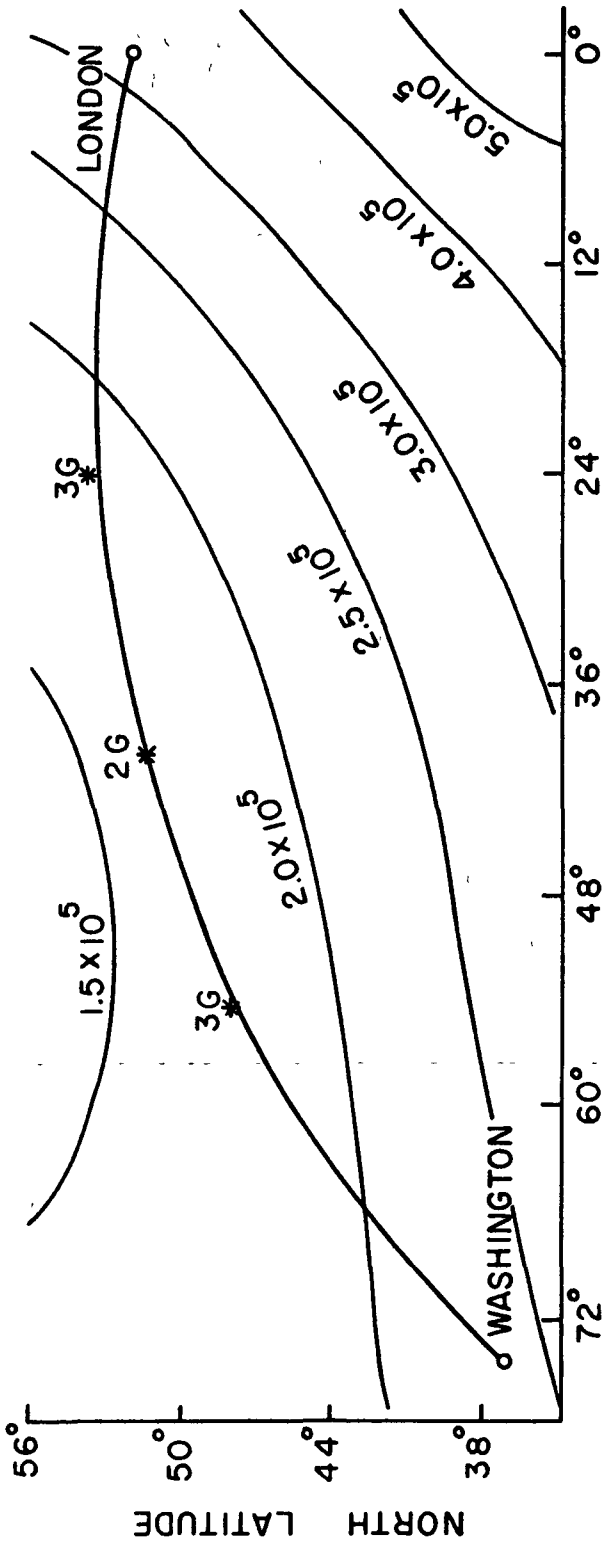

Figure 23 Projection of the Ray Path on the Ground

an attempt was made to see what success might be obtained in predicting the shape of an oblique incidence ionogram.

A virtual path-versus-frequency record is called an oblique incidence ionogram and is obtained by photographing the B scan on slowly moving film or paper in which the propagation time delay between the time a pulsed sinusoidal signal is transmitted from a remote site and the time the signal is received is determined.

Figure 24 shows an oblique incidence ionogram taken from NBS Report No. 31 Atlas of Oblique Incidence Ionograms along with the theoretical predictions. It is for a 1150 km path from Sterling, Virginia (39.0°N, - 77.5°E) to St. Louis, Missouri (38.7°N, - 90.3°E) measured at about 9 o'clock in the morning local time on April 24, 1952. Since the records of 10.7 cm solar flux for the time of the measurement were not available it was decided to bracket the estimated Zurich Sun-spot Number of 30 with 2800 MHz fluxes of 83 and 110 in the units of 10^{-22} $w/m^2/Mz$.

The frequency scale is greatly expanded so the small differences are magnified. The corresponding take-off angle versus frequency curves for the predictions are shown in Figure 25. It can be seen that, as the wave frequency increases, the height of reflection of the low-angle ray increases very slowly, whereas that of the high-angle ray decreases more rapidly. The frequency at which the low-angle ray and high-angle ray traces join is called the

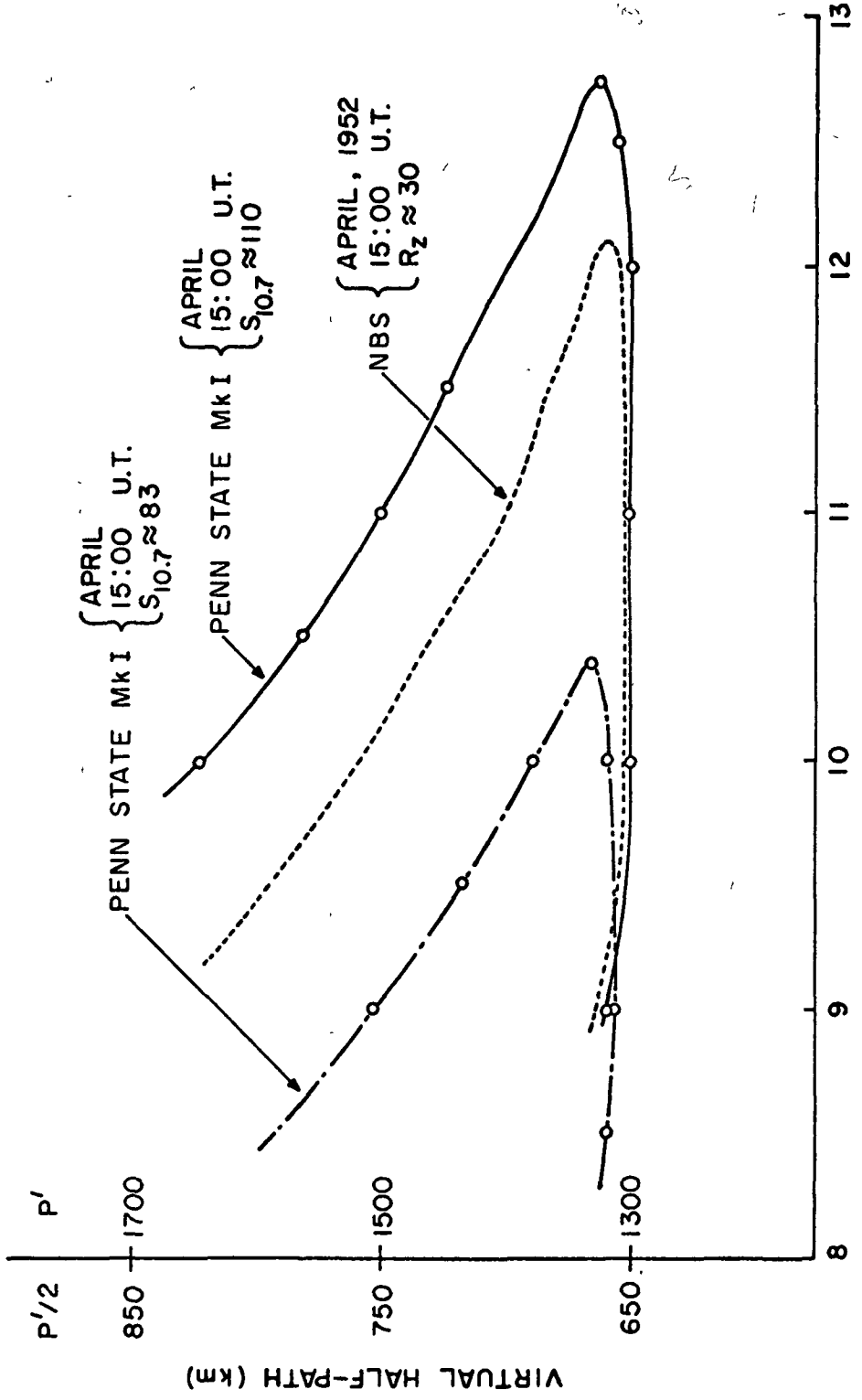

Figure 24. Oblique Incidence Sounding for Sterling - St Louis, 1150 Km

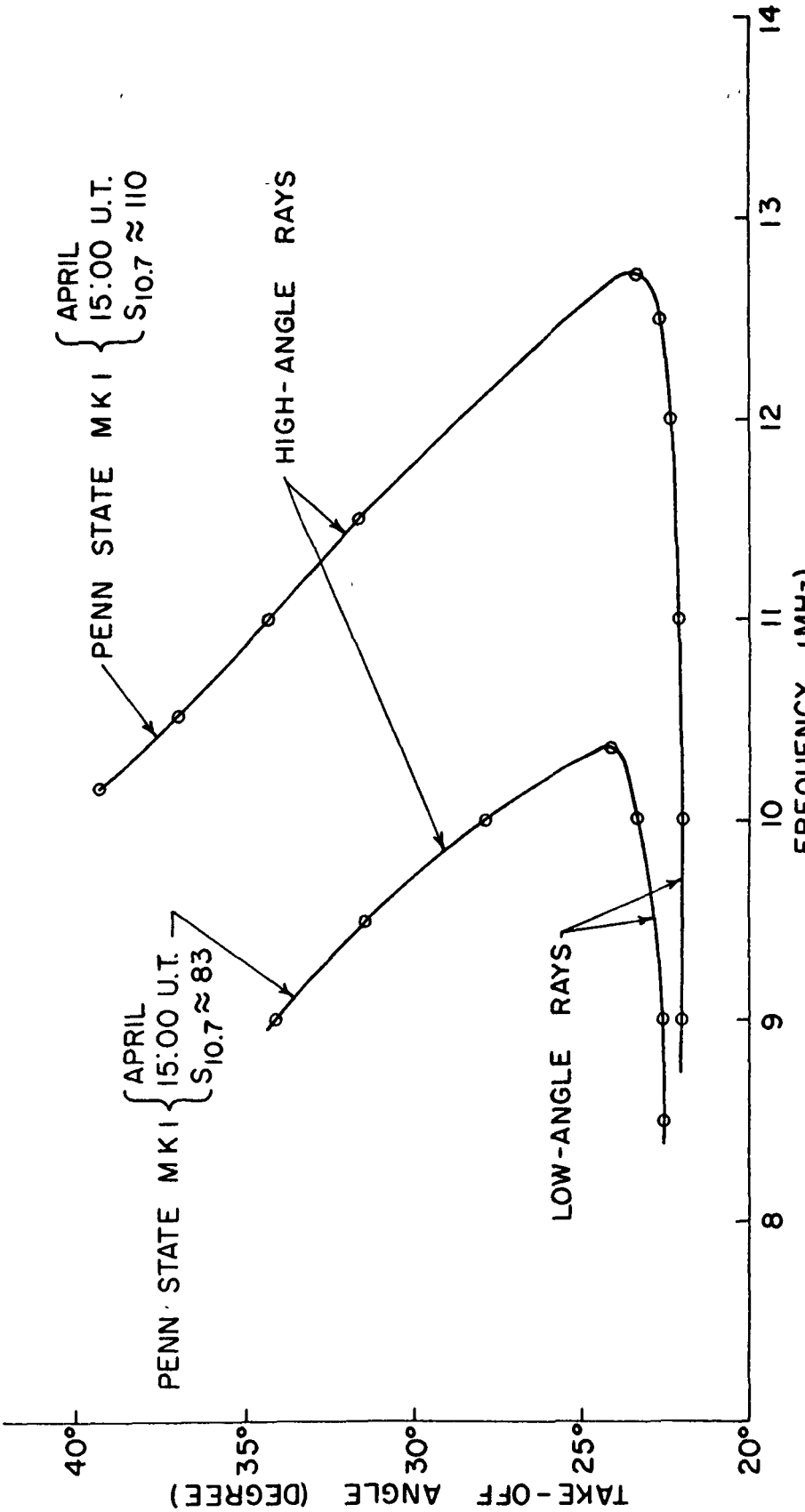

Figure 25. Variation of Take-Off Angle with Frequency

junction frequency, and represents the maximum usable frequency (MUF) for the given path and condition.

The MUF of the prediction for the solar activity, $S_{10.7}$ = 83 is 10.4 MHz and that for $S_{10.7}$ = 110 is around 12.7 MHz. This prediction shows therefore that the MUF for this path is proportional to the 1.4th power of the 10.7 cm solar flux.

Another prediction was made for the path between Washington and London, and compared with those obtained by the ITS prediction method. The maximum usable frequencies for the distances 3000 km and 4000 km from the transmitter were predicted by the model and compared with those obtained by the ITS method. The results are shown in Table 4.

Using the procedure based on the two control point method, the path MUF was also predicted and compared. It can be seen that the predictions for a reasonable range of solar activities bracket the observations in a satisfactory manner.

3.3 Prediction of the Path Loss of High Frequency Radio Waves

3.3.1 Theoretical Prediction of the Absorption Compared with A3 Absorption Measurements and Its Relation to the Ionospheric D- and E-Region

The purpose of the work described in this section is to re-examine the absorption of obliquely propagated high

Table 4: Comparison of MUF Model Calculation with ITS Prediction Method

		Ray Tracing Penn State Mk 1	ITS Prediction Method
		April 10, 1971	April 1971
7.00 UT	4000 MUF	12.00 MHz	12.40 MHz
	3000 MUF	11.00 MHz	11.50 MHz
	M(4000)	3.00	3.10
	M(3000)	2.76	2.90
	Path MUF	12.00 MHz	12.40 MHz
	Path FOT	10.20 MHz	10.50 MHz
23.00 UT	4000 MUF	21.00 MHz	22.00 MHz
	3000 MUF	20.00 MHz	21.00 MHz
	M(4000)	3.00	3.14
	M(3000)	2.86	3.00
	Path MUF	16.10 MHz	16.30 MHz
	Path FOT	13.67 MHz	13.70 MHz

frequency waves and to determine in particular how A3 absorption measurements are related to the D region of the ionosphere.

Recent papers such as those of Schwentek (1971) have presented extensive studies of D region absorption over the season and solar cycle based on A3 measurements.

First the prediction was made for the path from Annapolis (39°N, - 76.5°E) to State College (40.8°N, - 78°E) at 3.36 MHz.

The attenuation figures were calculated using the three dimensional ray tracing program of Jones (1966).

For the earth's magnetic model, the constant gyro-frequency and the dip angle of the path midpoint were used. The gyro-frequency and the dip angle are 1.5 MHz and 71.3° respectively for the height range of interest.

Since the attenuation figures of the measurement are not the absolute calculations of the daytime ionospheric absorption, but the daytime signal strength normalized to the nighttime value, the predictions are also made to give the normalized path loss. Figure 26 shows the observed normalized path loss for this path compared with predictions based on the model. The current ionospheric models used here seem to give too little attenuation compared with the measurements, and the electron density at the lower heights is probably greater than given by the Mitra-Rowe model. For the path from Annapolis to State College, the absolute daytime absorption is greater than the normalized path loss by

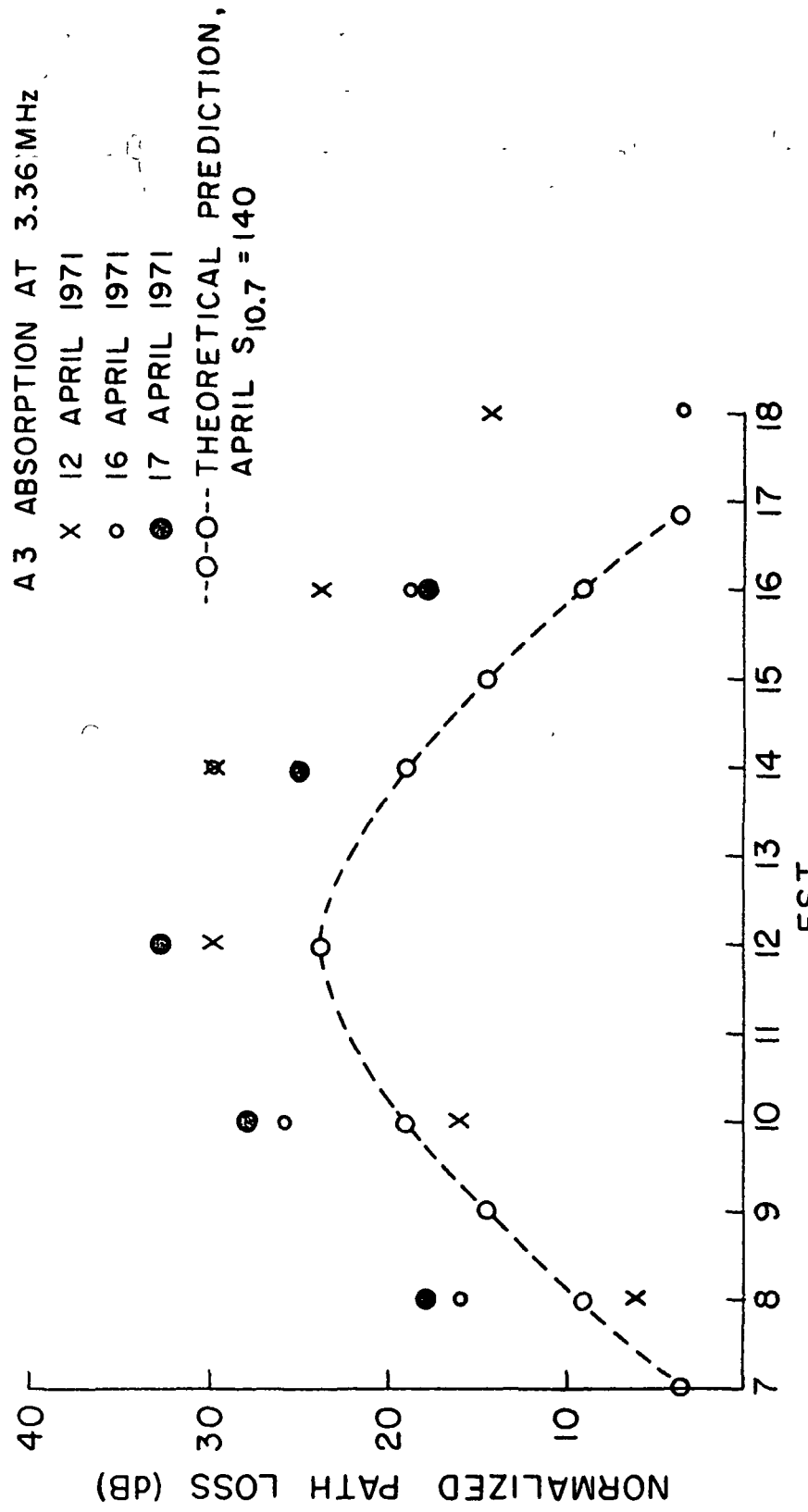

Figure 26 Diurnal Variation of A3 Absorption with the Prediction for the Path from Annapolis to State College, at 3.36 MHz

about 5 db. The remaining figures in this section show the relation of the daytime absorption to the ionospheric D- and E- regions. The differences between the absolute daytime absorption and the normalized path loss will be discussed fully in the following section.

Figure 27 shows the variation of absorption with height. It is apparent that the E region attenuation in this case is rather large compared with the attenuation lower down. It should also be noted that there is a considerable amount of attenuation close to the maximum altitude where the rays are traveling horizontally.

Figure 28 shows the variation of the reflection height with time for the model. It is apparent that these are, as would be expected, quite large. As the solar zenith angle increases the reflection height also increases.

Figure 29 shows the relative contributions from the region up to 85 km and also for the region above 85 km. It is apparent that the E region absorption dominates at all times in this instance.

Another prediction for the A3 measurement from Ft. Collins (40.6°N, - 105.1°E) to White Sands Missile Range (32.23°N, - 106.5°E) is shown in Figure 30. The frequency used is 5 MHz and the ground range is 940 km. This figure shows different aspects from the previous figure. However, the attenuation above 85 km is still not negligible compared with D region absorption.

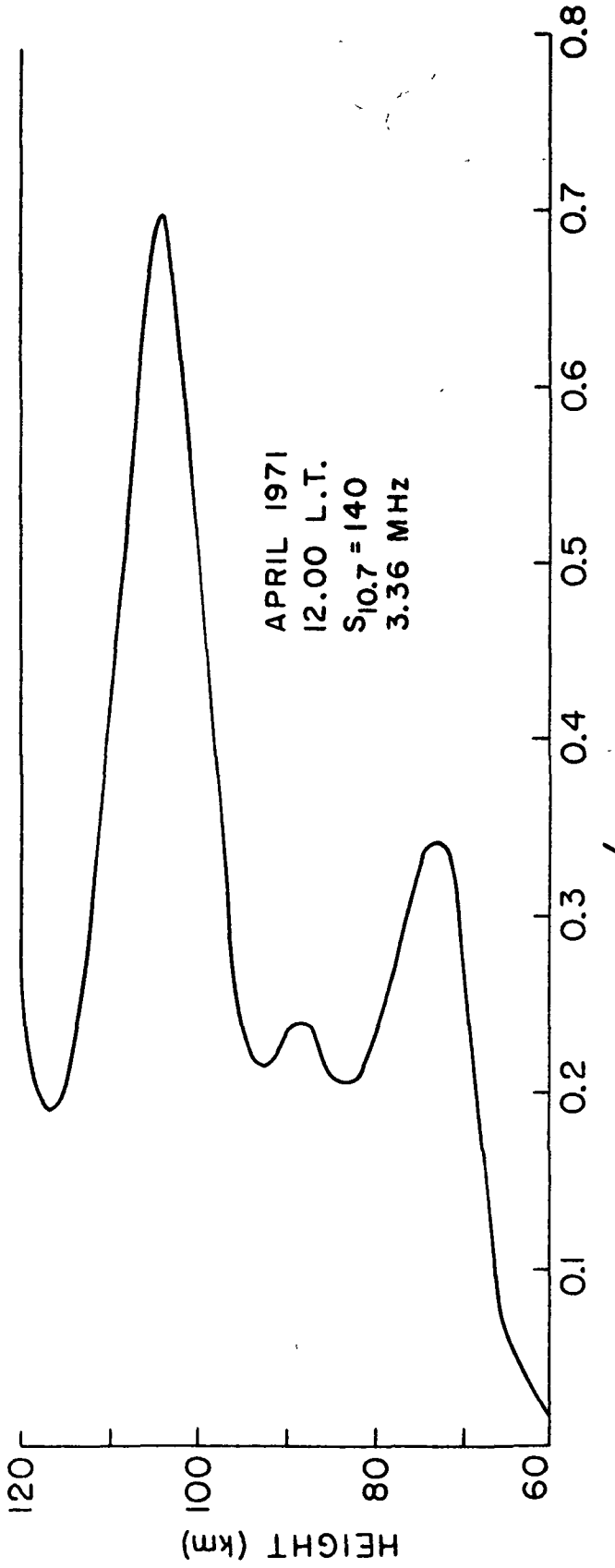

Figure 27 Variation of Absorption with Height

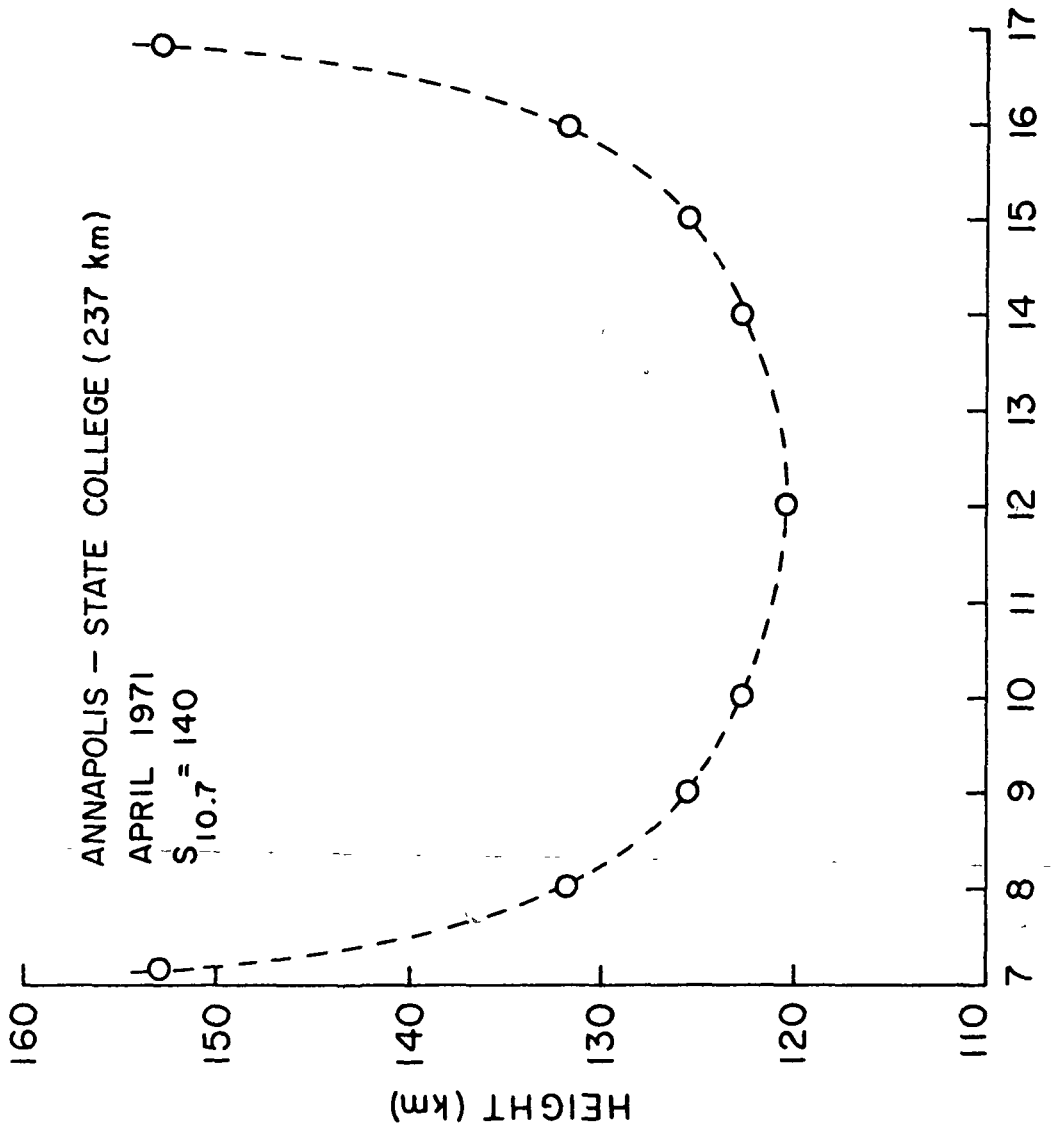

Figure 28 Diurnal Variation of Reflection Height

C-2

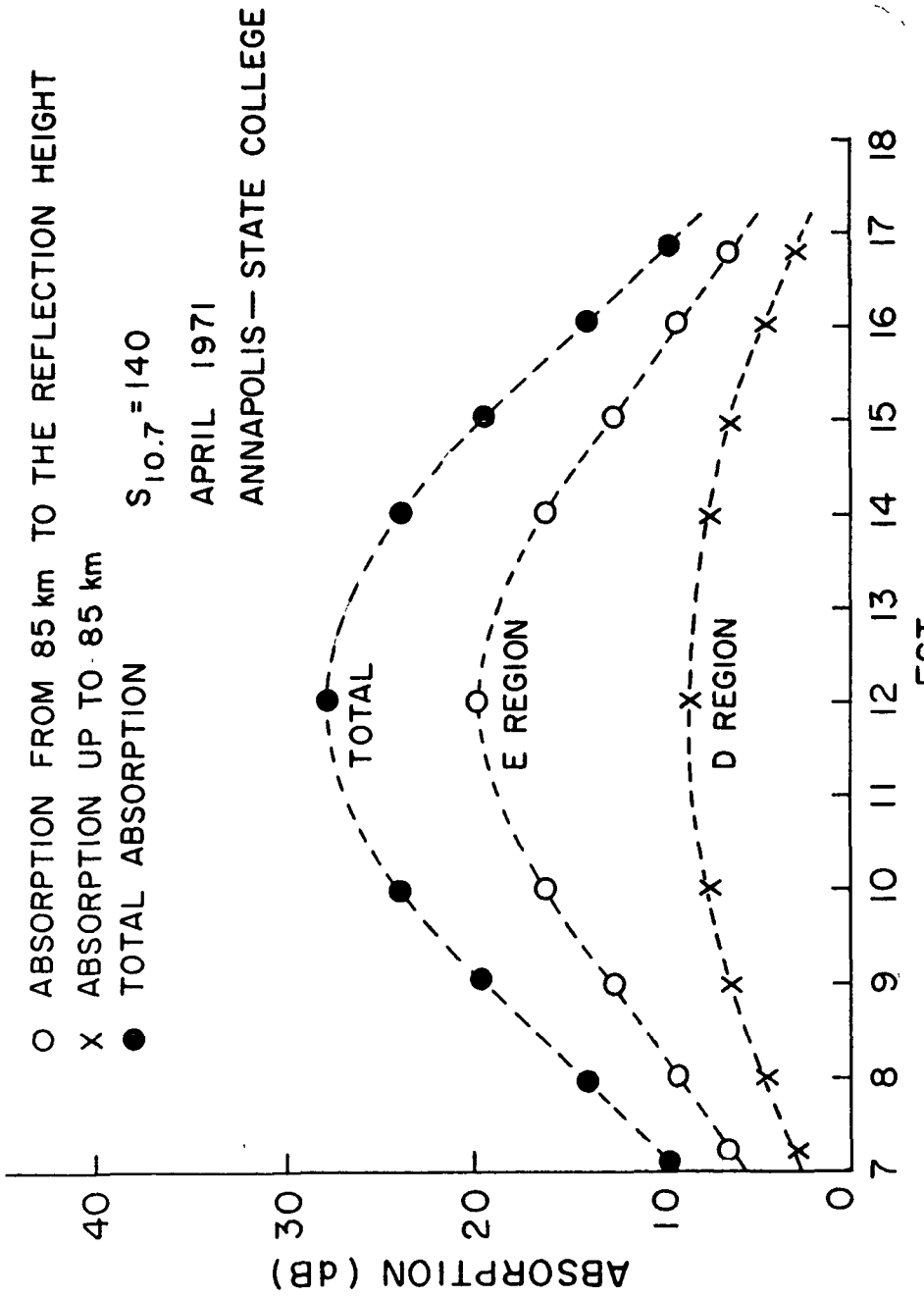

Figure 29 Diurnal Variation of A3 Absorption in the D- and E-Regions

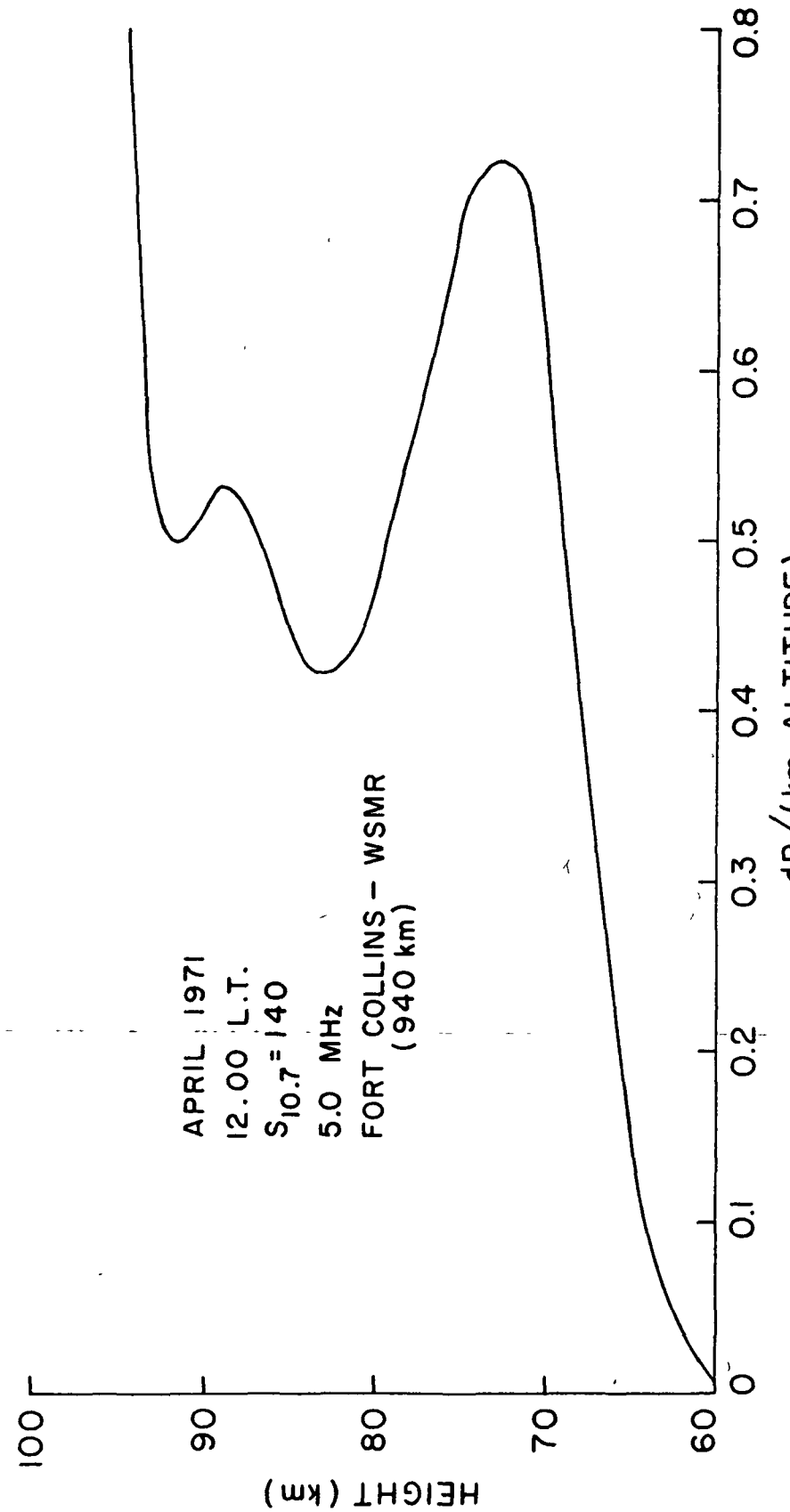

Figure 30 Variation of Absorption with Height

The model has been developed to allow rapid estimates to be made of the absorption of obliquely propagated radio waves in the high frequency band. It has been tested for a variety of frequencies, path lengths, and solar zenith angles. Reasonable agreement with A3 measurements was also obtained. In many cases the E region absorption is not negligible and great care must be taken to interpret A3 absorption measurements as indicating D region conditions.

3.3.2 The Prediction of Loss Calculation Due to Power Spreading

In high frequency propagation via the ionosphere, the path loss consists of several components, such as the spatial loss, the ionospheric absorption, and the focusing loss. For most cases the loss figures show that the spatial loss due to simple inverse square distance or dispersion of the energy is the main loss mechanism in radio wave propagation. In this section an attempt was made to see the contribution of the spatial loss to the path loss, and thus to deduce the absolute value for the daytime ionospheric absorption by comparing the nighttime path loss with the daytime path loss.

From the concept of the effective distance (which is the square root of the ratio of the actual defocused cross-section to the cross-section at unit distance from the source), Davies (1969) combined the spatial loss and the focusing loss to give the following expression.

$$L_t = 20 \log_{10} d_e = 10 \log_{10} \frac{A}{A_u}$$

$$= 10 \log_{10} [a \sin\phi \tan\theta \frac{dR}{d\theta}]$$

where

L_t = the spatial loss combined with the focusing loss, and will be called the spatial loss hereafter.

d_e = the effective distance.

A = the receiver cross-section.

A_u = the reference cross-section at unit distance (1 km) away from the source.

a = the radius of the earth, 6370 km.

θ = the elevation angle (take-off angle).

R and ϕ = the ground range in km and in radians respectively as shown in Figure 31.

$dR/d\theta$ = the derivative of ground range with respect to elevation angle and determined from the ray tracing results in this work.

An attempt was made to see what differences between daytime spatial loss and nighttime spatial loss might be obtained for both the Annapolis - State College path and the Ft. Collins - White Sands Missile Range path.

For the nighttime model only the Penn State Mk 1 Model is used to give the nighttime values for the electron densities and the collision frequency.

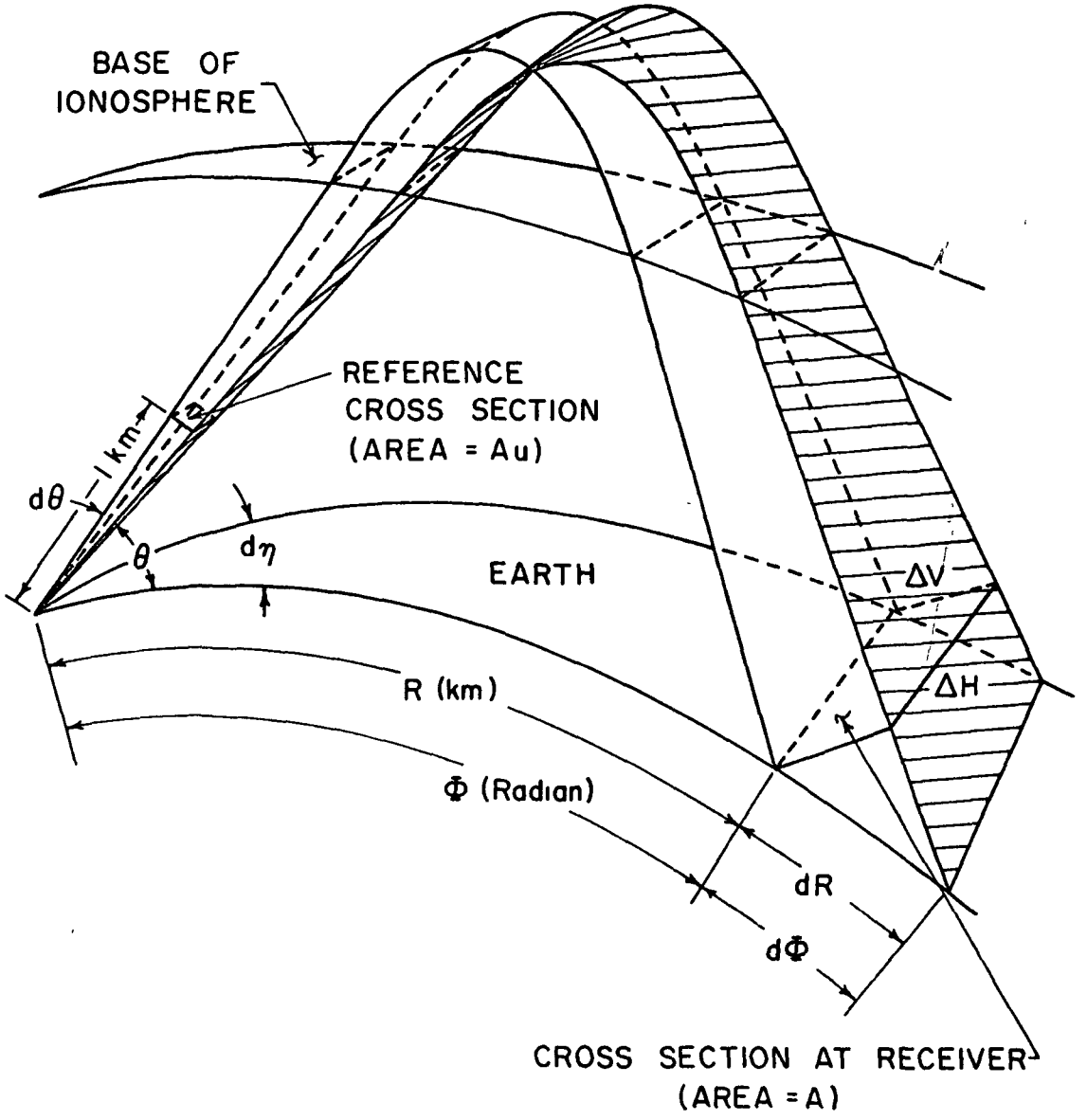

Figure 31 Divergence of a Narrow Radio Beam Reflected from a Curved Ionosphere

From the results shown in Table 5, there are 5 to 6 db differences between nighttime spatial loss and that of daytime for Annapolis to State College path while the path from Ft. Collins to White Sands Missile Range shows only a 2 db difference.

Since the attenuation figures shown in Figure 26 represent the normalized path loss, the differences of daytime and nighttime intensities have to be increased in this case by about 5 db to give a reasonable estimate of the daytime absorption assuming the antenna gain remains the same at the different zenith angles.

Here the ionospheric absorption by nighttime E layer below 120 km is neglected due to the assumed model. When the nighttime E layer electron densities are large, there is some absorption depending on the path geometry (Wakai, 1972) and therefore care must be taken.

To give some idea about the attenuation figures due to the spatial loss, an attempt was made to calculate the spatial losses for the same conditions on which the values of the ionospheric absorption were made as will be shown in Chapter IV. Due to the complexity of the ray paths the values shown in Table 6 are somewhat scattered.

3.3.3 Discussion of the Absorption Calculation Near the Reflection Level

The propagation of radio waves through the ionosphere can be described quite simply if the index of refraction does

Table 5: Calculations of Path Loss for Annapolis to State College Path and for Ft. Collins to White Sands Missile Range Path

Solar Zenith Angle (degree)	Elevation Angle (degree)	Reflection Height (km)	Ionospheric Absorption (db)	Spatial Loss (db)	Path Loss (db)	Path Loss Normalized to Nighttime Value (db)
		Annapolis to State College Path (237 km)				
$\chi = 30$	53	121	28.7	52.1	80.8	23.6
$\chi = 50$	53	126	19.5	52.1	71.6	14.4
$\chi = 70$	62	153	9.8	51.1	60.9	3.7
Nighttime (at midnight)	70	312	0.3	56.9	57.2	0
		April, $S_{10.7} = 140$				
		Ft. Collins to White Sands Missile Range Path (940 km)				
$\chi = 30$	10	96	33.5	57.8	91.3	31.0
Nighttime (at midnight)	33	310	0.2	60.1	60.3	0
		April, $S_{10.7} = 140$				

Table 6: Calculations of Spatial Loss

Spatial Loss for April, $S_{10.7} = 140$

Frequency (MHz)	Elevation Angle (degree)	Spatial Loss for $\chi = 30°$ (db)	Spatial Loss for $\chi = 50°$ (db)	Spatial Loss for $\chi = 70°$ (db)
5	1	55.7	52.5	56.0
	10	55.2	58.0	58.2
	20	53.8	53.0	56.1
	30	57.7	55.6	50.0
	40	53.2	50.7	52.4
	50	50.3	47.4	53.7
	60	52.6	55.6	55.7
	70	55.4	56.6	55.4
10	1	55.8	55.9	51.0
	10	65.6	61.4	57.0
	20	60.0	59.9	63.4
	30	61.9	60.3	50.8
	40	57.4	58.3	
	50	54.2		
20	1	53.0	59.7	58.6
	5	65.2	65.6	55.7
	10	65.0	63.8	70.6
	15	54.9	68.1	
	20	67.1		
30	1	58.3		
	5	77.7		

Table 6 Continued

Spatial Loss for April, $S_{10.7} = 70$

Frequency	Elevation Angle	Spatial Loss for $\chi = 30°$	Spatial Loss for $\chi = 50°$	Spatial Loss for $\chi = 70°$
(MHz)	(degree)	(db)	(db)	(db)
5	1	55.9	55.9	56.1
	10	57.9	58.0	58.1
	20	64.7	60.4	60.8
	30	56.6	51.8	52.4
	40	43.6	58.1	59.7
	50	60.0	60.1	56.9
	60	57.9	55.5	
	70	56.4		
10	1	55.8	58.4	57.5
	5	64.3	61.7	61.0
	10	60.0	57.8	64.2
	15	59.9	60.4	63.9
	20	65.7	53.2	68.5

not change appreciably over the distance of a wave length. In this case the reflection and transmission coefficients, the height of reflection, and so on, can be determined by the W.K.B. Solution.

The W.K.B. solutions at oblique incidence, when the effect of the earth's magnetic field is not included, are discussed in Chapter 9 of Budden (1961).

For horizontal polarization the W.K.B. solutions are invalid if

$$\frac{1}{k^2}\left|\frac{3}{4}\left(\frac{1}{q^3}\frac{dq}{dz}\right)^2-\frac{1}{2}\frac{1}{q^3}\frac{d^2q}{dz^2}\right| >> 1$$

and for vertical polarization

$$\frac{1}{k^2}\left|\frac{3}{4}\left(\frac{1}{q^2}\frac{dq}{dz}\right)^2-\frac{1}{2q^3}\frac{d^2q}{dz^2}+\frac{1}{q^2}\left[\frac{1}{q}\frac{d^2q}{dz^2}-2\left(\frac{1}{q}\frac{dq}{dz}\right)^2\right]\right| >> 1$$

where

k = the free space propagation constant

q = the normal component of the phase refractive index

Thus the W.K.B. solutions are invalid for 1) long wave length (low frequencies), 2) near reflection levels or coupling levels, 3) electron density not slowly varying.

The W.K.B. solutions also fail if the derivatives dq/dz, d^2q/dz^2 are large even when q is large. This would

be the case of reflection at a sharp boundary between two homogeneous media where the derivatives are infinite. Note that when the effect of collision is present, q^2 is complex and never takes on the value of zero. However, there is a region where $|q|$ is small and the W.K.B. solution is not valid. The W.K.B. solutions also break down for the case of partial reflection and partial transmission as discussed in chapter 17 of Ratcliff (1959).

The generalization of the W.K.B. solution can be found in chapter 18 of Budden (1961) and in the paper by Budden and Clemmow (1957).

When the W.K.B. solutions are invalid, the phase integral method or full wave solution must be used.

The purpose of this section is to discuss the absorption claculations by the ordinary ray theory and the full wave solution for the high frequencies of interest.

For some N(z) or X(z) profiles, it is possible to make a change of variable in such a way as to obtain a standard form of differential equation such as Bessels equation or the Hypergeometric equation. After obtaining the set of independent solutions of the equations and applying boundary conditions to obtain the required solution, the reflection coefficient is determined by separating the solution into the upgoing and downgoing parts and taking their ratio.

In this way Budden (1961) obtained the reflection

coefficient for the purely linear profile and the constant collision frequency as follows:

$$R = i \exp\{-2\ ikCh_o - \frac{4}{3}\ iC^3k(1-iZ)/a\}$$

where

$C = \cos \theta_I$

θ_I = the angle of incidence

k = the free space propagation constant

$i = \sqrt{-1}$

for the linear electron density profile,

$$X = a(z-h_o)$$

and for the constant collision frequency profile, Z. Thus the absorption per one hop can be obtained as follows:

$$L = -8.68 \ell n|R| \text{ (db)}$$

where

$$|R| = \exp\{-\frac{4}{3}\ C^3kZ/a\}$$

For the purpose of comparison the following linear electron density profile is used to represent the practical profile for the region between 85 km and around 120 km.

$$N = 1.314 \times 10^3 \cdot (z-85), \text{ electrons cm}^{-3}$$

where

z = the altitude in km

Table 7 shows the absorption calculated from the ordinary ray tracing program used and the values from the full wave solution.

As shown in the table the agreement between the two methods is not bad when the assumed value of the collision frequency is close to the collision frequency at the level where the reflection occurs. Since absorption near the reflection level is the main interest here, it will be wise to choose the value for the assumed constant collision frequency such that this value is close to the value near the reflection level occurring when this assumed collision frequency is included.

Since the ray tracing program tries to calculate the absorption near the reflection level where $|q|$ is very small, it tends to overestimate the absorption in this region. This is why the ray tracing program gives higher absorption than those obtained from the full wave solution as shown in Table 7.

For waves of higher frequencies which are reflected at higher levels where the collision frequency is smaller, there should be smaller discrepancies between the two methods for the absorption near the reflection level. It should be remembered that the ray theory discussed here is the ordinary ray theory, not a ray theory applied in the complex space. Jones (1970) explained the details of

Table 7: Comparison of Absorption Calculation by the Full Wave Solutions with the Ray Tracing Program

Frequency = 3 MHz
Elevation Angle = 30°

Assumed Constant Collision Frequency	Reflection Height	Absorption by Ray Theory	Absorption by Full Wave Solution
8.5×10^5 [85* km]	107.0 km	407.0 db	348.8 db
2.0×10^4 [107* km]	105.8 km	9.6 db	8.2 db
3.0×10^4 [104* km]	105.8 km	14.3 db	12.3 db

Electron Density Profile

$$N = 1.314 \times 10^3 \, [z - 85] \text{ electrons cm}^{-3}$$

where z = the height in km

* The height in the bracket indicates the height at which the collision frequency has the assumed value indicated on the left hand side of the bracket when the practical profile is considered.

complex ray tracing as discussed in section 1.2.2 of Chapter I.

Recently Gnanalingam (1972) calculated 3.2 db, 1.5 db, 1.3 db, 1.0 db, and 0.8 db for the phase integral corrections for the absorption of vertically incident waves of 1.33 MHz, 2.0 MHz, 2.2 MHz, 2.6 MHz, and 3.2 MHz, respectively. These absorption measurements were made at Colombo which is just outside the region where the quasi-transverse approximation is applicable to vertical propagation of the frequencies employed. (Dip angle 5°S, f_L = 0.093 Mhz at 100 km).

It can be seen that there are lower values for the phase integral correction for waves of higher frequency. For the oblique incidence this phase integral correction can be expected to be less than that for vertical incidence of the same frequency.

Recent papers, such as that of Jones and Foley (1972), consider the reflection and coupling points to be located away from the real axis in the complex X-plane when the effects of electron collisions are included. The conditions for reflection and coupling were derived using the Booker quartic equation. The behavior of the reflection levels in the complex X-plane was also shown as the angle of incidence is varied.

This is equivalent to a complex reflection height as discussed in Chapter 16 of Budden (1961). When the phase integral is calculated in the complex z-plane, the phase

integral along the imaginary axis gives the additional contribution to the phase shift and the reduction of amplitude. These were not predicted from simple ray theory (Budden, 1961). Thus the limiting factor of ordinary ray tracing programs is their failure to include the complex contribution to the phase integral (Jones, 1970).

It would be worthwhile to compare the result of ordinary ray tracing and full wave solution for more practical profiles of the electron density and the collision frequency.

CHAPTER IV

THE VARIATION OF ABSORPTION WITH SOLAR ZENITH ANGLE, GROUND RANGE, AND SOLAR ACTIVITY

4.1 The Diurnal Variation of Absorption

The absorption of radio waves is a complicated function of frequency, geographic location, season, ground range, solar zenith angle, and solar activity. The interrelationship between these controlling factors makes it very difficult to calculate the absorption of HF radio waves in a simple manner.

As shown in Figure 26 the absorption varies with the solar zenith angle χ. This diurnal variation is often expressed in terms of the power of cos χ. In Figure 32 the solar zenith angle dependence of the predicted absorption for the path from Annapolis to State College is shown. In the prediction the absorption both in the morning and in the afternoon were restricted by the model assumptions to be the same for the same solar zenith angle.

The predicted absorption can be approximated as follows

$$L \text{ (prediction)} = 32.1 \cos^{1.11} \chi \quad \text{db}$$

Many experimental results show a wide variation in the value for n, the power of cos χ, ranging from 0.75 to

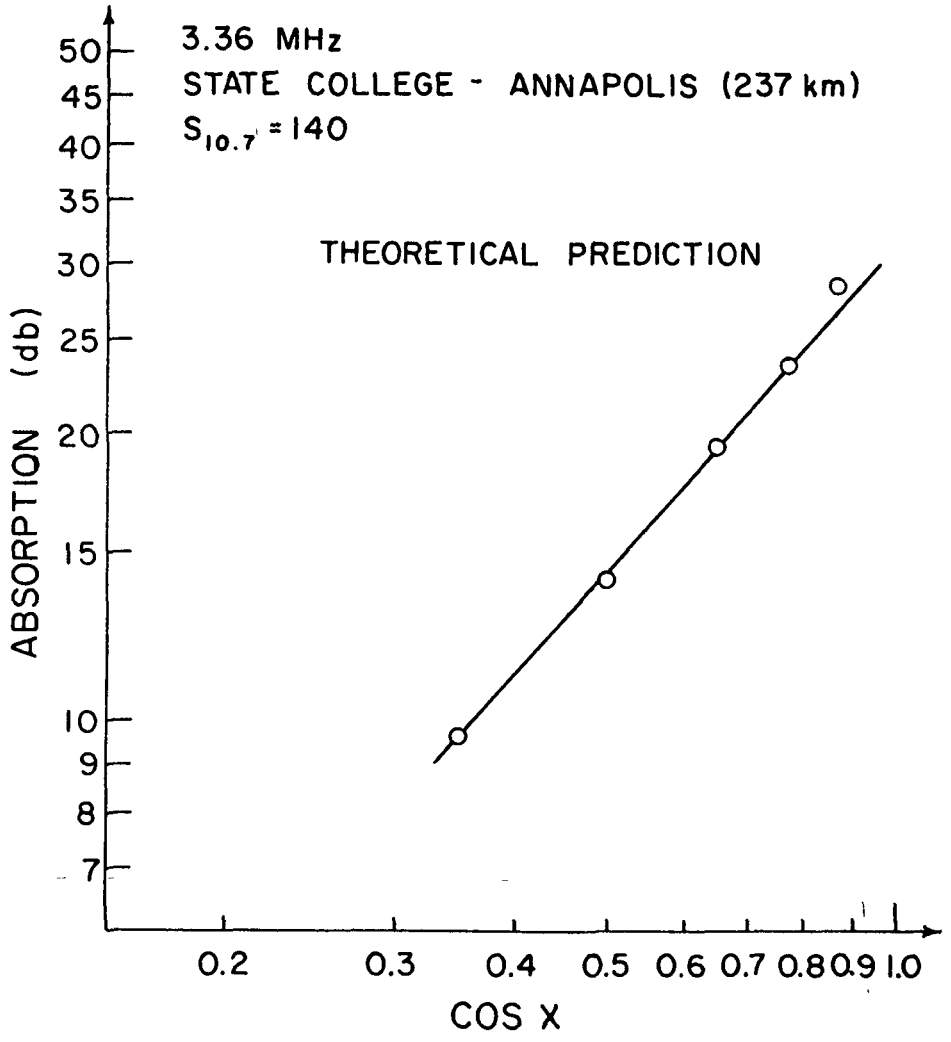

Figure 32 Variation of Absorption with Solar Zenith Angle

1.5 depending on the other controlling factors such as solar activity, season, etc.

Figure 33 shows the variation of absorption with solar activity for the same path. This prediction shows that the absorption increases with solar activity expressed here in 10.7 cm solar flux. Assuming a linear dependence of absorption on the solar activity, the figure on the right hand side shows the variation of the absorption with 10.7 cm solar flux for three different solar zenith angles. For the low solar activity, the dependence of absorption on cos χ is similar to that for high solar activity shown in Figure 32.

4.2 The Variation of Absorption with Ground Range

An attempt was made to predict the absorption of the waves of higher frequencies in middle latitudes for spring equinox. For this purpose the path between Washington and London was chosen. Electron density and collision frequency profiles are assumed to be the same along the path. The magnetic field model of Jensen and Caine (1962) was used to give the earth's magnetic field elements.

Figure 34 shows the variation of absorption with the angle of incidence. The predictions are compared with a formula given by Rawer (1952) shown below

$$L_a = 430(1+0.0035\ R)\cos^{3/4}\chi \sec\phi_D (f \pm f_L)^{-2} \quad \text{db}$$

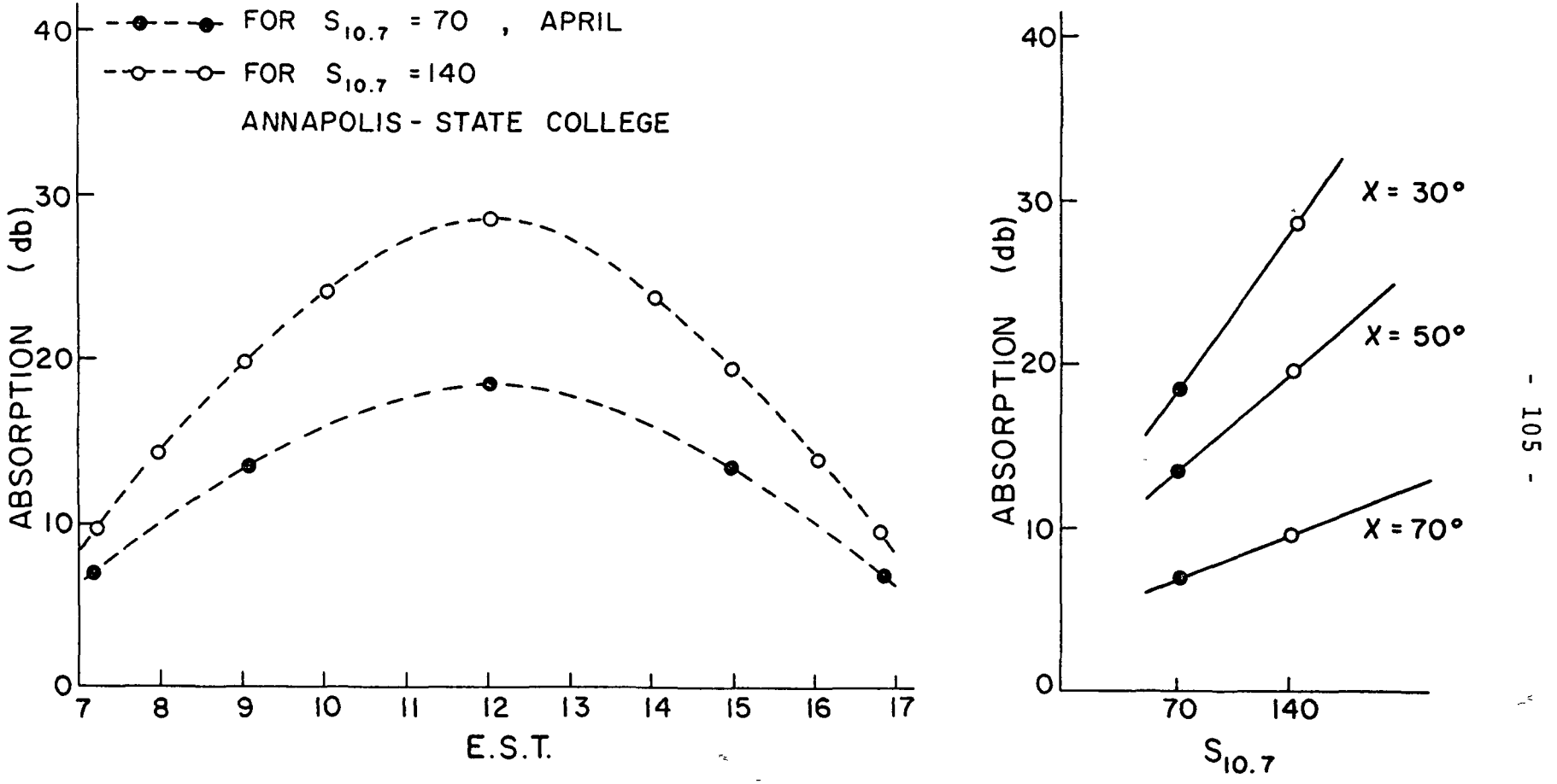

Figure 33 Diurnal Variation of Absorption for Two Different Solar Activities

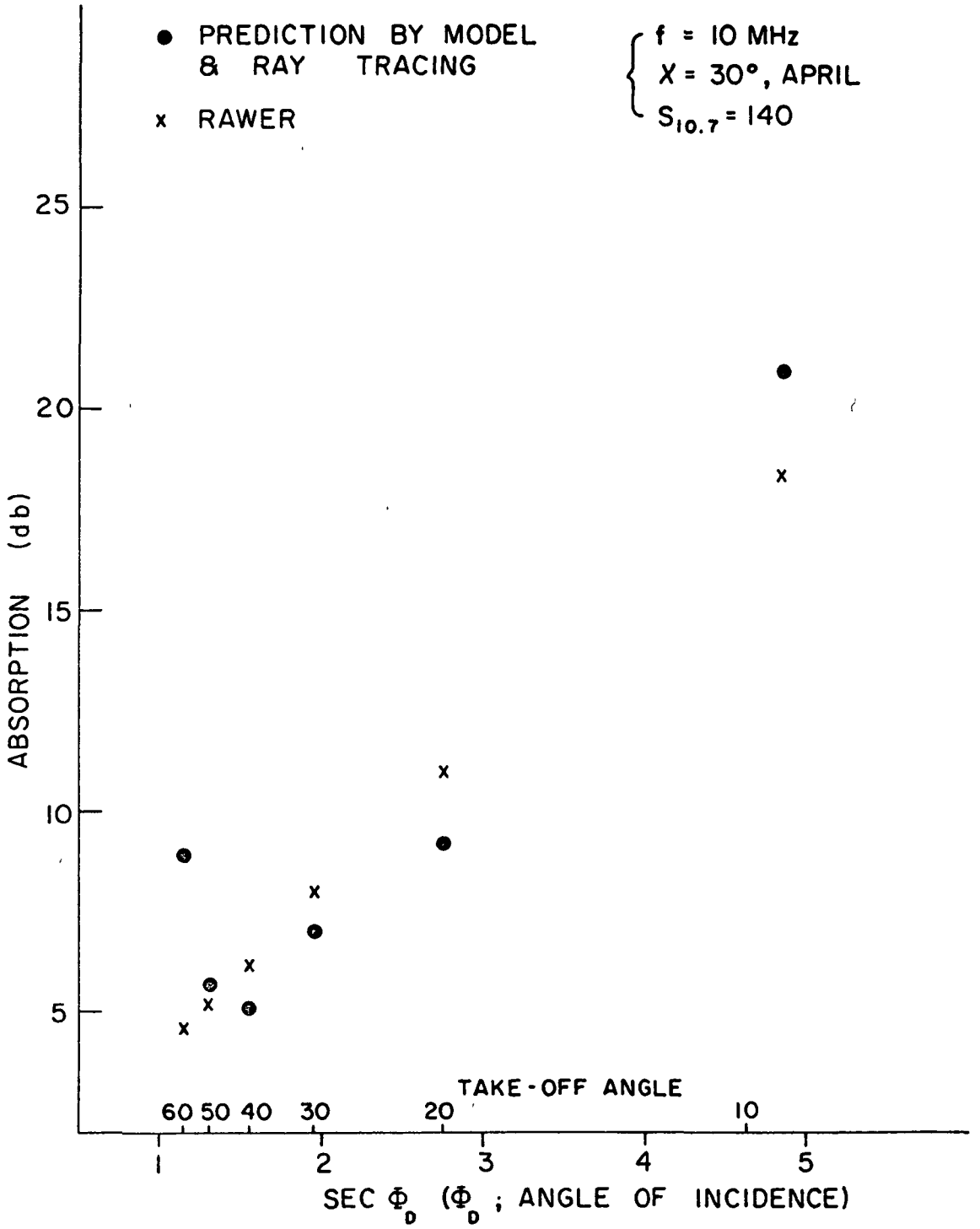

Figure 34 Variation of Absorption with the Angle of Incidence

where

L_a = the absorption in decibels per hop

R = the sunspot number

χ = the solar zenith angle

ϕ_D = the angle of incidence

f = the wave frequency in MHz

f_L = the longitudinal component of the gyro frequency

This formula represents the absorption in middle latitudes and the numerical values in this formula are based on analysis of vertical-incidence absorption measurements as Slough, England.

As shown in the figure the empirical formula given by Rawer has a linear variation of absorption with sec ϕ_D, while the prediction shows the relation to be non-linear. This is because of the importance of the deviative absorption in the calculations.

For the same conditions the variation of the absorption with ground range is shown in Figure 35 with the values of elevation angles indicated beside the dots.

The figure shows the possible existence of high-angle rays and low-angle rays for a given ground range. For example three possible rays can be found to have the same ground range around 950 km. One with an elevation angle of 16° is reflected at 127 km, the others with elevation angles of 20° and 30° are reflected at 137 km and 194 km respectively. These multiple modes are often seen in oblique ionograms.

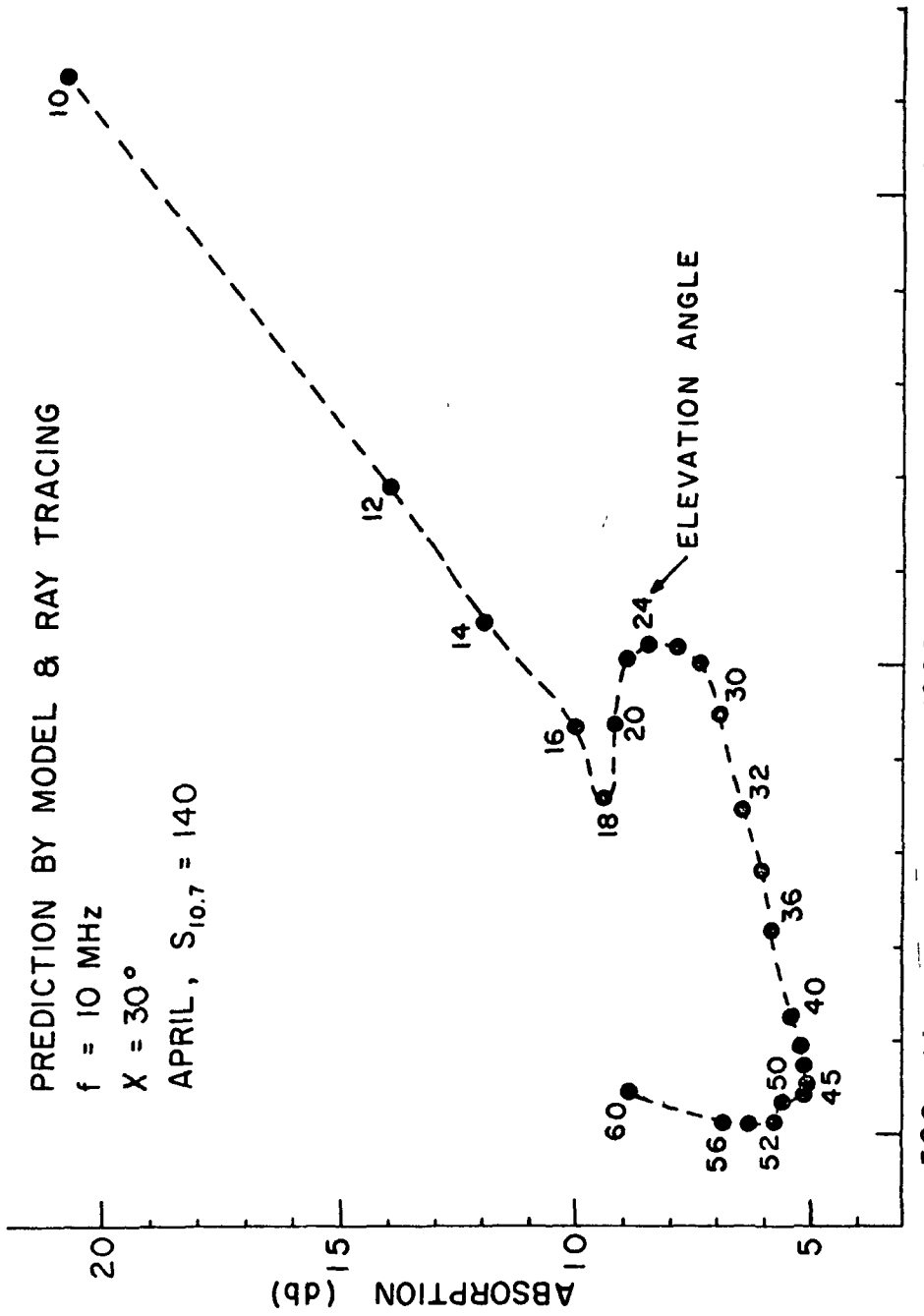

Figure 35 Variation of Absorption with Ground Range

For high elevation angles, above about 45° it can be seen that the absorption increases with the elevation angle. The reason for this is that the electron density increases as the wave approaches the height of the peak, while the collision frequency (mainly with ions) remains almost constant in this instance.

For an elevation angle of 60°, the variation of absorption with height is shown in Figure 36. A large amount of deviative absorption can be seen at high altitudes while the height variation of absorption for low elevation angles, such as 20°, shows different relative contributions as shown in Figure 37. For both cases the total absorption per hop is about 9 db.

Figure 38 shows the oblique ionogram for a path about 1000 km long and the values of absorption corresponding to low-and high-angle rays. In this case the absorption of low angle rays is higher than that of high angle rays. However, the variation in the magnitude of the absorption of low-angle rays is somewhat different from that of high-angle rays. Even though the absorption of low-angle rays is higher than than of high-angle rays for the same ground range, the spatial loss due to the energy spreading will be expected to be higher for high-angle rays than for low-angle rays. Details of the spatial loss were discussed in the previous chapter.

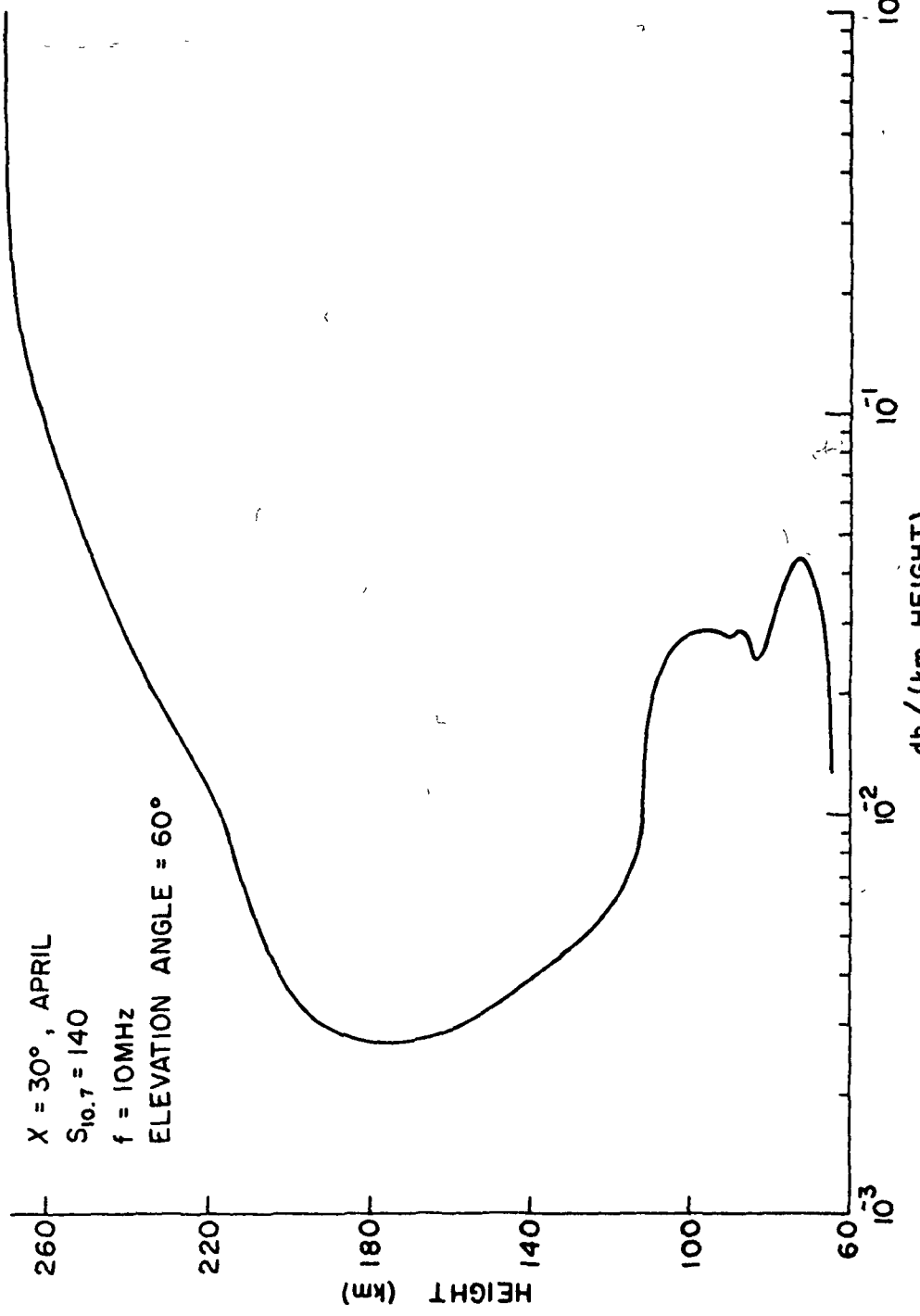

Figure 36 Variation of Absorption with Height for an Elevation Angle of 60°

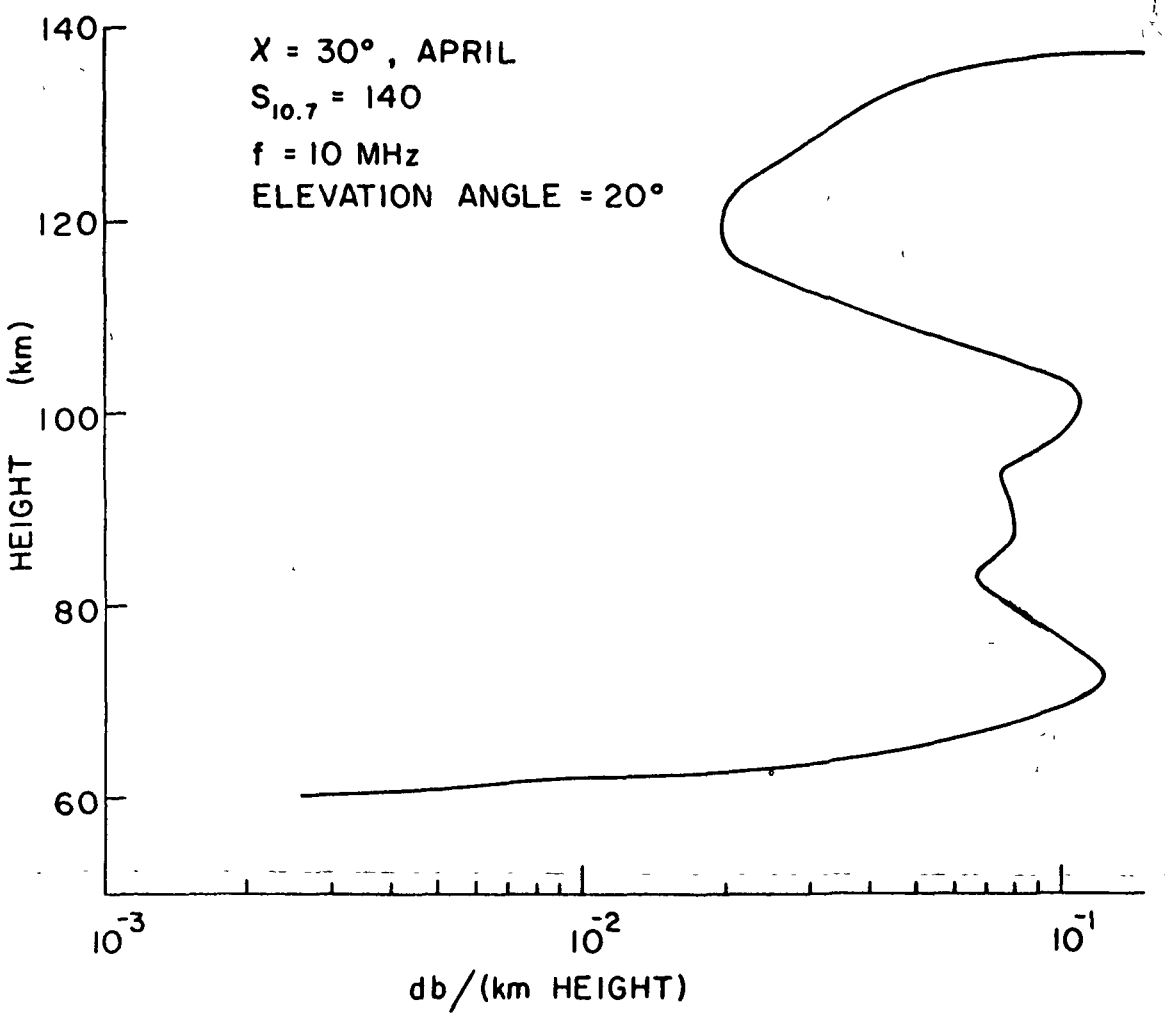

Figure 37 Variation of Absorption with Height for an Elevation Angle of 20°

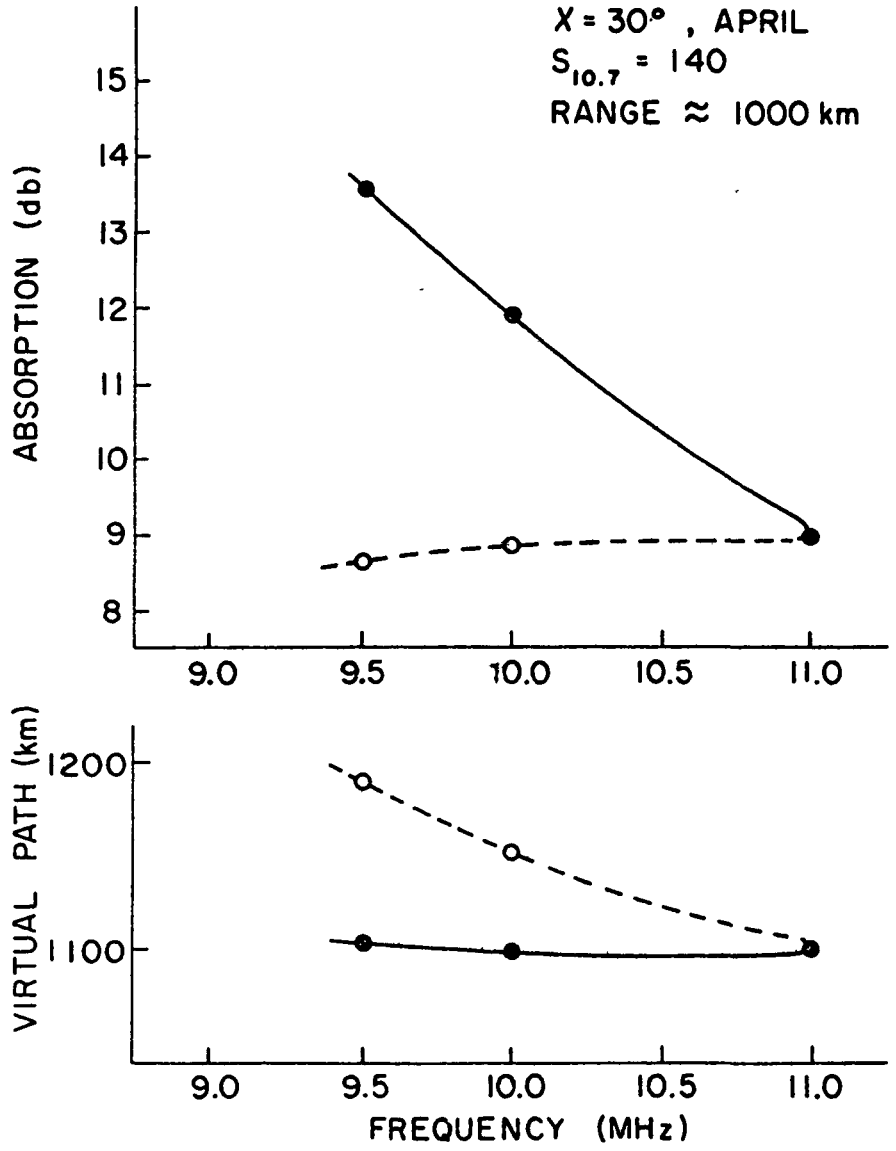

Figure 38 Oblique Ionogram with the Corresponding Values of Absorption

4.3 The Variation of Absorption with Solar Zenith Angle and Ground Range for Two Different Solar Activities

It was decided to attempt to derive an empirical equation relating the ground range, solar zenith angle, and 10.7 cm solar flux. Calculations were made of the absorption for three different solar zenith angles and a set of frequencies ranging from 5 MHz to 30 MHz. Two solar activities $S_{10.7} = 70$ and $S_{10.7} = 140$, which correspond approximately to the sun-spot numbers R = 0 and R = 100 respectively, were used to represent two phases of solar activities. The results are tabulated in Table 8.

It should be remembered that within a small range of elevation angle there can be possible low-and high-angle rays even though the results are tabulated with a large interval of elevation angle.

Even though the correct value for the absorption can only be obtained from the ray tracing, it is worthwhile to have an empirical equation to give a quick estimate of the absorption.

For this purpose the data obtained from the ray tracing were fitted to give the following equation.

$$L = 200\cos^{0.71}\chi(1+0.0031 \cdot S_{10.7})(1+0.0041D) \cdot \{(f+f_H \cdot \sin(I))^2+(\nu_o/2\pi)^2\}^{-1} \quad \text{db}$$

where

Table 8: Calculations of Ionospheric Absorption

$S_{10.7} = 140$

$\chi = 30°$, April

f Frequency (MHz)	θ Elevation Angle (degree)	h_r Reflection Height (km)	R Range (km)	L Absorption (db)
5	0	92.0	2225	57.8
	10	95.4	945	37.4
	20	99.3	545	25.9
	30	119.2	535	27.4
	40	126.5	358	16.9
	50	136.4	315	14.3
	60	157.4	302	13.1
	70	173.5	221	11.7
10	0	98.3	2282	16.0
	10	117.6	1629	20.0
	20	137.0	938	9.2
	30	194.5	951	7.0
	40	213.6	630	5.4
	50	232.7	536	5.7
	60	270.0	544	8.9
20	0	151.5	3997	6.2
	5	182.8	3315	5.5
	10	204.8	2225	4.1
	15	218.0	1687	3.3
	20	257.0	1930	4.4
30	0	233.4	4431	3.2
	5	265.6	6205	6.5

Table 8 continued

$S_{10.7} = 140$

$\chi = 50°$, April

f Frequency (MHz)	θ Elevation Angle (degree)	h_r Reflection Height (km)	R Range (km)	L Absorption (db)
5	0	93.1	2274	51.0
	10	97.5	966	31.0
	20	102.0	567	21.7
	30	124.1	517	18.4
	40	134.2	405	13.2
	50	154.0	399	11.4
	60	171.5	335	9.9
	70	190.0	224	8.8
10	0	100.7	2307	13.2
	10	123.3	1375	11.8
	20	158.8	1212	7.4
	30	204.5	884	5.2
	40	220.0	643	4.3
20	0	191.0	4323	4.6
	5	201.0	3073	4.0
	10	211.0	2169	3.1
	15	235.7	2046	3.2

Table 8 continued

$S_{10.7} = 140$

$\chi = 70°$, April

f Frequency (Mhz)	θ Elevation Angle (degree)	h_r Reflection Height (km)	R Range (km)	L Absorption (db)
5	0	96.9	2357	35.3
	10	101.8	1016	20.2
	20	121.9	977	19.2
	30	140.9	605	10.0
	40	169.0	604	7.9
	50	196.4	493	6.4
	60	206.2	314	5.2
	70	211.1	200	4.6
10	0	109.1	2520	9.3
	10	141.2	1573	6.3
	20	202.2	1345	4.1
	30	221.5	919	3.1
20	0	215.4	3821	2.4
	5	219.4	2861	2.2
	10	251.2	3064	2.8

Table 8 continued

$S_{10.7} = 70$

$\chi = 30°$, April

f Frequency (MHz)	θ Elevation Angle (degree)	h_r Reflection Height (km)	R Range (km)	L Absorption (db)
5	0	94.0	2261	53.3
	10	97.2	961	33.9
	20	105.1	640	28.0
	30	127.3	530	17.8
	40	143.2	477	13.7
	50	193.0	589	11.9
	60	210.0	369	9.5
10	0	102.0	2363	15.9
	10	126.2	1363	11.4
	20	202.1	1592	7.6

$S_{10.7} = 70$

$\chi = 50°$, April

5	0	95.4	2321	47.6
	10	99.2	983	28.2
	20	120.6	831	23.0
	30	133.8	567	13.9
	40	161.9	610	11.1
	50	199.6	520	9.0
	60	212.0	361	7.6

Table 8 continued

$S_{10.7} = 70$

$\chi = 50°$, April

f Frequency (MHz)	θ Elevation Angle (degree)	h_r Reflection Height (km)	R Range (km)	L Absorption (db)
10	0	119.5	3131	16.6
	10	113.0	1469	8.9
	20	205.4	1442	5.8

$S_{10.7} = 70$

$\chi = 70°$, April

5	0	97.5	2378	35.4
	10	104.0	1052	20.2
	20	135.2	868	13.0
	30	161.3	756	8.8
	40	201.4	674	6.7
	50	216.3	479	5.4
10	0	136.3	2966	8.3
	10	168.8	2072	5.6
	20	225.9	1534	3.8

L = total absorption per hop in db

χ = solar zenith angle

$S_{10.7}$ = solar activity expressed in 10.7 cm solar flux

D = ground range in km

f = wave frequency in MHz

f_H = gyro frequency in MHz

I = dip angle (at the midpoint of the path)

$\nu_o/2\pi$ = collision frequency at 90 km in MHz

A nonlinear least square fitting method was used in this analysis. The standard deviation of the predicted values by this empirical equation from the data is around 3 db.

CHAPTER V

SUMMARY AND CONCLUSION

5.1 Development of a General Theoretical Approach to Radio Wave Propagation Prediction by Combining a Theoretical Ionospheric Model with a Ray Tracing Program

It was not the purpose of this work to develop new ionospheric models or ray tracing programs. Modification was made to allow the D region model to be matched to the bottom of the Penn State Mk 1 Model and to ensure that a collision frequency model was developed that was consistent with both the most up-to-date atmospheric model in the lower ionosphere and the Penn State Mk 1 electron densities in the F region.

In contrast to current prediction techniques the method described in this report allows many properties of high frequency radio wave propagation to be predicted in a consistent manner. It has been shown that Faraday rotation and differential Doppler velocities from satellites, propagation modes for long distance high frequency propagation including the effect of longitudinal and transverse gradients, group delays and azimuth and zenith angles for each mode, ionospheric absorption, and spatial loss including the effects of focusing can all be predicted.

While the method requires large amounts of computer time for the ray tracing program, it does not require a

great deal of knowledge about ionospheric conditions or wave propagation on the part of an eventual user. The complexities in these areas are built into the program. The restrictions on the use of the technique depend on those of the ionospheric models and on the ray tracing program. The current level of knowledge of the ionosphere only allows average monthly ionospheric conditions to be predicted. It is probably a fair summary of the work reported here to say that in each case studied, the departures of the predictions from the measurements were no larger than the range of variation encountered in a given month. While the measurements of the densities and contents were within these limits, the estimation of gradients in the density was much more difficult. Large departures from average gradients were observed and would be expected, so that prediction of such things as the departure of the ray path from the great circle path and focusing should be regarded with great caution. A model, to account for these effects fully, will presumably require frequent updating with real time ionospheric data.

5.2 Comparison of Oblique Incidence Ionospheric Sounding with the Predictions of the Propagation Condition for an Ionospheric Model

An oblique incidence sounding for the 1150 km path from Sterling, Virginia to St. Louis, Missouri was compared. It was shown that the group delay and the relation of group

delay with frequency for both low-and high-angle ray modes were very similar to the measurements. The group delays measured were bracketed by curves calculated based on a variation of ± 10% on the solar flux about the estimated value for the time of measurements.

5.3 Comparison of the Predictions of the Model with Current Techniques

Comparisons were made of the predictions of the model for a path from Washington, D.C. to London, England for 7:00 U.T. and 23:00 U.T. and the ITS Ionospheric Predictions for the same period. The results of these investigations are given in Table 4. The maximum percentage difference between the maximum usable frequencies for the paths was in all cases tested within 5%. It should be pointed out, however, that the methods use common data for the predictions and the errors are not independent. The current prediction techniques have a long history of being checked against actual operating conditions, and thus the agreement seems to validate the results reported in this work. The present method does, of course, predict much more than just the maximum usable frequency or the optimum working frequency. It is upon those other parameters, such as the ionospheric absorption, group delays on the various paths, and the spatial losses, that the importance of the present method rests.

5.4 Comparison of Predicted Satellite to Ground Propagation with Observations

The diurnal variations of the electron content over State College, Pennsylvania and Stanford, California were predicted and compared with the measurements from satellites. The day-to-day variation was predicted and compared with the measurements for the different local times as the satellite precessed. At Stanford the predictions were compared with data for 4 years and 3 seasons.

Even though the general agreement was good, discrepancies of up to 40% were shown in Figures 11, 14, and 16. These variations were of the same order as the day-to-day variation in the electron content. The predictions are for monthly average conditions and it remains to be determined whether the departures are due to changes in the neutral atmosphere, the ionizing radiation or some other effect.

The assumptions of the Penn State Mk 1 Model break down for low latitudes, but the predictions of the electron content at Huancayo, Peru shown in Figure 12 were in satisfactory agreement. The reason for this appears to be that the electron content can be estimated quite well provided that the peak electron density and the height of the peak are correct, and the scale height of the ionization is well estimated. It is probably unwise to assume that the agreement found between the current predictions and measurements extends to the electron density profiles in regions far above the peak.

The gradients of the electron content were also predicted for a few cases. The gradients caused by predictable inputs, such as sunrise and sunset can be treated well by the models.

It is not possible at present to treat irregularities with short wave lengths such as are produced by gravity waves which pass through the atmosphere and produce gradients which change with time or by winds which are not always regular and can change from one night to the next.

5.5 The Predictions of the Path Loss

The predictions of the absorption at 3.36 MHz for the path from Annapolis to State College and at 5 MHz for the path from Ft. Collins to White Sands Missile Range were made.

The current ionospheric models seem to give too little attenuation, and the electron density at the lower heights is probably greater than given by the Mitra-Rowe Model. Some models based on rocket measurements which show substantially higher densities were also tried, and these showed much greater attenuations than were observed. It would appear that the method can serve as a useful technique in checking models.

The method showed in a very clear way the percentage of the absorption that took place at different altitudes. While it has been realized for some time that great care had to be exercised in interpreting ionospheric absorption

measurements in terms of D region densities, it was very difficult for people making measurements to interpret their data and determine what they were seeing. The present technique allows readily interpretable results to be presented in a very simple manner so that an experimenter can determine the sensitivities of his technique or results to the parameters of interest.

5.6 Recommendations for Future Work

Many experimental data are now available for the satellite electron content measurements, oblique incidence ionograms, and A3 absorption measurements. Wider comparison of the predictions by model calculations with actual data are needed for different seasons and locations.

One disadvantage of this technique is the cost of the ray tracing, which requires a large amount of computer time. In this instance, the cost of ray tracing was of the order of a few thousand dollars, while the cost of calculating the complete ionospheric models was only a few dollars. This means that when ray tracing of this type is contemplated the extra expense of a rather sophisticated ionospheric model is quite small, and much greater complexities could be included in the ionospheric model program without greatly increasing the total cost. The ray tracing program also needs to be simplified if possible to reduce the cost without affecting its accuracy.

The Penn State Mk 1 Model and Mitra-Rowe Model must be coupled together by matching the boundary conditions so that the electron density and collision frequency profiles can be obtained without a discontinuity from the base of the ionosphere to the upper F region as a function of time, day number, season, and solar activity. This model coupled with the magnetic field model can then supply the necessary quantities which the ray tracing program needs to calculate the ray path for any desired transmitter and receiver. This could allow technicians to run the program by simply supplying the proper input data. In this case error estimates as well as parameter estimates will be required.

BIBLIOGRAPHY

Appleton, E. V., Wireless Studies of the Ionosphere, J. Inst. Elect. Engrs., 71, 652-650, October 1932.

Appleton, E. V., and W. J. G. Beynon, The Application of Ionospheric Data to Radio-Communication Problems; Part I, Proc. Phys. Soc. (London), 52 (202), 518-533, July 1940.

Appleton, E. V., and W. J. G. Beynon, The Application of Ionospheric Data to Radio-Communication Problems; Part II, Proc. Phys. Soc. (London), 59 (331), 58-76, January 1947.

Barghausen, A. F., J. W. Finney, L. L. Proctor, and L. D. Schultz, Predicting Long-Term Operational Parameters of High-Frequency Sky-Wave Telecommunication Systems, ESSA, Tech. Rept., ERL 110-ITS 78, May 1969.

Barron, D. W., and K. G. Budden, The Numerical Solutions of Differential Equations Governing Reflection of Long Radio Waves from the Ionosphere III, Proc. Roy. Soc. A, 249, 387-401, 1959.

Belrose, J. S., Radio Wave Probing of the Ionosphere by the Partial Reflection of Radio Waves (from Heights Below 100 km), J. Atm. Terr. Phys., 32 (4), 567-596, April 1970.

Booker, H. G., The Propagation of Wave Packets Incident Obliquely on a Stratified Doubly Refracting Ionosphere, Phil. Trans. Roy. Soc. A, 237 (781), 411-451, September 1939.

Bowhill, S. A., The Faraday-Rotation Rate of a Satellite Radio Signal, J. Atm. Terr. Phys., 13 (1/2), 175-176, December 1958.

Bowhill, S. A., The Formation of the Daytime Peak of the Ionospheric F2-Layer, J. Atm. Terr. Phys., 24 (6), 503-519, June 1962.

Bowman, M. R., L. Thomas, and J. E. Geisler, The Effect of Diffusion Processes on the Hydrogen and Oxygen Constituents in the Mesosphere and Lower Thermosphere, J. Atm. Terr. Phys., 32 (10), 1661-1674, October 1970.

Budden, K. G., The Numerical Solutions of Differential Equations Governing Reflection of Long Radio Waves from the Ionosphere I, Proc. Roy. Soc. A, 227, 516-537, 1955a.

Budden, K. G., The Numerical Solutions of Differential Equations Governing Reflection of Long Radio Waves from The Ionosphere II, Phil. Trans. Roy. Soc. A, 248, 45-71, 1955b.

Budden, K. G., Radio Waves in the Ionosphere, The University Press, Cambridge, 1961.

Budden, K. G., Effect of Electron Collisions on the Formulas of Magneto-ionic Theory, Radio Sci., 69 (2), 191-211, February 1965.

Budden, K. G. and P. C. Clemmow, Coupled Form of the Differential Equations Governing Radio Wave Propagation in the Ionosphere II, Proc. Camb. Phil. Soc., 53, 669-682, 1957.

C.C.I.R., The International Radio Consultative Committee, C.C.I.R. Rep. 340, Atlas of Ionospheric Characteristics, Union Internationale des Telecommunications, Geneva, Switzerland, 1967.

Chapman, S., and J. Bartels, Geomagnetism, Vol. II, Oxford at the Clarendon Press, 1962.

CIRA, Cospar International Reference Atmosphere, compiled by working group IV, COSPAR, North-Holland, Amsterdam, 1965.

Clemmow, P. E. and J. Heading, Coupled Forms of the Differential Equations Governing Radio Propagation in the Ionosphere I, Proc. Camb. Phil. Soc., 50, 319-333, 1954.

Croft, A. C., Methods and Applications of Computer Ray Tracing, Tech. Rept. No. 112, Radio Science Laboratory, Stanford Electronics Laboratory, Stanford University, January 1969.

da Rosa, A. V., and O. K. Garriot, Protonospheric Electron Concentration Profiles, J. Geophys. Res., 74 (26), 6386-6402, December 1, 1969.

Davies, K., The Effect of the Earth's Magnetic Field on M.U.F. Calculations, J. Atm. Terr. Phys., 16 (1/2), 187-189, 1959.

Davies, K., Ionospheric Radio Propagation (NBS Monograph 80) U.S. Department of Commerce, U.S. Government Printing Office, April 1965.

Davies, K., Ionospheric Radio Waves, Blaisdell Publishing Co., 1969.

Davies, R. M. Jr., Short-term Prediction of F2-layer MUFs from Local Magnetic Activity, ESSA Tech. Rept. ERL 157-ITS 100, March 1970.

Deeks, D. G., Generalized Full Wave Theory for Energy-Dependent Collision Frequencies, J. Atm. Terr. Phys., 28 (8), 839-846, September 1966.

Evans, W. F. J., and E. J. Llewellgn, Molecular Oxygen Emissions in the Airglow, Annales Geophys., 26 (1), 167-177, January-February-March 1970.

Ferraro, A. J. and H. S. Lee, Winter D-Region Electron Concentration and Collision Frequency Features Obtained with High-Power Interaction Measurement, J. Geophys. Res., 74 (5), 1184-1194, March 1, 1969.

Garriot, O. K., A. V. da Rosa, and W. J. Ross, Electron Content Obtained from Faraday Rotation and Phase Path Length Variations, J. Atm. Terr. Phys., 32, 705-727, 1970.

Ginzburg, V. L., Propagation of Electromagnetic Waves in Plasma, Gordon and Breach Science Publishers, Inc., New York, 1961.

Gnanalingam, S., Equatorial Ionospheric Absorption During Half a Solar Cycle (1964-1970), X-625-72-276, Laboratory for Planetary Atmospheres, NASA/Goddard Space Fleight Center, Greenbelt, Maryland, 1972.

Groves, G. V., Seasonal and Latitudinal Models of Atmospheric Temperature, Pressure and Density, 25 to 110 Km, COSPAR 14th Plenary Meeting, June 18 - July 2, Seattle, Washington, 1971.

Hanson, G. H., H. V. Serson, and W. Campbell, Maximum Usable Frequencies for the Path Washington to Resolute Bay, J. Geophys. Res., 58 (4), 487-491, December 1958.

Haselgrove, J., Ray Theory and a New Method for Ray Tracing, Report of the Physical Society Conference on the Physics of the Ionosphere, published by Physical Society (London), 355-364, 1955.

Hays, P. B. and J. J. Olivero, Carbon Dioxide and Monoxide above the Troposphere, Planet. Space Sci., 18 (12), 1729-1733, December 1970.

Heaviside, O., Telegraphy, Encyclopedia Britanica, 10th Ed. 9, 213-235, Adams and Charles Block, London and Edinburgh, 1902.

Heisler, R., and G. L. Hower, Comparisons between Calculated Ionospheric Absorption and Riometer Measurements, J. Atm. Terr. Phys., 32 (11), 1755-1764, November 1970.

Itikawa, Y., Effective Collision Frequency of Electrons in Atmospheric Gases, Planet. Space Sci., 19, 993-1007, 1971.

Jacchia, L. G., New Static Models of the Thermosphere and Exosphere with Empirical Temperature Profiles, Smithsonian Astrophys. Obs. Spec. Rept., No. 313, 1-88, May 6, 1970.

Jensen, D. C., and J. C. Cain, Interim Geomagnetic Field (abstr.), J. Geophys. Res., 67 (9), 3568-3569, August 1962.

Jones, R. M., A Three Dimensional Ray Tracing Computer Program, ESSA Tech. Rept., IER 17-ITSA 17, 1966.

Jones, R. M., Ray Theory for Lossy Media, Radio Sci., 5 (5) 793-801, May 1970.

Jones, T. B., and G. Foley, Reflection Conditions of a Radiowave Propagated Obliquely through a Horizontally Stratified Ionosphere, J. Atm. Terr. Phys., 34 (5), 837-844, May 1972.

Jones, W. B., and R. M. Gallet, Ionospheric Mapping by Numerical Methods, ITU Telecomm. Journal, No. 12, 260-264, 1960.

Jones W. B., and R. M. Gallet, Representation of Diurnal and Geographical Variations of Ionospheric Data by Numerical Method, J. Res., NBS 66D (Radio Propagation), No. 4, 419-438, 1962a.

Jones W. B., and R. M. Gallet, Methods for Applying Numerical Maps of Ionospheric Characteristics, J. Res., NBS 66D (Radio Propagation), No. 6, 649-662, 1962b.

Jones, W. B., R. P. Graham, and M. Leftin, Advances in Ionospheric Mapping by Numerical Methods, ESSA Tech. Rept. ERL 107-ITS 75, Boulder, Colorado, May 1969.

Kelso, J. M., Radio Ray Propagation in the Ionosphere, McGraw-Hill Book Co., 1964.

Kelso, J. M., Ray Tracing in the Ionosphere, Radio Sci., 3 (1), 1-8, January 1968.

Kennely, A. E., On the Elevation of Electrically Conducting Strata of the Earth's Atmosphere, Electrical World and Engineering, 39 (11), 473, 1902.

Ladato, R. F., and E. A. Mechtly, Rocket Measurement of Electron Collision Frequency, Aeronomy Rept. No. 45, Aeronomy Laboratory, University of Illinois, September 1971.

Lucas, D. L., and G. W. Haydon, Predicting Statistical Performance Indexes for High Frequency Ionospheric Telecommunication Systems, ESSA Tech. Rept., IER 1-ITSA 1, 1966.

Meira, L. G., Rocket Measurements of Upper Atmospheric Nitric Oxide and Their Consequences to the Lower Ionosphere, J. Geophys. Res., 76 (1), 202-212, January 1, 1971.

Mitra, A. P., HF and VHF Absorption Techniques in Radio Wave Probing of the Ionosphere, J. Atm. Terr. Phys., 32 (4), 623-646, April 1970.

Mitra, A. P., Summary of COSPAR Assembly, Madrid, 1972, IRL Internal Rept. No. 14, Ionosphere Research Laboratory, The Pennsylvania State University, October 2, 1972.

Mitra, A. P. and J. N. Rowe, Ionospheric Effects of Solar Flares-VI. Changes in D-region in Chemistry During Solar Flares, J. Atm. Terr. Phys., 34, 795-806, 1972.

Mitra, A. P., and C. A. Shain, The Measurement of Ionospheric Absorption Using Observations of 18.3 Mc/s Cosmic Radio Noise, J. Atm. Terr. Phys., 4 (4/5), 204-218, December 1953.

Nisbet, J. S., On the Construction and Use of the Penn State Mk 1 Ionospheric Model, Ionosphere Research Laboratory, Sci. Rept. No. 355, The Pennsylvania State University, May 1, 1972a.

Nisbet, J. S., Tables from the Penn State Mk 1 Ionospheric Model, Ionosphere Research Laboratory, Sci. Rept. No. 362(E), The Pennsylvania State University, August 20, 1970b.

Ostrow, S. M., Handbook for CRPL Ionospheric Predictions Based on Numerical Methods of Mapping, Handbook 90, ESSA, ITSA, Boulder, Colorado, August 1966.

Phelps, A. V., and J. L. Pack, Electron Collision Frequencies in Nitrogen and in the Lower Ionosphere, Phys. Rev. Letters, 3, 340-342, 1959.

Piggot, W. R. and G. M. Brown, IQSY Instruction Manual No. 4, Part II, Absorption Measurements, Compiled from contributions by K. H. Gerswald, K. Oberlander, G. Umlauft, H. Schwentek, and C. G. Little CIG-IQSY Committee, London, 1963.

Piggot, W. R., M. L. V. Pitteway, and E. V. Thrane, The Numerical Calculation of Wave-Fields, Reflection Coefficients and Polarizations for Long Radio Waves in the Ionosphere, II., Phil. Trans. Roy. Soc. A, 257, 243-271, 1965.

Pitteway, M. L. V., The Numerical Calculation of Wave-Fields, Reflection Coefficients and Polarizations for Long Radio Waves in the Ionosphere, I., Phil Trans. Roy. Soc. A, 257, 219-241, 1965.

Ratcliff, J. A., Magneto-ionic Theory and Its Application to the Upper Atmosphere, Cambridge University Press, Cambridge, 1959.

Rawer, K., Calculation of Sky Wave Field Strength, Wireless Engineers, 29 (349), 287-301, November 1952.

Ross, W. J., Second-order Effects in High Frequency Trans-ionospheric Propagation, J. Geophys. Res., 70, 597-612, 1965.

Ross, W. J., Measurement of Electron Content at the Magnetic Equator, J. Geophys. Res., 71 (15), 3671-3676, August 1, 1966.

Ross, W. J., O. K. Garriot, F. De Mendonca, and A. V. da Rosa, Comments on Local Electron Concentration Determination from Doppler Dispersion Measurements of Satellite Radio Beacons, J. Geophys. Res., 73 (3), 1102-1106, February 1, 1968.

Saha, A. K. and R. Venkatachari, A Re-examination of Collision Frequency Estimates in the Ionospheric F- and E-layers from Derivative Absorption Measurements, J. Atm. Terr. Phys., 32 (4), 303-314, 1970.

Schwentek, H., The Determination of Absorption in the Ionosphere by Recording the Field Strength of a Distant Transmitter (Fundamentals of the Method A3 and Results of the Continuous Measurements Since 1956). Annales Geophys., 2, 276-288, April-June 1966.

Schwentek, H., The Sunspot Cycle 1958/70 in Ionospheric Absorption and Stratospheric Temperature, J. Atm. Terr. Phys., 33 (12), 1839-1852, 1971.

Seliga, T. A., Electron Density in the D Region of the Ionosphere from Low Frequency Signal Strength Measurement in Rockets, Ionosphere Research Laboratory, Sci. Rept. No. 254, The Pennsylvania State University, November 1, 1965.

Sen, H. K., and Wyller, A. A., On the Generalization of the Appleton-Hartree Magnetoionic Formulas, J. Geophys. Res., 65 (12), 3931-3950, December, 1970.

Silberstein, R., The Use of Sweep-Frequency Backscatter Data for Determining Oblique Incidence Ionospheric Characteristics, J. Geophys. Res., 63 (2), 335-351, 1958.

Smith, N., The Relation of Radio Sky-wave Transmission to Ionosphere Measurements, Proc. IRE, 27, 332-347, 1939.

Solomon, S. L., Variation in the Total Electron Content of the Ionosphere at Mid-latitudes During Quiet Sun Conditions. Ionosphere Research Laboratory, Sci. Rept. No. 256, The Pennsylvania State University, November 30, 1965.

Thomas, J. O., J. Haselgrove and A. R. Robbins, The Electron Distribution in the Ionosphere Over Slough-I. Quiet Days, J. Atm. Terr. Phys., 12 (1), 46-56, 1958a.

Thomas, J. O., J. Haselgrove and A. R. Robbins, Tables of Ionospheric Electron Density, Series B No. 1 Cavendish Laboratory, Cambridge, 1958b.

Thomas J. O. and A. R. Robbins, Ionospheric True Height and M.U.F. Calculations, J. Atm. Terr. Phys., 12 (1), 77-79, 1958.

Thrane, E. V., and W. R. Piggot, The Collision Frequency in the E-and D-regions of the Ionosphere, J. Atm. Terr. Phys., 28, 721-737, 1966.

Vickers, M. D., The Calculation of the M.U.F. Factor for a Non-Parabolic Ionospheric Layer, J. Atm. Terr. Phys., 17, 34-45, 1959.

Wakai, N., Ray Paths and Absorption of MF and HF Radio Waves Incident on the Nighttime Ionosphere, J. Rad. Res. Labs., 18 (97), 191-208, Printed in Tokyo, Japan, May, 1971.

Wentzel, G., H. A. Kramers, and Brillouin, Z. Physik, 38, 518, (1926), Z. Physik, 828 (1926), and Compt. Rend., 183, 24 (1926), respectively.

Wider, B., Some Results of a Sweep Frequency Propagation Experiments Over an 1150-Km East-West, J. Geophys. Res., 60 (5), 395-409, 1955.

APPENDIX 1

ESTIMATION OF INITIAL AZIMUTH ANGLE AND A GREAT CIRCLE PATH

Before the ray tracing program can be run, it is necessary to make an estimate of the initial azimuth angle and of the great circle path so that the ionospheric models can be run for the appropriate geographical regions.

The first parameter to be calculated, given the geographic latitudes and longitudes of the transmitting and receiving locations, is the path length, which is taken to be the shorter of the great-circle distances between the two points, and which is computed from the spherical trigonometry as shown in Figure 39.

$$\cos d = \sin \lambda_1 \sin \lambda_2 + \cos \lambda_1 \cos \lambda_2 \cos (\theta_1 - \theta_2)$$

where

λ_1 = geographic latitude of transmitter

θ_1 = geographic longitude of transmitter

λ_2 = geographic latitude of receiver

θ_2 = geographic longitude of receiver

d = path length in radians

Having obtained the path length, the bearing (the azimuth angle from the north pole) of the transmitter along the great circle path can be calculated;

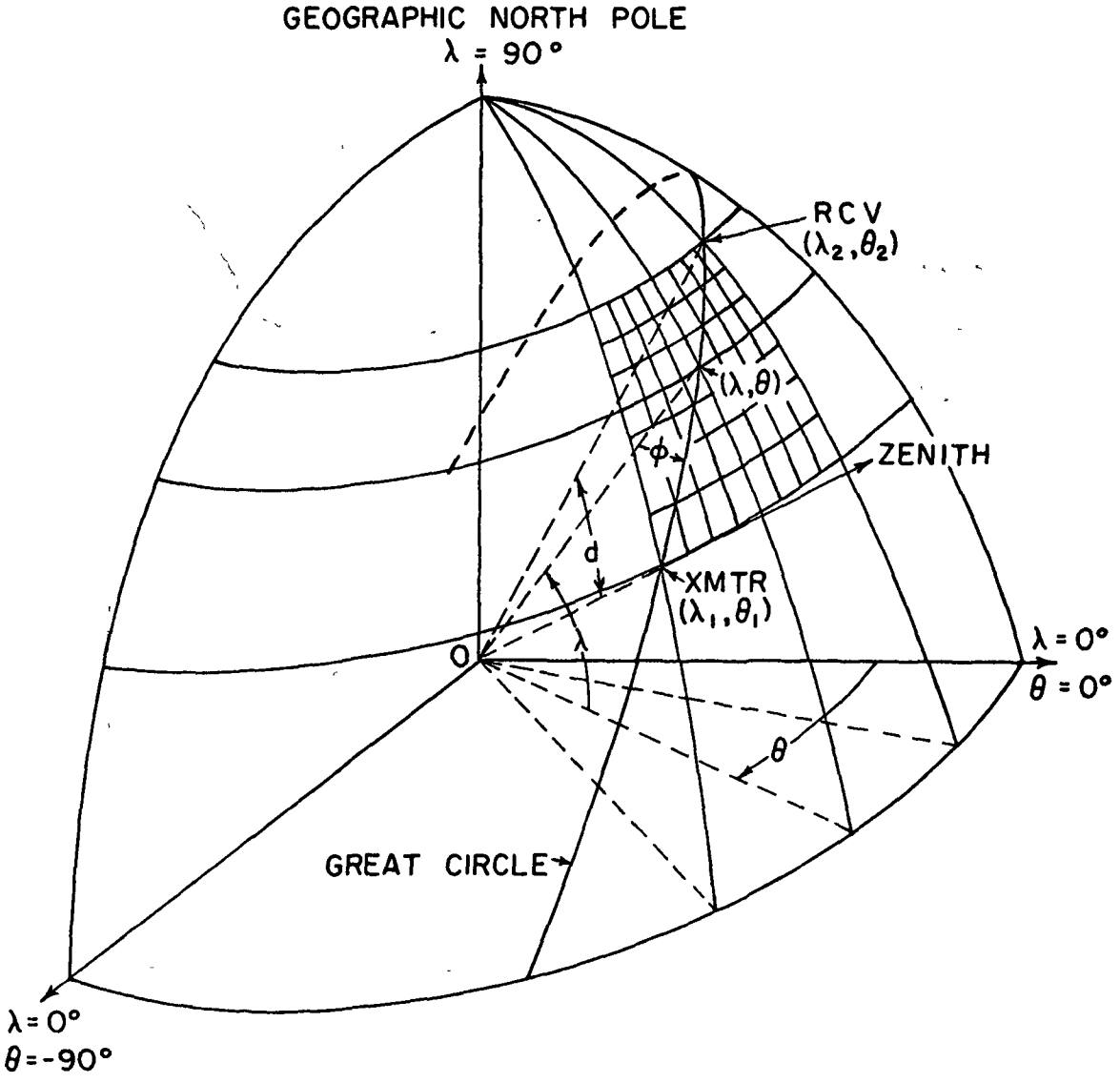

Figure 39 Geometry of the Path

$$\cos \phi_1 = (\sin \lambda_2 - \sin \lambda_1 \cos d)/\cos \lambda_1 \sin d$$

$$\cos \phi_2 = (\sin \lambda_1 - \sin \lambda_2 \cos d)/\cos \lambda_2 \sin d$$

where

ϕ_1 = bearing of transmitter to receiver in radians

ϕ_2 = bearing of receiver to transmitter in radians

Using the bearing obtained, the geographic latitude and longitude of any point on the great circle path which is a certain distance away from the transmitter can also be calculated in the same way.

APPENDIX 2

LIST OF MAIN COMPUTER PROGRAMS

1. Penn State Mk 1 Ionospheric Model

This program gives the complete electron density profile from 210 km to 1250 km as a function of latitude, longitude, day number and solar activity. More details are described in Chapter I. This program also can calculate the electron collision frequency with neutrals and ions using Itikawa's Equation.

2. Ray Tracing Program

This program was originally developed by Jones (1966) and modified a little at Stanford Radioscience Laboratory. The modified version was used in this work. This program calculates the ray path by numerical integration of six simultaneous differential equations as discussed in Chapter I.

3. Magnetic Field Model

This program calculates the elements of the earth's magnetic field vector as discussed in Chapter I.

4. D Region Model

This model gives the electron density profile from 60 km to 120 km for middle latitudes (for dip latitude 30° ~ 60°) as a function of the solar zenith angle, season, and solar activity. This program also gives the electron collision frequency with neutrals by using Itikawa's equation and Groves' neutral atmospheric model.